INVESTIGATING THE TIMING OF DEGLACIATION AND THE EFFICIENCY OF SUBGLACIAL EROSION IN CENTRAL-WESTERN GREENLAND WITH COSMOGENIC ^{10}BE AND ^{26}AL

A Thesis Presented

by

Lee Corbett

to

The Faculty of the Graduate College

of

The University of Vermont

In partial Fulfillment of the Requirements
for the Degree of Master of Science
Specializing in Geology

October, 2011

Accepted by the Faculty of the Graduate College, The University of Vermont, in partial fulfillment of the requirements for the degree of Master of Science, specializing in Geology.

Thesis Examination Committee:

_____**Advisor**
Paul Bierman, Ph.D.

_____
Stephen Wright, Ph.D.

_____**Chairperson**
Shelly Rayback, Ph.D.

_____**Dean, Graduate College**
Domenico Grasso, Ph.D.

Date: **May 12, 2011**

ABSTRACT

This work aims to study the behavior of the western margin of the Greenland Ice Sheet during a period of pronounced ice retreat roughly 10,000 years ago, after the end of the last glacial period. It explores the efficiency of subglacial erosion, the spatial dynamics of ice retreat, and the rates of ice retreat. To address these questions, I use the radionuclides ^{10}Be and ^{26}Al, which form in rocks due to the bombardment of cosmic rays, only after the rocks have been exposed from underneath retreating ice. These nuclides can be used as a geologic dating technique to explore exposure history.

Before applying this dating technique to address geological questions, it was critical to first perform methodological development. My work in the University of Vermont's new Cosmogenic Nuclide Laboratory served to improve the precision and efficiency of the pre-existing laboratory methods. New methodological advances ensured that samples from Greenland, which contained only low concentrations of ^{10}Be and ^{26}Al, could be used to yield meaningful results about ice behavior.

Cosmogenic nuclide dating was applied at two sites along the ice sheet margin in central-western Greenland. At both of these sites, I collected paired bedrock and boulder samples in a transect normal to and outside of the present-day ice sheet margin. Samples were collected from a variety of elevations at numerous locations along the transects, thus providing three-dimensional coverage of the field area. After isolating the mineral quartz from the rocks, and isolating the elements Be and Al from the quartz, isotopic analysis was performed using accelerator mass spectrometry to quantify the relative abundances of the radionuclides against their respective stable isotopes.

The southern study site, Ilulissat, is located on the western coast of Greenland at a latitude of 69°N. Much previous work has been conducted here due to the presence of one of the largest ice streams in the northern hemisphere, Jakobshavn Isbræ. My work in Ilulissat demonstrated that subglacial erosion rates were high during previous glacial periods, efficiently sculpting and eroding the landscape. Ice retreat across the land surface began around 10,300 years ago, and the ice sheet retreated behind its present-day margin about 7,600 years ago. Ice retreat occurred at a rate of about 100 meters per year. My work in this area suggests that retreat in the large ice stream set the pace and timing for retreat of the neighboring ice sheet margin.

The northern site, Upernavik, is located on the western coast of Greenland at a latitude of 73°N. Little research has been conducted here in the past. Unlike in Ilulissat, my work here shows that the ice sheet did not efficiently erode the landscape, especially at high elevations, during previous glacial periods. This is likely because the ice was thinner, and therefore had a colder base, than the ice in Ilulissat. My work suggests that ice cover was lost from this area very rapidly, likely at rates of about 170 meters per year, in a single episode around 11,300 years ago. Comparison between the two study sites reveals that ice characteristics can vary appreciably over relatively small distances.

CITATIONS

Material from this thesis was published in *Quaternary Science Reviews* on May 14, 2011 in the following form:

Corbett, L.B., Young, N.E., Bierman, P.R., Briner, J.P., Neumann, T.A., Rood, D.H., and Graly, J.A. (2011). ^{10}Be concentrations in bedrock and boulder samples resulting from early Holocene ice retreat near Jakobshavn Isfjord, western Greenland. Quaternary Science Reviews DOI 10.1016/j.quascirev.2011.04.001.

DEDICATION

To my parents, for always letting me keep rocks in the pockets of my overalls.

ACKNOWLEDGEMENTS

Thank you to the Middlebury College Geology faculty for your continued support, enthusiasm, mentoring, and friendship. I was thrilled and honored to be a part of your department during January of 2011, and learned an astonishing amount. Your love of teaching has inspired me throughout my time as a graduate student and will continue to motivate me as I look ahead in my career. A very special thank you to Dave for inspiration in both science and in life, and for always understanding me to the core.

I have a wonderful group of friends who served as cheerleaders for me throughout my research. Thank you for celebrating my accomplishments, for always being there when things weren't going well, and for feigning interest during my impromptu mini-lectures about various geological phenomena. Thank you especially to Ross for answering hundreds of questions about Excel and statistics, and for showing me what really matters.

Finally, I have only been able to achieve what I have due to the unconditional support of my parents, Pam and Pat Corbett. Thank you for always putting my education first, for encouraging me every step of the way, and for being my number one fans. You taught me to follow my dreams and to tackle my pursuits with passion.

TABLE OF CONTENTS

Chapter 2: Manuscript for *Quaternary Geochronology*

Chapter 3: Manuscript for *Quaternary Science Reviews*

LIST OF TABLES

LIST OF FIGURES

CHAPTER 1. INTRODUCTION

1. Motivations and Overview

The Greenland Ice Sheet plays a critical role in modern anthropogenic climate warming and sea level rise (Alley et al., 2005). Recent work has focused on quantifying how increasing temperatures have impacted the ice sheet, and has demonstrated that change is occurring at a rapid rate (IPCC, 2007). There has been a statistically significant increase in Greenland temperatures and ice sheet runoff (Hanna et al., 2008), contributing to an accelerating loss of ice mass (Wouters et al., 2008). Melting of the Greenland Ice Sheet has contributed between about 15 and 30% of the total global sea level rise since 2003 (Long, 2009), and will continue to be an important player in the future. Since the Greenland Ice Sheet holds about 6-7 meters of global sea level equivalent (Alley et al., 2005), melting ice has the potential to cause profound global change.

However, it is necessary to place the current changes in Greenland within a larger paleoclimatic context in order to more fully understand their meaning (Long, 2009). Accumulation and ablation rates of the Greenland Ice Sheet vary greatly over space and time, and paleoclimatic insight will help to make recent investigations of the Greenland Ice Sheet more meaningful. The goal of this project, therefore, is to explore behavior of the Greenland Ice Sheet on longer time scales.

To understand how the Greenland Ice Sheet behaves during a period of warming climate, it is important to study the transition between glacial and interglacial periods in order to determine how rapidly ice cover can be lost. In this project, I investigate the latest Pleistocene deglaciation at two sites in central-western Greenland (Ilulissat, 69°N,

and Upernavik, 73°N, Fig. 1). I perform these investigations by quantifying the abundance of two radioactive isotopes (^{10}Be and ^{26}Al) that are produced in rock when it is uncovered by glacial ice and exposed to the bombardment of cosmic radiation. This technique provides important information about various aspects of ice sheet behavior, including subglacial erosion efficiency and deglaciation chronology.

2. Study Site: Greenland and the Greenland Ice Sheet

The Greenland Ice Sheet (Fig. 1) occupies about 1.7 x 10^6 km^2 of land area and is the second largest ice sheet in the world after the Antarctic Ice Sheet. It covers 81% of Greenland, with the unglaciated areas found predominately around the coast and in the southwestern region. Although the thickness of the ice sheet near the coast is only 10's of meters, it increases to roughly 3,400 m at the center (Huybrechts et al., 1991). Because of Greenland's polar climate, the ice sheet is frozen to the bed in most locations and only reaches the pressure melting point in the areas of thickest ice and in the relatively warm coastal regions (Huybrechts, 1996). Greenland has been at least partially glaciated since about 7 Ma, although continuous ice cover did not develop until the late Pliocene (Larsen et al., 1994).

This project will investigate two sites along the western coast of Greenland. The southern site, Ilulissat, hosts the third largest settlement in Greenland and is located at 69°N. It is in close proximity to Jakobshavn Isbræ, a fast-flowing calving glacier, and sits directly on the iceberg-choked Ilulissat Isfjord. The northern site, Upernavik is located at 73°N. The settlement of Upernavik sits on a currently unglaciated offshore island, as the ice sheet on the mainland extends almost completely to the sea.
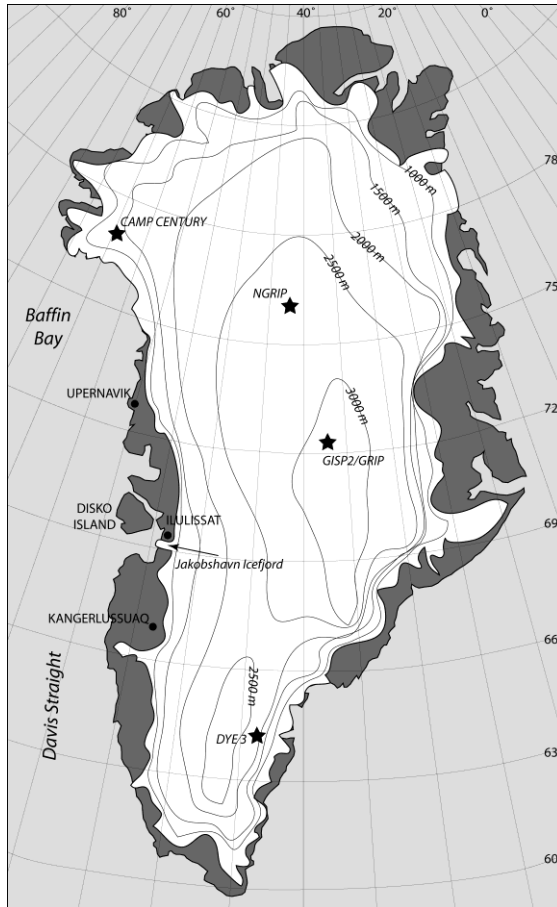
Figure 1. Map of Greenland. Relevant location names are shown. Stars indicate location of ice cores, and contour lines indicate ice sheet elevation.

3. Cosmogenic Nuclide Dating: An Overview

3.1. Principles of Cosmogenic Nuclide Dating

The basis of cosmogenic dating is a process that involves bombardment of terrestrial material by two types of cosmogenic particles: nucleons and muons (Granger and Muzikar, 2001). These high-energy cosmic-ray particles cause the formation of about two-dozen different isotopes that are not produced by any other common mechanism (Lal, 1988; Sharma and Middleton, 1989). The most frequently used isotopes for dating purposes include ^{3}He, ^{21}Ne, ^{10}Be, ^{26}Al, ^{36}Cl, and ^{14}C. The first two are stable noble

gasses, while the latter four are solid phase radionuclides listed by decreasing half-life (1.38 Ma, 0.7 Ma, 0.3 Ma, and 5.7 ka respectively) (Gosse, 2007; Nishiizumi et al., 2007).

Cosmogenic nuclide dating is based on the assumption that terrestrial cosmogenic nuclides are formed through bombardment of rock surfaces by cosmogenic particles at known rates, although these rates vary spatially as a function of geomagnetic field strength, altitude, latitude, and time (Lal, 1991). Cosmogenic nuclides are produced slowly, at rates of several atoms to several tens of atoms per gram of quartz per year. Knowing the cosmogenic nuclide concentration in a sample, as well as the production rate of that particular nuclide, allows inferences to be made about a sample's exposure history to cosmic radiation.

3.2. Exposure Dating

The traditional form of cosmogenic dating, called exposure dating, is concerned with determining how recently a surface (e.g. striated bedrock, or a boulder on a glacial moraine) was exposed. Assuming that the surface had no cosmogenic nuclides leftover from previous periods of exposure and has not eroded since exposure, measuring the abundance of cosmogenic nuclides in the sample would therefore indicate how long that bedrock surface has been uncovered and subjected to bombardment by cosmogenic particles (Phillips et al., 1990). If using a radioactive cosmogenic nuclide, the rate of decay must also be taken into account.

3.3. Burial Dating

A related technique, called cosmogenic burial dating, can be used on surfaces that have seen exposure followed by burial (Granger and Muzikar, 2001). Cosmogenic burial dating relies on the principle that radioactive cosmogenic nuclides are formed at a known rate and decay at another known rate. If two cosmogenic nuclides are used, the ratio of their concentrations can be correlated to the amount of time the surface spent exposed (thus accumulating cosmogenic nuclides) and the amount of time the surface spent shielded from radiation (thus decaying radioactive cosmogenic nuclides) (Granger and Muzikar, 2001). For example, in an area where glaciers have periodically advanced and retreated, the ratio of ^{26}Al to ^{10}Be can indicate what fraction of the time the bedrock was exposed versus buried by ice (Nishiizumi et al., 1991).

Because nuclides with different production rates and half-lives behave differently, examining two nuclides together provides information about complex exposure histories. Assuming that a rock surface was exposed for a long duration, the ratio of the concentrations of the cosmogenic nuclides follows a curved path as shown by the thick black "constant exposure" line (Fig. 2). The starting point of this graph is determined by the ratio of production rates of the two cosmogenic nuclides (~6.75, in the case of ^{26}Al/^{10}Be). The path that the line follows is determined by the decay constants of the cosmogenic nuclides and the duration of exposure. Eventually, if no burial or erosion occurs, the path will reach a point of secular equilibrium where the rate of decay is equal to the rate of production.
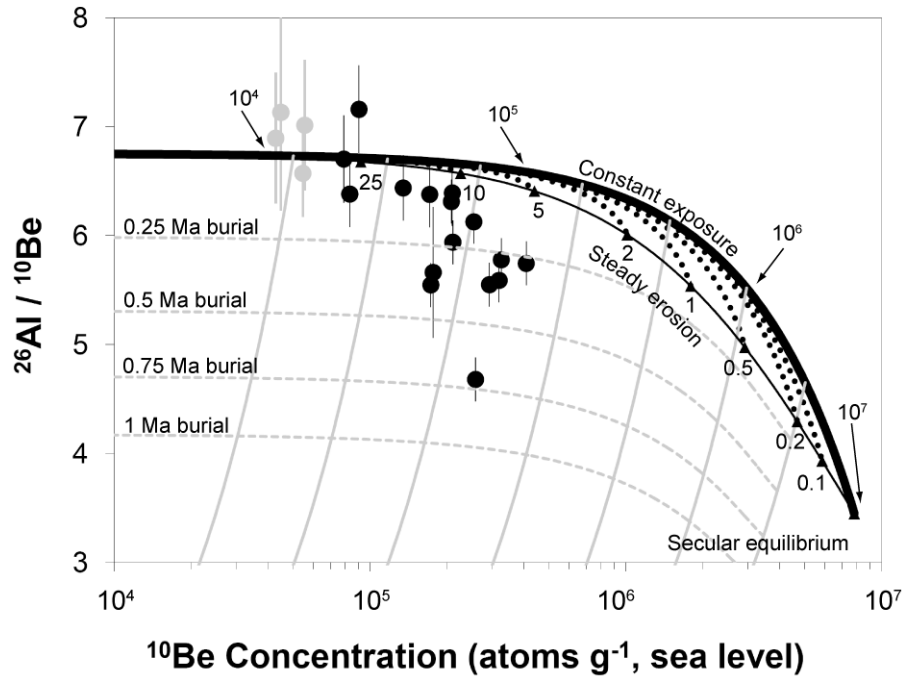
Figure 2. Example plot of paths in the two-isotope system of ^{10}Be and ^{26}Al in quartz. Exposure durations (in years) are shown along the thick black "constant exposure" path. Erosion rates, in m Ma^{-1}, are shown along the bottom of the "steady erosion" envelope. Individual erosion paths for the erosion rates mentioned are shown with black dotted lines. Burial paths are shown with thin gray lines, and burial isochrones are shown with thin gray dashed lines. Gray and black dots represent some of the samples that will be discussed in Chapter 4.

If the rock surface is eroding, material and cosmogenic nuclides are removed from the surface. Erosion mimics an increase in the decay constants of the nuclides, causing the exposure path to shift leftward (Fig. 2). The endpoints of all possible erosion paths serve to define the bottom of the "erosion envelope". Any samples that plot within this envelope can be considered to have experienced constant surface exposure with steady erosion.

In the simplest model of burial dating, a surface is exposed to cosmic radiation for an amount of time much shorter than the half-lives of the cosmogenic nuclides, and then buried deeply enough to halt all production (Granger and Muzikar, 2001). In Figure 2,

this would equate to traveling along the curved "constant exposure" line for a certain amount of time proportional to the duration of cosmic ray exposure, and then traveling perpendicularly to that path across the burial isochrones for an amount of time proportional to the duration of burial. As shown by the path described above, the $^{26}Al/^{10}Be$ ratio decreases with burial because the half-life of ^{26}Al is less than that of ^{10}Be. This model can get increasingly complex if multiple periods of exposure and burial are involved. Using two nuclides together can yield information about minimum exposure and burial durations.

4. The History of Glaciation in Greenland

4.1. The Onset of Glaciation

Although the Greenland Ice Sheet is a large and important player in Earth's climate system, the age of its formation is poorly constrained. Thus far, there has been no reliable way to determine the age of the ice sheet directly since the oldest ice from the bottom of ice cores taken from Greenland's summit only dates to the last glacial period. The onset of glaciation can, however, be dated indirectly by determining the onset of ice-rafted debris deposition in deep sea sediment in the North Atlantic. The oldest widespread ice-rafted debris found in North Atlantic deep sea cores dates back to around 2.4 Ma (Shackleton et al., 1984). Other work off the southeast coast of Greenland, however, indicates that the first ice-transported dropstones were deposited in the Late Miocene, roughly 7 Ma (Larsen et al., 1994).

These dates, however, do not necessary represent the actual onset of northern hemisphere glaciation because ice-rafted debris is only produced when glaciers or ice

sheets become large enough to reach the sea. Larsen et al. (1994) suggest that glaciation actually began much earlier, likely at the onset of cooling in the early Late Miocene around 10 Ma. Full glacial conditions would have been established by about the middle Late Miocene (7 Ma), allowing glaciers in Greenland to reach the sea, calve icebergs, and contribute to the deposition of ice-rafted debris in deep sea sediments. It is suspected that Northern Hemisphere glaciation would have nucleated in southeastern Greenland where temperatures were warmer and precipitation higher, rather than in the cold, dry interior (Larsen et al., 1994).

4.2. Glaciation in the Miocene and Pliocene (10 – 1.8 Ma)

Few paleoclimate records exist that provide information about ancient glacial advances and retreats, primarily because any land-based evidence of glacial retreat gets erased when the ice re-advances. Again, it is most helpful to turn to the marine record. If, as described above, glaciation began in the middle Late Miocene, then subsequent pulses of ice-rafted debris may be indicators of periods of heightened glacial activity. Conversely, units of sediment devoid of ice-rafted debris would indicate warm interglacial periods when ice had retreated back from the coast. Using these assumptions, Larsen et al. (1994) identify several major warm periods in the sediment that date to 3.1, 2.7, 2.6, and 2.4 Ma BP. These periods correlate roughly with warm marine oxygen isotope stages measured through oxygen isotope ratios (δ^{18}O) in benthic foraminifera by Lisiecki and Raymo (2005) (Fig. 3).

In shallow marine areas, sediments preserve records of biologic activity on land. Funder et al. (1985) documented terrestrial vegetation remains and invertebrate fauna in

8

sediments off the northern shore of Greenland from 2 Ma. These biological climate proxies suggest that Greenland was covered by a forest tundra environment during the late Pliocene, implying that arctic tree line was 2500 km to the north of its present-day position.

4.3. Glaciation in the Early and Middle Pleistocene (1.8 Ma – 130 ka)

Many of the records from this time period point to an anomalous warm period ~400 ka. Nishiizumi et al. (1996) used cosmogenic burial dating to assess the concentration of cosmogenic nuclides in the rock below the center of the Greenland Ice Sheet. This rock was obtained during the drilling of the Greenland Ice Sheet Project 2 ice core. The nuclide concentration indicated that the bedrock had been exposed to cosmic rays in the past, suggesting that Greenland's summit was completely or nearly ice-free 0.5 +/- 0.2 Ma BP, possibly in association with marine oxygen isotope stage 11 (Nishiizumi et al., 1996). Pollen at the base of the Dye3 ice core indicated the presence of a boreal forest, and was dated to somewhere between 800 and 450 ka (Willerslev et al., 2007), hypothesized to possibly be coincident with marine oxygen isotope stage 11 (Steig and Wolfe, 2008). Similarly, spruce pollen from deep sea cores also suggests that a boreal forest covered Greenland ~400 ka (De Vernal and Hillaire-Marcel, 2008).

4.4. The Last Interglacial (130 – 120 ka)

The last interglacial period (the Eemian) lasted from roughly 130 to 120 ka and has been the subject of abundant research efforts because it may be the best analogue of how climate will respond to anthropogenic forcings. While much of this research relies

on modeling, Koerner (1989) used chemical properties of Eemian-age ice from Greenland and Antarctic cores to infer information about climate. He notes that $\delta^{18}O$ values from Eemian ice suggest a smaller, thinner ice sheet at lower elevation. Additionally, Eemian ice is often characterized by high porosity and abundant debris, indicating that the material originally accumulated in a snowfield during the initial stages of ice sheet re-growth. These two lines of evidence suggest that the Greenland Ice Sheet had receded significantly during the last interglacial, forcing the ice sheet to rebuild at the onset of the latest Pleistocene glaciation.

Many records show that sea level was significantly higher during the Eemian. To account for this, modeling efforts have attempted to infer how much smaller the Greenland Ice Sheet actually was. Data from Letréguilly et al. (1991), Cuffey and Marshall (2000), Otto-Bliesner et al. (2006), and Overpeck et al. (2006) all suggest that ice cover during the Eemian was significantly reduced from present-day ice cover. While there is debate over whether the ice sheet split into northern and southern domes, or whether the southern dome disappeared entirely, all agree that significant melting occurred.

4.5. The Latest Pleistocene Glaciation (120 – 10 ka)

The Greenland Ice Sheet was again extensive during the Last Glacial Maximum (~21 ka). At the height of the Last Glacial Maximum, it is thought that the entire island of Greenland, plus much of the surrounding continental shelf, was glaciated (Bennike and Björck, 2002). The latest Pleistocene deglaciation chronology is complicated (Fig. 3),

with ice melting first on the southern peninsula and latest on the northern tip, with

substantial local variability between the two extremes.
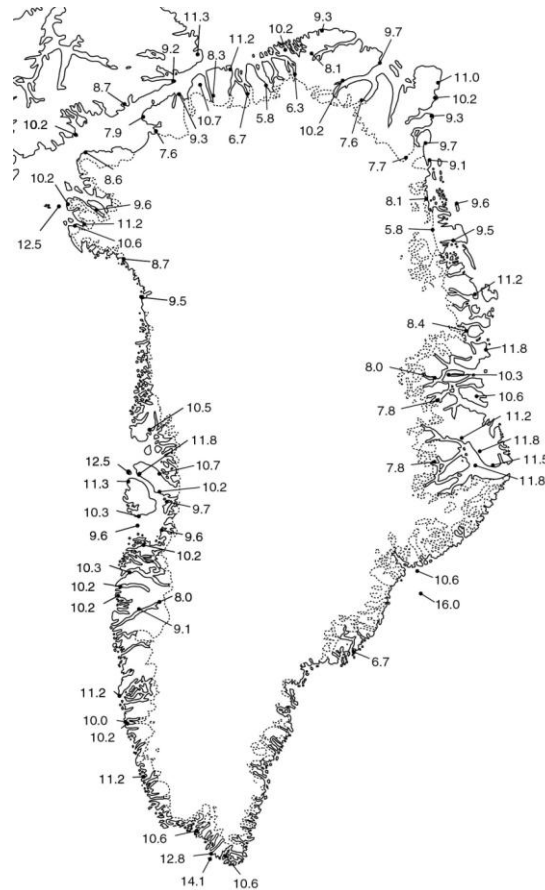
Figure 3. Ages of the last recession of the Greenland Ice Sheet from Bennike and
Bjorck (2002). Ages are radiocarbon dates obtained from all published studies of glacial
retreat after the Last Glacial Maximum.

4.6. The Holocene (10 ka – present)

Even though Holocene climate has been relatively stable, variation in the size of

the Greenland Ice Sheet has occurred. Weidick et al. (1990) suggest that the ice sheet, at

least in the Jakobshavn Isfjord area on the west coast, retreated during the Holocene

climatic optimum about 6 to 4 ka BP. During the mid Holocene, hypothesized

temperatures in the Jakobshavn area were roughly 2˚C warmer than today with a 10-15%

11

longer ablation season, allowing the ice sheet to retreat back beyond its present day margin. Weidick et al. (1990) speculate that this receded state may have allowed ancient peoples to settle the coastal areas, but that these people were forced to relocate when the ice began to re-advance around 4 ka.

Since the end of the Little Ice Age, ice extent has slowly shrunk due to warmer temperatures. This pattern has been especially pronounced for Jakobshavn Isbræ on the west coast. Jakobshavn, an outlet glacier, drains an impressive 7% of the ice sheet, but has thinned and retreated significantly since 1850. Csatho et al. (2008) showed that the terminus position has retreated unevenly over the past 150 years, with the most active periods of change being 1902-1913, 1930-1959, and 1999 to present. During these periods, thinning rates reached 5-11 m/year. The speed of ice flow has also increased dramatically from 5,700 m/year in 1992 to 9,400 m/year in 2000 and 12,600 m/year in 2003 (Joughin et al., 2004). This retreat of almost 30 km since 1950 may have been facilitated by the disintegration of the ice shelf which served to provide friction and contain the outflow of ice. This single glacier is estimated to contribute 0.06 mm/year of sea level rise (Joughin et al., 2004).

4.7. The Future

The Greenland Ice Sheet is a dynamic system that is closely linked with climate. Since climate is changing rapidly due to anthropogenic warming, it is likely that the characteristics of the ice sheet will change as well. The ice sheet's response depends on how much Arctic climate warms. Huybrechts et al. (1991) suggest that a warming of only 1˚C over Greenland would result in a 40% increase in runoff volume and would

contribute 0.22 mm/year of sea level rise. According to modeling performed by

Huybrechts et al. (1991), there is a 65% chance that mean annual temperature will be

between 2.7 and 5.7˚C higher by 2100. Although there is still considerable uncertainty

surrounding how much greenhouse gas concentrations and global temperature will rise

during the next centuries, it is possible that the ice sheet could undergo significant

melting in the next several centuries, resulting in the disappearance of the ice sheet

entirely (Gregory et al., 2004; Overpeck et al., 2006).

5. Climate Forcings

5.1. Glacial-Interglacial Cycles

The changes in the extent of the Greenland Ice Sheet described above were

largely driven by external climate forcings. The most dominant of these forcings, which

cause the cyclic pattern of glacial and interglacial periods, control the amount of

incoming solar radiation reaching Earth's surface (Imbrie et al., 1992). Known as

"Milankovitch cycles", these variations in Earth's orbital parameters encompass three

separate aspects: eccentricity, obliquity, and precession of the equinoxes (Berger, 1988;

Milankovitch, 1969). Eccentricity refers to the shape of Earth's orbit around the sun, and

varies on cycles of 400,000 years. Obliquity quantifies the tilt of Earth's axis, and varies

on cycles of 41,000 years. Precession of the equinoxes describes the wobbling of Earth's

axis, and varies on cycles of 19,000 and 22,000 years. All of these parameters control the

strength of seasonality, and the amount of solar radiation reaching Earth at different times

of the year (Berger, 1988; Milankovitch, 1969). When the influences of these parameters

are combined, they dictate changes in global ice volume (Lisiecki and Raymo, 2005).

5.2. Post-glacial Climate Variability

Global climate has varied appreciably over time, even since the end of the last glacial period. Two pronounced cold reversals likely impacted the Greenland Ice Sheet during the time periods that will be investigated in this thesis: the Younger Dryas and the "8200 Event". The Younger Dryas lasted between 12.7 and 11.5 ka and represented a brief but extreme return to glacial conditions during the transition from the last glacial period to the warmer Holocene (Alley, 2000). Ice cores from Greenland suggest that this event was characterized by cool temperatures and interruption of the North Atlantic deepwater formation (Alley, 2000); however, finding evidence of an ice sheet re-advance associated with the Younger Dryas in Greenland has been difficult (Kelly et al., 2008). The Younger Dryas ended rapidly, with abundant short-lived pulses between warm and cool climate phases (Dansgaard et al., 1989; Taylor et al., 1993; Taylor et al., 1997). The Younger Dryas was likely caused by meltwater diversion from the melting Laurentide Ice Sheet that interfered with thermohaline circulation in the North Atlantic (Alley, 2000).

The "8200 Event", also known as 8.2 ka cold reversal, was likely the most prominent and extreme climate fluctuation of the Holocene. Like the Younger Dryas, the cooling event probably occurred when large volumes of freshwater from the outburst of an ice-damned lake in front of the Laurentide Ice Sheet entered the North Atlantic Ocean, thereby slowing thermohaline circulation (Alley and Ágústsdóttir, 2005). Evidence for colder climate during this time period is widespread within the northern hemisphere, and is especially prevalent around the North Atlantic region (Alley and Ágústsdóttir, 2005).

6. Thesis Outline

Before using cosmogenic radionuclides to understand the glacial history of Greenland's coast, I first performed methodological development to improve the efficiency and precision of the ^{10}Be and ^{26}Al dating approaches. The methodological advances made at University of Vermont's new Cosmogenic Nuclide Laboratory optimized sample preparation techniques to maximize Be yield and purity, improving the isotopic counting efficiency of the accelerator mass spectrometer, and thereby increasing data precision. Methodological optimization is the focus of the second chapter of this thesis.

Cosmogenic nuclide concentrations were analyzed in samples from two sites in western Greenland to provide information about ice sheet behavior. I focus on determining the chronology of ice margin retreat after the last glacial period, estimating rates of ice loss, and studying the efficiency of subglacial erosion. My research in central-western Greenland will be the focus of the third and fourth chapters of this thesis.

References

Alley, R., 2000, The Younger Dryas cold interval as viewed from central Greenland: Quaternary Science Reviews, v. 19, p. 213-226.

Alley, R., and Ágústsdóttir, A., 2005, The 8k event: cause and consequences of a major Holocene abrupt climate change: Quaternary Science Reviews, v. 24, p. 1123-1149.

Alley, R., Clark, P., Huybrechts, P., and Joughin, I., 2005, Ice-sheet and sea-level changes: Science, v. 310, p. 456-460.

Bennike, O., and Björck, S., 2002, Chronology of the last recession of the Greenland Ice Sheet: Journal of Quaternary Science, v. 17, p. 211-219.

Berger, A., 1988, Milankovitch theory and climate: Reviews of Geophysics, v. 26, p. 624-657.

Csatho, B., Schenk, T., Van der Veen, C., and Krabill, W., 2008, Intermittent thinning of Jakobshavn Isbræ, West Greenland, since the Little Ice Age: Journal of Glaciology, v. 54, p. 131-144.

Cuffey, K., and Marshall, S., 2000, Substantial contribution to sea-level rise during the last interglacial from the Greenland ice sheet: Nature, v. 404, p. 591-594.

Dansgaard, W., White, J., and Johnsen, S., 1989, The abrupt termination of the Younger Dryas climate event: Nature, v. 339, p. 532-534.

De Vernal, A., and Hillaire-Marcel, C., 2008, Natural variability of Greenland climate, vegetation, and ice volume during the past million years: Science, v. 320, p. 1622-1625.

Funder, S., Abrahamsen, N., Bennike, O., and Feyling-Hanssen, R., 1985, Forested arctic: evidence from north Greenland: Geology, v. 13, p. 542-546.

Granger, D., and Muzikar, P., 2001, Dating sediment burial with in situ-produced cosmogenic nuclides: theory, techniques, and limitations: Earth and Planetary Science Letters, v. 188, p. 269-281.

Gregory, J., Huybrechts, P., and Raper, S., 2004, Threatened loss of the Greenland ice-sheet: Nature, v. 428, p. 616.

Hanna, E., Huybrechts, P., Steffen, K., Cappelen, J., Huff, R., Shuman, C., Irvine-Fynn, T., Wise, S., and Griffiths, M., 2008, Increased runoff from melt from the Greenland Ice Sheet: a response to global warming: Journal of Climate, v. 21, p. 331-341.

Huybrechts, P., 1996, Basal temperature conditions of the Greenland ice sheet during the glacial cycles: Annals of Glaciology, v. 23, p. 226-236.

Huybrechts, P., Letreguilly, A., and Reeh, N., 1991, The Greenland ice sheet and greenhouse warming: Global and Planetary Change, v. 3, p. 399-412.

Imbrie, J., Boyle, E., Clemens, S., Duffy, A., Howard, W., Kukla, G., Kutzbach, J., Martinson, D., McIntyre, A., Mix, A., Molfino, B., Morley, J., Peterson, L., Pisias, N., Prell, W., Raymo, M., Shackleton, N., and Toggweiler, J., 1992, On the structure and origin of major glaciation cycles 1, linear responses to Milankovitch forcing: Paleoceanography, v. 7, p. 701-738.

IPCC, 2007, Climate Change 2007: The Physical Science Basis. Contribution of Working Group I to the Fourth Assessment Report of the Intergovernmental Panel on Climate Change, Cambridge University Press.

Joughin, I., Abdalati, W., and Fahnestock, M., 2004, Large fluctuations in speed on Greenland's Jakobshavn Isbrae glacier: Nature, v. 432, p. 608-610.

Kelly, M., Lowell, T., Hall, B., Schaefer, J., Finkel, R., Goehring, B., Alley, R., and Denton, G., 2008, A [10]Be chronology of lateglacial and Holocene mountain glaciation in the Scoresby Sund region, east Greenland: implications for seasonality during lateglacial time: Quaternary Science Reviews, v. 27, p. 2273-2282.

Koerner, R., 1989, Ice core evidence for extensive melting of the Greenland ice sheet in the last interglacial: Science, v. 244, p. 964-968.

Lal, D., 1988, In situ-produced cosmogenic isotopes in terrestrial rocks: Annual Review of Earth and Planetary Sciences, v. 16, p. 355-388.

—, 1991, Cosmic ray labeling of erosion surfaces: in situ nuclide production rates and erosion models: Earth and Planetary Science Letters, v. 104, p. 424-439.

Larsen, H., Saunders, A., Clift, P., Beget, J., Wei, W., and Spezzaferri, S., 1994, Seven million years of glaciation in Greenland: Science, v. 264, p. 952-955.

Letréguilly, A., Reeh, N., and Huybrechts, P., 1991, The Greenland ice sheet through the last glacial-interglacial cycle: Global and Planetary Change, v. 4, p. 385-394.

Lisiecki, L., and Raymo, M., 2005, A Plio-Pleistocene stack of 57 globally distributed benthic [18]O records: Paleoceanography, v. 20, p. 522–533.

Long, A., 2009, Back to the future: Greenland's contribution to sea-level change: GSA Today, v. 19, p. 4-10.

Milankovitch, M., 1969, Canon of isolation and the Ice-Age problem: Jerusalem, Israel Program for Scientific Translations, 484 p.

Nishiizumi, K., Finkel, R., Ponganis, K., Graf, T., Kohl, C., and Marti, K., 1996, *In situ* produced cosmogenic nuclides in GISP2 rock core from Greenland summit: EOS Transactions of the American Geophysical Union, v. 77, p. Abstract 06945142.

Nishiizumi, K., Kohl, C., Arnold, J., Klein, J., Fink, D., and Middleton, R., 1991, Cosmic ray produced [10]Be and [26]Al in Antarctic rocks: exposure and erosion history: Earth and Planetary Science Letters, v. 104, p. 440-454.

Otto-Bliesner, B., Marshall, S., Overpeck, J., Miller, G., and Hu, A., 2006, Simulating Arctic climate warmth and icefield retreat in the last interglaciation: Science, v. 311, p. 1751-1753.

Overpeck, J., Otto-Bliesner, B., Miller, G., Muhs, D., Alley, R., and Kiehl, J., 2006, Paleoclimatic evidence for future ice-sheet instability and rapid sea-level rise: Science, v. 311, p. 1747-1750.

Phillips, F., Zreda, M., Smith, S., Elmore, D., Kubik, P., and Sharma, P., 1990, Cosmogenic chlorine-36 chronology for glacial deposits at Bloody Canyon, eastern Sierra Nevada: Science, v. 248, p. 1529-1532.

Shackleton, N., Backman, J., Zimmerman, H., Kent, D., Hall, M., Roberts, D., Schnitker, D., Baldauf, J., Desprairies, A., and Homrighausen, R., 1984, Oxygen isotope calibration of the onset of ice-rafting and history of glaciation in the North Atlantic region: Nature, v. 307, p. 620-623.

Sharma, P., and Middleton, R., 1989, Radiogenic production of ^{10}Be and ^{26}Al in uranium and thorium ores: Implications for studying terrestrial samples containing low levels of ^{10}Be and ^{26}Al: Geochimica et Cosmochimica Acta, v. 53, p. 709-716.

Steig, E., and Wolfe, A., 2008, Sprucing Up Greenland: Science, v. 320, p. 1595-1596.

Taylor, K., Lamorey, G., Doyle, G., Alley, R., Grootes, P., Mayewski, P., White, J., and Barlow, L., 1993, The 'flickering switch'of late Pleistocene climate change: Nature, v. 361, p. 432-436.

Taylor, K., Mayewski, P., Alley, R., Brook, E., Gow, A., Grootes, P., Meese, D., Saltzman, E., Severinghaus, J., and Twickler, M., 1997, The Holocene-Younger Dryas transition recorded at Summit, Greenland: Science, v. 278, p. 825-827.

Weidick, A., Oerter, H., Reeh, N., Thomsen, H., and Thorning, L., 1990, The recession of the Inland Ice margin during the Holocene climatic optimum in the Jakobshavn Isfjord area of West Greenland: Global and Planetary Change, v. 2, p. 389-399.

Willerslev, E., Cappellini, E., Boomsma, W., Nielsen, R., Hebsgaard, M., Brand, T., Hofreiter, M., Bunce, M., Poinar, H., and Dahl-Jensen, D., 2007, Ancient biomolecules from deep ice cores reveal a forested southern Greenland: Science, v. 317, p. 111-114.

Wouters, B., Chambers, D., and Schrama, E., 2008, GRACE observes small-scale mass loss in Greenland: Geophysical Research Letters, v. 35, p. L20501.

CHAPTER 2. MANUSCRIPT FOR "QUATERNARY GEOCHRONOLOGY"

OPTIMIZING SAMPLE PREPARATION FOR [10]BE ANALYSIS BY ACCELERATOR MASS SPECTROMETRY

Lee B. Corbett[1]*
Paul R. Bierman[1]
Lucas J. Reusser[1]
Dylan H. Rood[2,3]
Robert C. Finkel[2]

[1]Department of Geology, University of Vermont, Burlington VT 05405
[2]Center for Accelerator Mass Spectrometry, Lawrence Livermore National Laboratory, Livermore CA 94550
[3]Earth Research Institute, University of California, Santa Barbara CA 93106
*Contact Author: Ashley.Corbett@uvm.edu, (802) 656-4411

Abstract

We investigate data collected during preparation and isotopic analysis of ~500 ^{10}Be samples for cosmogenic nuclide dating. Samples were prepared after implementing laboratory modifications and methodological advances targeted at optimizing both the quality and efficiency of the Be isolation process. These data show which factors control a sample's behavior, specifically the resulting beam current during accelerator mass spectrometry (AMS). Procedural modifications increased average beam currents from 13.4 ± 5.4 µA (old laboratory; 1 SD, n = 63) to 22.5 ± 3.4 µA (new laboratory, 1 SD, n = 446), while reducing beam current variability. In this data set, initial quartz purity, final Be yield, and final Be purity do not predict AMS beam current; this may be because all samples had high Be yields and low levels of impurities, and slight deviations from this norm were not sufficient to depress beam currents. The variation in beam currents is instead likely derived from factors not quantified in this analysis, including variability in the AMS, trace elements in the samples, and differences in packing of the cathodes.

1. Introduction

The measurement of *in situ* produced cosmogenic ^{10}Be in geologic samples provides valuable insight about a wide variety of geologic processes (Bierman and Nichols, 2004; Gosse and Phillips, 2001; Nichols et al., 2006). Isotope concentrations are derived by isotope dilution using added ^{9}Be carrier and measuring the ^{10}Be/^{9}Be ratio by accelerator mass spectrometry (AMS). The precision of such ratio measurements is most often limited by the number of ^{10}Be atoms that can be counted before all sample material is consumed. The quality of the isotopic data is therefore typically controlled by two factors: the AMS beam current, which determines the number of atoms counted per unit time, and the final Be yield, which determines for how long a sample can be counted (Rood et al., 2010). The ^{10}Be blank levels also control the precision of measured ratios, with relatively higher blanks hindering the ability to measure samples with little ^{10}Be. Therefore, the best analyses are provided by samples with consistently high beam currents, high final Be yields, and comparatively low blank levels. Especially for low-concentration samples, such as those derived from young glacial deposits or rapidly eroding terrains, the utility of the results is controlled, at least partially, by the effectiveness of the sample processing.

Cosmogenic dating is a widely used technique that answers important questions about Earth's surface. For example, quantifying ^{10}Be concentrations in moraine boulders (Phillips et al., 1990) or previously-glaciated bedrock surfaces (Bierman et al., 1999) indicates when the ice last left those positions (Balco, 2011; Fabel and Harbor, 1999), thus providing valuable paleoclimatic information. Cosmogenic ^{10}Be is useful for measuring displacement rates on fault systems by dating offset landforms (Bierman et al.,

1995). It can also be used to study landscape erosion rates, both on outcrop scales (Nishiizumi et al., 1991; Nishiizumi et al., 1986) and basin scales (Bierman and Steig, 1996; Brown et al., 1995; Granger et al., 1996; Von Blanckenburg, 2005), thereby shedding light on the processes that shape Earth's surface (Portenga and Bierman, *In Press*).

There are several reasons why it makes sense to optimize the preparation of samples for isotopic analysis. For a limited subset of applications, the highest precision isotopic data are required to make meaningful interpretations: for example, burial dating using multiple isotope systems (Gillespie and Bierman, 1995), precise dating of glacial events (Kelly et al., 2008), and the calibration of cosmogenic nuclide production rates (Balco et al., 2009). Very low concentration samples, such as those from very young exposures (Licciardi et al., 2009), require high efficiency AMS counting to lower detection limits and provide meaningful ages. High beam currents reduce counting times required to achieve nominal precisions, speeding AMS throughput, and better utilizing the limited beam time available for analysis.

Isolating Be from a sample of rock or sediment is a time-intensive process (Fig. 1). After a sample is collected, the mineral quartz is isolated from the other mineral phases through a series of physical and chemical processes. Next, the quartz is dissolved and Be is isolated through a series of chemical processes. Finally, the ratio of cosmogenic ^{10}Be to stable ^{9}Be (added through a spike, since its abundance in quartz is very low) is measured by AMS. Failing to remove impurities or losing Be can easily occur during numerous phases of the process, leading to less effective AMS analysis (Hunt et al., 2008) and therefore less precise data.

Over the past two years, after the construction of a new extraction laboratory at the University of Vermont, we have optimized sample preparation procedures in order to process ^{10}Be samples for AMS analysis that have high and consistent beam currents. We place particular emphasis on rethinking the cation chromatography methodology. Samples are tested twice during the extraction process: the initial purity of the quartz is tested before sample dissolution, and the final Be yield and purity are tested after cation chromatography. We use the results of these analyses to perform on-the-fly methodological optimization tailored to each individual sample's chemistry and behavior. In this paper, we summarize our extraction methods and explore the chemical and isotopic data related to ~500 samples processed during 2009-2010. We use this analysis to understand the factors that control AMS beam currents.

2. Background and Previous Methodological Advances

In situ cosmogenic ^{10}Be forms when high-energy cosmic rays bombard rock in the upper-most few meters of Earth's surface. In the mineral quartz, ^{10}Be is produced by spallation of oxygen (Lal, 1988) at low rates, on the order of a few to a few tens of atoms g^{-1} quartz yr^{-1} (Nishiizumi et al., 2007). Production is dependent on latitude and elevation, and ceases if the surface is buried to a sufficient depth (for example, by thick glacial ice). Cosmogenic ^{10}Be is a radionuclide with a half-life of ~1.38 million years (Nishiizumi et al., 2007); therefore, while concentrations of ^{10}Be initially increase in exposed rock over time, they eventually level off as production and decay reach equilibrium.

23

Over time, different methods have been used to extract *in situ* cosmogenic ^{10}Be. Initially, abundances of cosmogenic ^{10}Be were quantified by decay counting after Be was isolated from silicate minerals by dissolution in acid (Fairhall, 1960). However, this proved to be a daunting task because the long half-life of ^{10}Be made atomic emissions difficult to detect.

Later, it became possible to measure ^{10}Be/^{9}Be ratios via AMS (Lanford et al., 1980; Southon et al., 1983). Yields were typically high (85-90%), but samples frequently retained impurities, especially Al. Samples were measured in relation to known standards; precisions were generally 5-10%, and detection was limited to ^{10}Be/^{9}Be ratios greater than ~10^{-13} (Southon et al., 1983). Although ^{10}Be had become a widely used technique and abundant measurements had been made, average AMS beam currents remained relatively low at ~7 µA (Klein and Middleton, 1984). By 1990, the quality of AMS measurements had increased, and precisions of several percent were attainable (Suter, 1990).

At around the same time, *in situ* ^{10}Be became a dating technique of interest as AMS precisions increased and after it was confirmed that meteoric ^{10}Be could be removed from the grain coatings of a sample (Nishiizumi et al., 1991; Nishiizumi et al., 1986; Nishiizumi et al., 1989). Controlled cleaning experiments showed that repeated etches in HCl efficiently removed meteoric ^{10}Be from sample grains (Brown et al., 1991; Kohl and Nishiizumi, 1992). Adding a column chromatography step ensured that Ti, Be, and Al fractions could be separated (Ditchburn and Whitehead, 1994).

More recent methodological advances have served to further increase the quality of AMS ^{10}Be measurements. Although commercially-available ^{9}Be carrier is commonly

used, its $^{10}Be/^9Be$ ratio is $\sim10^{-14}$, which hinders the analysis of low-level samples. Experimentation has demonstrated that ^9Be carriers made from phenakite (Be_2SiO_4) and beryl ($Be_3Al_2Si_6O_{18}$) minerals yielded ratios two orders of magnitude lower (Merchel et al., 2008), which are more suited for the analysis of low-level samples. BeO had traditionally been mixed with Ag before being packing into cathodes for AMS analysis; however, recent work has shown that using Nb instead of Ag improves beam currents and AMS counting efficiency (Hunt et al., 2006; Merchel et al., 2008).

The question of AMS "source poisons" (i.e., impurities which decrease AMS beam currents) is still being explored. Work by Merchel et al. (2008) suggests that additions of Ti did not directly decrease beam currents, although the resulting dilution of Be did. However, work by Hunt et al. (2008) found that Al and Ti both depressed beam currents (although Ca, Fe, Mg, and Mn did not). Experimentation at Lawrence Livermore National Laboratory suggests that the AMS detection limit is now as low as ~1000 atoms, making it possible to obtain high-precision measurements on small samples or samples with little ^{10}Be (Rood et al., 2010).

3. Methods

3.1. Study Design

Over the course of 2008, a new Cosmogenic Laboratory was built at the University of Vermont. We took the opportunity of moving into a new laboratory to re-evaluate the sample preparation methodology in order to improve process reliability, reduce blank and boron levels, and ensure that every cathode we produced had high beam currents and could be measured for at least three 5-minutes cycles on the Lawrence

Livermore National Laboratory AMS (Fig. 1). A thorough analysis of the prior methodology was conducted in the old laboratory (Hunt et al., 2008), which provided benchmarks against which progress could be measured. We primarily adapted and modified the extraction techniques developed first by J. Stone and others at the University of Washington laboratory.

During the first half of 2009, we experimented with and updated the sample processing procedures, focusing especially on the anion and cation column steps which Hunt et al. (2008) had identified as a source of inconsistency in the old laboratory. During the second half of 2009 and most of 2010, undergraduate (n=1), MS (n=3), and PhD (n = 2) students, as well as a faculty member, processed >500 ^{10}Be samples in the new laboratory using these new procedures. Samples were processed in batches of 12, including either one or two process blanks. We studied the results from two quality checks conducted in the laboratory process: the purity of quartz prior to dissolution and the yield and purity of Be after cation chromatography. We compared this information to AMS beam currents, which we use as a measure of a sample's performance during analysis.

3.2. Column Optimization

The anion and cation column chromatography methods were redesigned in order to separate more cleanly the desired sample fractions and to improve the efficiency with which samples can be processed. We implemented a double-fritted column for both the anion and cation steps (3mL resin bed for anion columns, 5 mL resin bed for cation columns, Fig. 2). The second frit sits 1-2 mm above the resin bed, and serves to maintain

a thin layer of solution in between the top of the resin bed and the bottom of the second frit. This prevents the column from drying out, thereby avoiding channeling in the resin. In addition, the second frit ensures that the resin bed is not disturbed while adding solutions, allowing the column steps to be performed more quickly. We have successfully regenerated and thus re-used columns for over a year (> 20 batches of samples) by stripping them with acid, flushing them with water, and storing them fully saturated between uses. Over that time, there has been no change in column performance.

The rate at which Ti, Be, and Al elute through the cation columns depends on multiple factors including column shape, resin type, resin bed volume, and most importantly acid strength. All of these factors can be adjusted to achieve an optimal elution curve, which cleanly splits the three fractions (Fig. 3). Since Ti is thought to be an AMS source poison (Hunt et al., 2008), even small amounts can compromise beam currents. To ensure that samples are Ti-free, Ti elution is continued until all Ti is removed, even if small amounts of Be (several percent of the total load) may be lost.

We performed cation column tests before beginning to use real samples. These tests used quartz spiked with differing concentrations of additional Al and Ti. During the earlier tests, the goal was to determine the cleanest way to separate the three elution peaks. We experimented with acid strength and elution volume, collecting all of the eluted solution for ICP-OES analysis. After optimizing the elution pattern for the cation columns, the later tests were targeted at determining the total cation load that the columns could handle. We accomplished this through spiking quartz to various impurity levels, and determining the threshold of column failure. Column failure was considered to occur

when cations oversaturated the resin and leaked out prematurely, contaminating the Be fraction.

4. Laboratory Data and Results

4.1. Quartz Purity

4.1.1. Testing Quartz Purity

Quartz is isolated and purified based on methods modified from Kohl and Nishiizumi (1992). Every sample is tested for purity (Al, Ca, Fe, K, Mg, Mn, Na, and Ti) by inductively-coupled plasma optical emission spectrometry (ICP-OES) before Be extraction. Quartz with no more than ~150 ppm Al and no more than several hundred ppm total cation load is considered acceptable; any quartz with higher impurity levels is sent back to the mineral separation process for an additional week of etching. Of the 762 quartz samples that passed the purity test during 2009-2010, the average total cation concentration was 262 ppm, of which almost half was Al (Fig. 4). Since only 0.25-0.5 g of quartz is used to test sample purity, in rare occasions this small amount may not accurately represent the sample as a whole, especially in the case of very heterogeneous samples.

Not all quartz processed during 2009-2010 had the same attainable levels of purity (Fig. 5). Some quartz, with low impurity levels, was easily purified. For example, quartz from Ilulissat, Greenland, was some of the purest quartz to enter the cosmogenic laboratory; it averaged only 30 ppm Al and 130 ppm total cations after the mineral separation process was complete. Other quartz, however, was difficult to clean even with repeated, long acid etches. Quartz from Panama had the highest total cation

28

concentrations (450 ppm) due to high levels of Ti, Fe, and alkaline metals. Quartz from

the southern Appalachian Mountains had the highest Al concentrations, averaging 170

ppm, but with isolated samples up to 1000 ppm. Different levels of attainable quartz

purity were also noted by Kohl and Nishiizumi (1992), and are likely caused by

inclusions that are not preferentially removed during acid etching.

The concentration of Al appears to be more variable than that of other cations.

The trend line drawn through the average quartz measurements from different sites in

Figure 5 intercepts the y-axis at ~100 ppm total non-Al cations, suggesting that, in

general, quartz can be expected to have ~100 ppm cations other than Al. Quartz

concentrations follow this trend more closely at lower cation concentrations, and deviate

from this trend at higher cation concentrations. This trend implies that Al is the dominant

cation that controls quartz purity, and therefore controls the ability to process clean quartz

suitable for Be isolation.

4.1.2. Quartz Purity and Beam Currents

Data from 446 samples analyzed by AMS during 2009-2010 suggest that purity of

the quartz at the beginning of the Be isolation process does not affect resulting beam

currents (Fig. 6). The data demonstrate that, as long as the quartz has cation

concentrations within the range of what the lab chemistry is able to remove, the actual

cation concentration is unimportant. In instances where samples are not able to reach high

levels of purity (for example, the Panama samples discussed above), knowing cation

concentrations alerts the laboratory worker to decrease the mass of quartz being used and

thereby avoid overloading the cation columns. The results of the regression shown in

29

Figure 6 would likely be different if quartz was not screened for purity before Be isolation began.

4.2. Final Be Yield and Purity

4.2.1. Testing Final Be Yield and Purity

At the end of the extraction process and before hydroxide precipitation, the Be fraction of every sample was tested for yield and purity. Because the dilution is done volumetrically and the ICP-OES measurements are made rapidly, precision of these data are ~5%. Optimal Be yield should be 94% because 6% of the total sample is removed during the aliquoting process after quartz dissolution. The average yield was $92.5 \pm 5.6\%$ (1 SD, Fig. 7), although ICP-OES error led to some yields of >100%. Of the 504 samples (including both samples and blanks) tested for Be yield, a small number (19 in total) were excluded from this analysis due to operator dilution error or malfunctions during ICP-OES measurement. Only a very small number of samples (8 in total) had yields below 80%. The majority of these poor-yield samples were caused by laboratory error such as spilling or splattering liquid sample. Overall, Be yield results demonstrate that it is possible to recover virtually all of the Be from a quartz sample.

4.2.2. Final Be Yield and Beam Currents

Results suggest that final Be yield is not an effective predictor of AMS beam current (Fig. 8). Even several samples with low Be yield (caused by laboratory error, such as spilling) still had AMS beam currents that were only slightly below the overall average. This lack of a relationship suggests that sample purity is likely a more important

controlling factor for beam currents than Be yield. Rood et al. (2010) documented that total Be mass did control beam currents, although a much wider variation of beam currents was investigated, including samples with as little as 80 µg Be (the smallest samples explored in this analysis had >100 µg).

4.2.3. Final Be Purity and Beam Currents

The purity of the sample just before it is precipitated, dried, and packed into the cathode does not predict AMS beam currents until high impurity concentrations are reached. Even cations that have been shown to depress beam currents, such as Al and Ti (Hunt et al., 2008), did not appear to control the beam currents for this set of 446 samples. However, the lack of relationship between AMS beam current and sample purity may be because the samples were generally very clean, and these cations appear not to reduce beam currents at such low concentrations (Fig. 9). Only several of the samples had detectable Al in the final Be fraction; three samples had almost 100 µg and two had almost 1000 µg of Al. These samples had depressed beam currents as low as ~15 µA. This analysis suggests that Al does not depress beam currents until relatively high amounts are reached; this may be because the Al is itself a source poison, or because the presence of Al serves to dilute the Be.

Many of the samples retained alkali metals (Ca, K, Mg, and Na) when analyzed after cation chromatography. However, these impurities do not negatively impact AMS beam currents even at high levels (Fig. 10) because they are removed later during BeOH precipitation and washing.

5. AMS Measurements

5.1. AMS Beam Currents

AMS beam currents for samples processed during 2009-2010 were high and consistent (Fig. 11). The average beam current for samples was 22.5 ± 3.4 µA (1 SD, n = 446). Considering both samples and blanks, this value increases slightly to 22.6 ± 3.4 µA (1 SD, n = 504). However, an independent samples t-test shows that beam currents of samples and blanks are not statistically separable (p = 0.149). The lowest beam current was 3.1 µA, although this is 6 SD outside of the sample average and was the only sample with a single-digit current. The highest beam current was 33.6 µA. Comparison with data from Hunt et al. (2008) demonstrates that laboratory modifications and methodological advances have greatly improved sample beam currents (Fig. 11). The average beam current using the former process in the old laboratory was 13.4 ± 5.4 µA (1 SD, n = 63). The new procedure not only increased beam currents, but also made them less variable; the relative standard deviation of beam currents decreased from 40% to 15%.

5.2. Best and Worst Beam Currents

Analysis of the top 5% and bottom 5% of sample beam currents does not clearly illustrate which factors led to the respective success and failure of these samples. Two of the worst beam currents were from samples which contained 33 and 70 µg of Al in the final Be sample, although this is near the detection limit of the ICP-OES and may not be a robust measurement. It is evident that at least some of the factors controlling beam currents are present at the level of whole batches rather than individual samples. This is especially true for the bottom 5% of beam currents, where eight of the 25 worst are from

a single batch, and 12 of the 25 are from two batches. This pattern also holds for the top 5% of beam currents, where five of the 25 best are from a single batch. Many of the worst beam currents are from samples run at Lawrence Livermore National Laboratory during December 2009; conversely, many of the best beam currents are from samples run during July of 2010.

5.3. Beam Currents Over Time

Average AMS beam current varied over time. Samples discussed in this paper were analyzed at Lawrence Livermore National Laboratory during December 2009 (n = 132), March 2010 (n = 36), April 2010 (n = 120), and July 2010 (n = 216). Average beam currents for samples and blanks analyzed during these runs were 20.1 ± 3.1, 20.6 ± 1.3, 22.5 ± 2.7, and 24.5 ± 3.0 µA, respectively (1 SD). A one-way ANOVA shows that these are statistically separable populations ($p < 0.001$). Subsequent independent samples t-tests show that AMS beam currents for all runs are distinguishable ($p < 0.001$ for all), except December 2009 and March 2010 ($p = 0.255$).

6. Discussion

6.1. Real-Time Optimization

The data generated during the quality control checks discussed above (quartz purity and final Be yield/purity) can be used to optimize the laboratory procedures in real-time, after sample processing has already begun. In this way, the laboratory methodology can be tailored as needed in order to reflect each sample's chemistry and behavior.

6.1.1. Quartz Purity

    After quartz purity is assessed, the initial cation concentration for each sample is
known, providing information about how best to treat the sample. Most importantly, this
information can be used to avoid overloading the cation columns. Experimentation has
shown that the cation column set-up discussed here can effectively handle a maximum
total cation load of ~8000 µg. For example, if a given sample of quartz has 400 ppm total
cations, then a maximum of 20 g can be used to avoid overloading. Quartz purity data is
also used to optimize the addition of a ^{27}Al spike, if necessary. Finally, having quartz
purity data highlights the rare instances where a sample contains measurable amounts of
native Be, which occurred in only 3 of the 762 samples. The presence of native Be can be
circumvented by high-precision quantification of the native Be load in aliquots removed
after sample digestion.

6.1.2. Final Be Yield and Purity

    Determining the yield and purity of the Be fraction at the end of the extraction
process and before precipitation provides additional information. Specifically,
quantifying the Be yield determines if enough Be is present for a successful AMS
measurement and if the Be is pure. After small aliquots are removed for ICP-OES
analysis, all sample processing is halted until Be yield information is available. If Al or
Ti are present at greater than trace levels, the sample can be neutralized, dried down, and
run through the cation columns a second time to remove impurities. If sufficient Be is not
present in the sample, the Ti fraction is analyzed by ICP-OES; in these rare cases, the
missing Be has eluted early and can be recovered by reprocessing the Ti fraction. Only

when the Be yield and purity levels are acceptable is the sample processing taken to completion. In this way, the rare problem-causing samples are identified and corrected before AMS analysis.

6.2. Variability in AMS Beam Currents

None of the factors explored in this analysis appear to exert strong control over AMS beam currents. A multiple regression model suggests that all of the factors discussed here (initial quartz purity, Be yield, and final Be purity) explain only 7% of the variability seen in the beam currents of the 446 samples that were analyzed. Instead, much of this variability is derived from factors not quantified in this analysis, such as changes in the behavior of the AMS. This pattern, however, would probably not hold if methodological modifications had not been made. Changes in the laboratory procedures have increased the overall quality of the samples being processed; slight impurities or a several percent reduction in total Be mass do not appear to depress beam currents. The results of a similar analysis conducted in the old laboratory were much different, and found that impurities were a strong controlling factor of AMS beam currents (Hunt et al., 2008).

6.3. Progress Over Time

Laboratory modifications and methodological advances have increased the average beam current of samples almost twofold. This progress can be attributed to numerous factors, including tighter quality control on incoming quartz purity, new column design and refined elution procedures, checking of final Be yields and purity, and

real-time sample-by-sample optimization. Careful testing of every quartz sample has ensured that only pure quartz enters the laboratory; furthermore, knowledge of cation contents allows subsequent steps in the process to be tailored accordingly, ensuring that the process is optimized for each sample. The new double-fritted columns improved results, efficiency, and consistency, which has allowed for precise and reproducible calibration of the column elution curves. Understanding maximum column loads and how to cleanly separate the three cation fractions enabled the production of higher-yield and more pure Be fractions. Quantifying final Be yield and purity ensures that any problematic samples are identified and corrected, and ensures that no substandard cathodes are sent to the AMS. These advances have optimized laboratory procedures and have improved the quality and consistency of samples and the efficiency with which they can be processed.

7. Conclusions

Analysis of ~500 ^{10}Be samples prepared at the University of Vermont and measured at Lawrence Livermore National Laboratory shows that the variability in AMS beam currents is not well-explained by factors explored in this investigation. This is likely because the sample population generally had high Be yields and low levels of impurities, and slight deviations from this norm were not sufficient to depress beam currents. The variability in beam currents is instead likely driven by factors not quantified in this analysis, such as behavior of the AMS. Methodological optimization increased average sample beam currents and decreased beam current variability.

References

Balco, G., 2011. Contributions and unrealized potential contributions of cosmogenic-nuclide exposure dating to glacier chronology, 1990-2010. Quaternary Science Reviews 30, 3-27.

Balco, G., Briner, J., Finkel, R., Rayburn, J., Ridge, J., Schaefer, J., 2009. Regional beryllium-10 production rate calibration for late-glacial northeastern North America. Quaternary Geochronology 4, 93-107.

Bierman, P., Marsella, K., Patterson, C., Davis, P., Caffee, M., 1999. Mid-Pleistocene cosmogenic minimum-age limits for pre-Wisconsinan glacial surfaces in southwestern Minnesota and southern Baffin Island: a multiple nuclide approach. Geomorphology 27, 25-39.

Bierman, P., Nichols, K., 2004. Rock to sediment- slope to sea with [10]Be- rates of landscape change. Annual Review of Earth and Planetary Sciences 32, 215-255.

Bierman, P., Steig, E., 1996. Estimating rates of denudation using cosmogenic isotope abundances in sediment. Earth Surface Processes and Landforms 21, 125-139.

Brown, E., Edmond, J., Raisbeck, G., Yiou, F., Kurz, M., Brook, E., 1991. Examination of surface exposure ages of Antarctic moraines using in situ produced [10]Be and [26]Al. Geochimica et Cosmochimica Acta 55, 2269-2283.

Brown, E., Stallard, R., Larsen, M., Raisbeck, G., Yiou, F., 1995. Denudation rates determined from the accumulation of in situ-produced [10]Be in the Luquillo Experimental Forest, Puerto Rico. Earth and Planetary Science Letters 129, 193-202.

Ditchburn, R., Whitehead, N., 1994. The separation of [10]Be from silicates, 3rd Workshop of the South Pacific Environmental Radioactivity Association, pp. 4-7.

Fabel, D., Harbor, J., 1999. The use of in-situ produced cosmogenic radionuclides in glaciology and glacial geomorphology. Annals of Glaciology 28, 103-110.

Fairhall, A., 1960. The Radiochemistry of Beryllium, Nuclear Science Series. National Academy of Sciences and National Research Council, Washington, DC.

Gillespie, A., Bierman, P., 1995. Precision of terrestrial exposure ages and erosion rates estimated from analysis of cosmogenic isotopes produced *in situ*. Journal of Geophysical Research 100, 24,637-624,649.

Gosse, J., Phillips, F., 2001. Terrestrial in situ cosmogenic nuclides: theory and application. Quaternary Science Reviews 20, 1475-1560.

Granger, D., Kirchner, J., Finkel, R., 1996. Spatially averaged long-term erosion rates measured from in situ-produced cosmogenic nuclides in alluvial sediment. The Journal of Geology 104, 249-257.

Hunt, A., Larsen, J., Bierman, P., Petrucci, G., 2008. Investigation of factors that affect the sensitivity of accelerator mass spectrometry for cosmogenic ^{10}Be and ^{26}Al isotope analysis. Analytical Chemistry 80, 1656-1663.

Hunt, A., Petrucci, G., Bierman, P., Finkel, R., 2006. Metal matrices to optimize ion beam currents for accelerator mass spectrometry. Nuclear Instruments and Methods in Physics Research Section B: Beam Interactions with Materials and Atoms 243, 216-222.

Kelly, M., Lowell, T., Hall, B., Schaefer, J., Finkel, R., Goehring, B., Alley, R., Denton, G., 2008. A ^{10}Be chronology of lateglacial and Holocene mountain glaciation in the Scoresby Sund region, east Greenland: implications for seasonality during lateglacial time. Quaternary Science Reviews 27, 2273-2282.

Klein, J., Middleton, R., 1984. Accelerator mass spectrometry at the University of Pennsylvania. Nuclear Instruments and Methods in Physics Research Section B: Beam Interactions with Materials and Atoms 5, 129-133.

Kohl, C., Nishiizumi, K., 1992. Chemical isolation of quartz for measurement of in-situ-produced cosmogenic nuclides. Geochimica et Cosmochimica Acta 56, 3583-3587.

Lal, D., 1988. In situ-produced cosmogenic isotopes in terrestrial rocks. Annual Review of Earth and Planetary Sciences 16, 355-388.

Lanford, W., Parker, P., Bauer, K., Turekian, K., Cochran, J., Krishnaswami, S., 1980. Measurements of ^{10}Be distributions using a Tandem Van De Graaff accelerator. Nuclear Instruments and Methods 168, 505-510.

Licciardi, J., Schaefer, J., Taggart, J., Lund, D., 2009. Holocene glacier fluctuations in the Peruvian Andes indicate northern climate linkages. Science 325, 1677-1679.

Merchel, S., Arnold, M., Aumaitre, G., Benedetti, L., Bourles, D., Braucher, R., Alfimov, V., Freeman, S., Steier, P., Wallner, A., 2008. Towards more precise ^{10}Be and ^{36}Cl data from measurements at the 10^{-14} level: Influence of sample preparation. Nuclear Instruments and Methods in Physics Research Section B: Beam Interactions with Materials and Atoms 266, 4921-4926.

Nichols, K., Bierman, P., Foniri, W., Gillespie, A., Caffee, M., Finkel, R., 2006. Dates and rates of arid region geomorphic processes. GSA Today 16, 4-11.

Nishiizumi, K., Imamura, M., Caffee, M., Southon, J., Finkel, R., McAninch, J., 2007. Absolute calibration of ^{10}Be AMS standards. Nuclear Instruments and Methods in Physics Research Section B: Beam Interactions with Materials and Atoms 258, 403-413.

Nishiizumi, K., Kohl, C., Arnold, J., Klein, J., Fink, D., Middleton, R., 1991. Cosmic ray produced ^{10}Be and ^{26}Al in Antarctic rocks: exposure and erosion history. Earth and Planetary Science Letters 104, 440-454.

Nishiizumi, K., Lal, D., Klein, J., Middleton, R., Arnold, J., 1986. Production of [10]Be and [26]Al by cosmic rays in terrestrial quartz in situ and implications for erosion rates. Nature 319, 134-136.

Nishiizumi, K., Winterer, E., Kohl, C., Klein, J., Middleton, R., Lal, D., Arnold, J., 1989. Cosmic ray production rates of [10]Be and [26]Al in quartz from glacially polished rocks. Journal of Geophysical Research 94, 17907.

Phillips, F., Zreda, M., Smith, S., Elmore, D., Kubik, P., Sharma, P., 1990. Cosmogenic chlorine-36 chronology for glacial deposits at Bloody Canyon, eastern Sierra Nevada. Science 248, 1529-1532.

Portenga, E., Bierman, P., *In Press*. Understanding Earth's eroding surface with [10]Be. GSA Today.

Rood, D., Hall, S., Guilderson, T., Finkel, R., Brown, T., 2010. Challenges and opportunities in high-precision Be-10 measurements at CAMS. Nuclear Instruments and Methods in Physics Research Section B: Beam Interactions with Materials and Atoms 268, 730-732.

Southon, J., Vogel, J., Nowikow, I., Nelson, D., Korteling, R., Ku, T., Kusakabe, M., Huh, C., 1983. The measurement of [10]Be concentrations with a tandem accelerator. Nuclear Instruments and Methods in Physics Research 205, 251-257.

Suter, M., 1990. Accelerator mass spectrometry: state of the art in 1990. Nuclear Instruments and Methods in Physics Research Section B: Beam Interactions with Materials and Atoms 52, 211-223.

Von Blanckenburg, F., 2005. The control mechanisms of erosion and weathering at basin scale from cosmogenic nuclides in river sediment. Earth and Planetary Science Letters 237, 462-479.

Figure 1.

Solutions can be added without disturbing the resin bed

Reservoir is clearly marked with column volume measurements

Frit #2 ensures that resin remains saturated, preventing air gaps and channelization

1-2 mm space between resin and frit, always retains solution

3 mL **resin bed** for anions
5 mL **resin bed** for cations

Frit #1 keeps resin in column
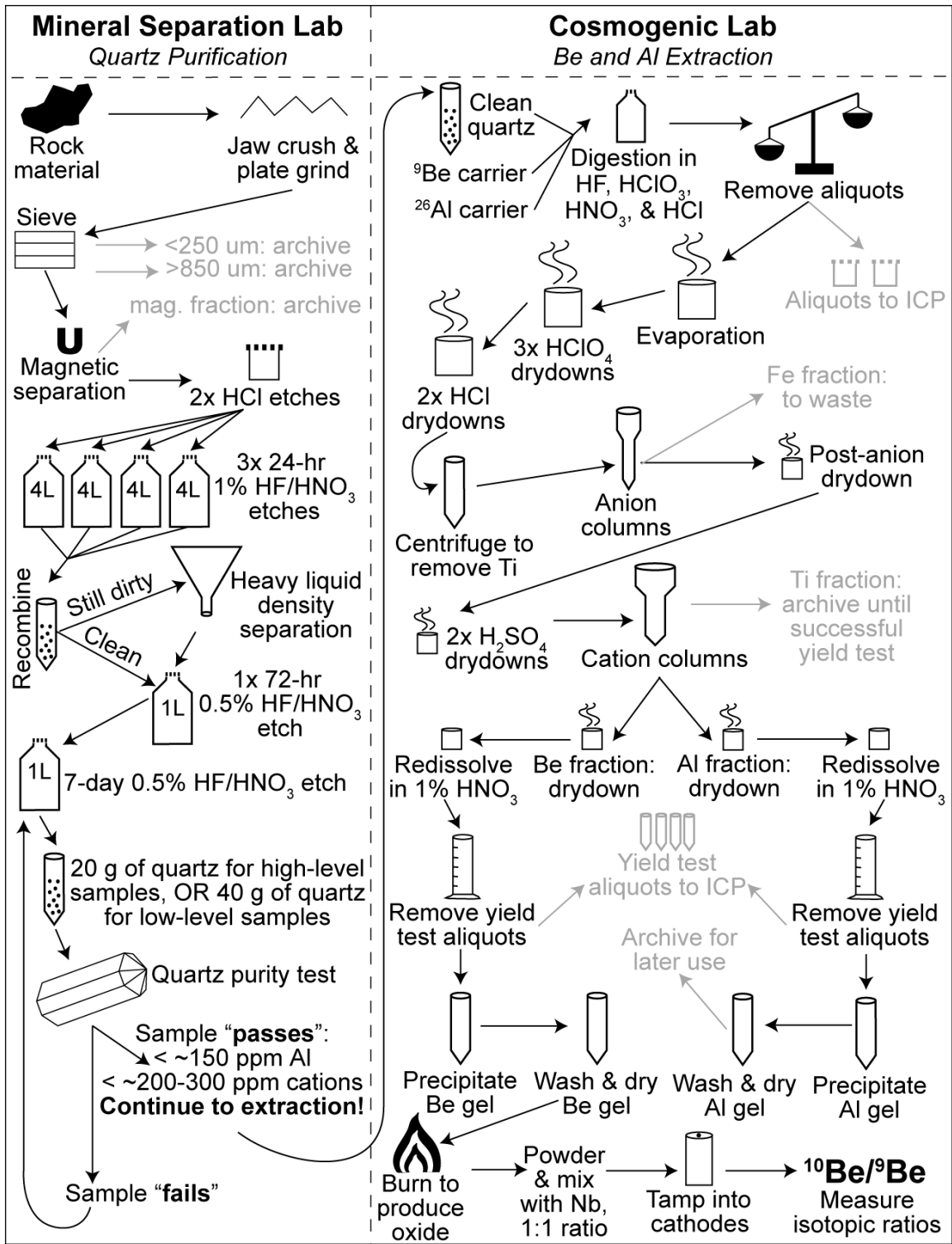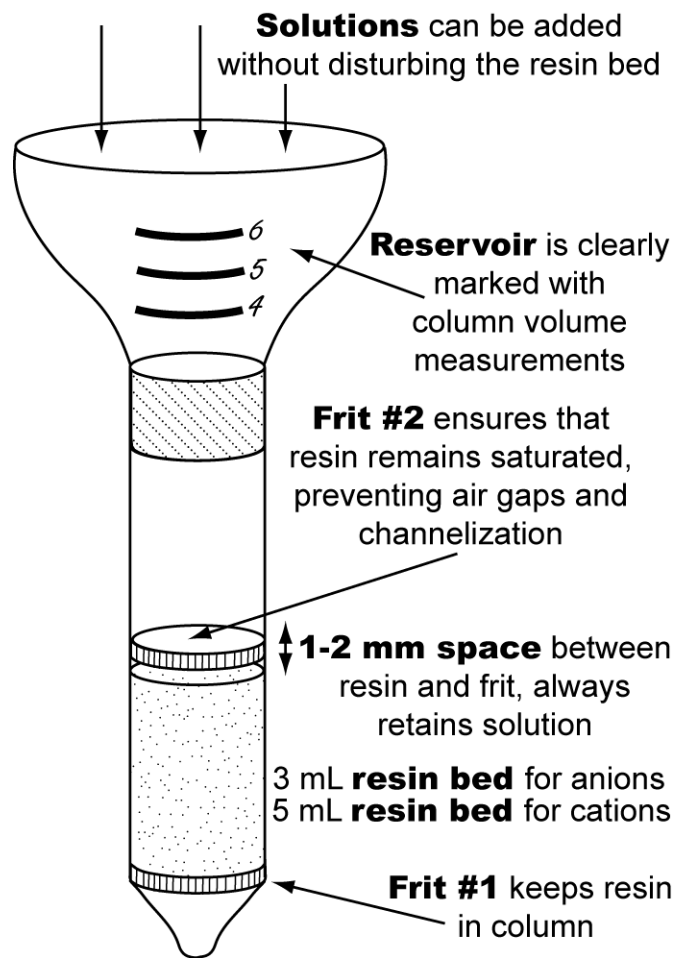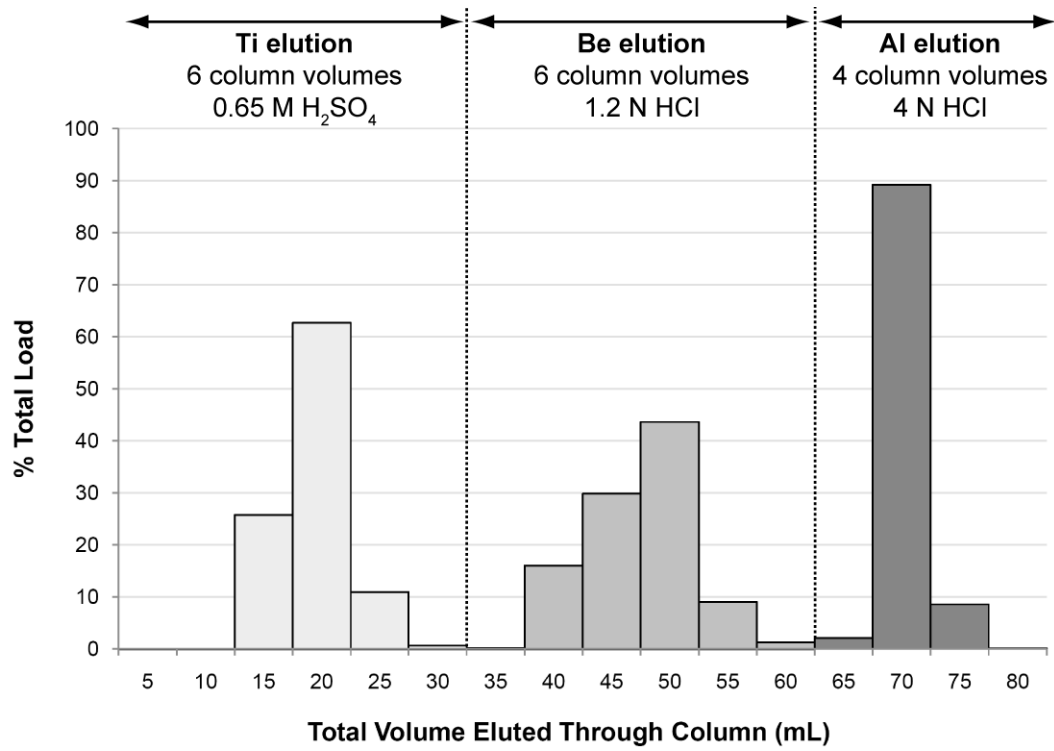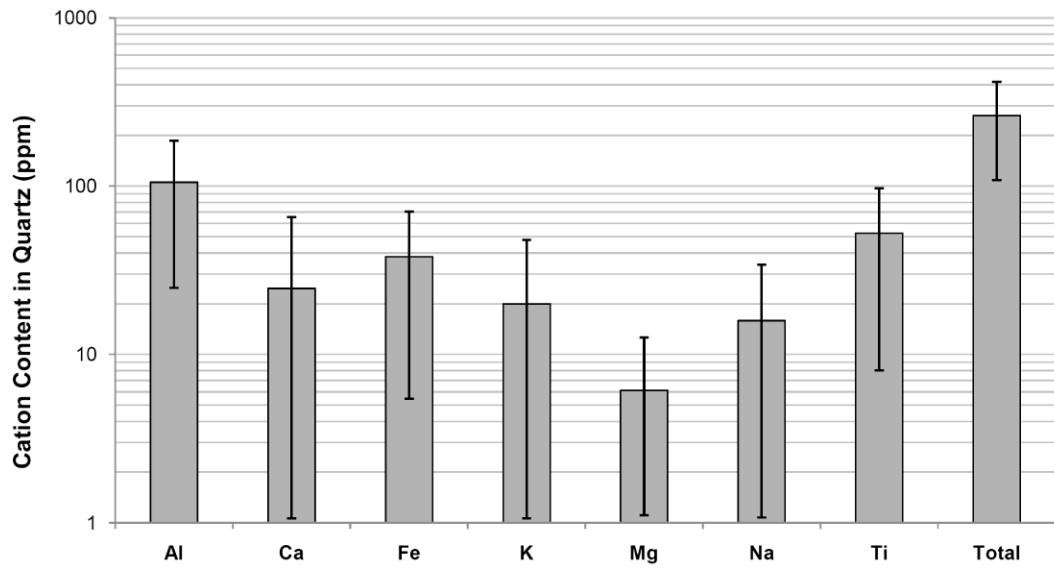
Figure 2.
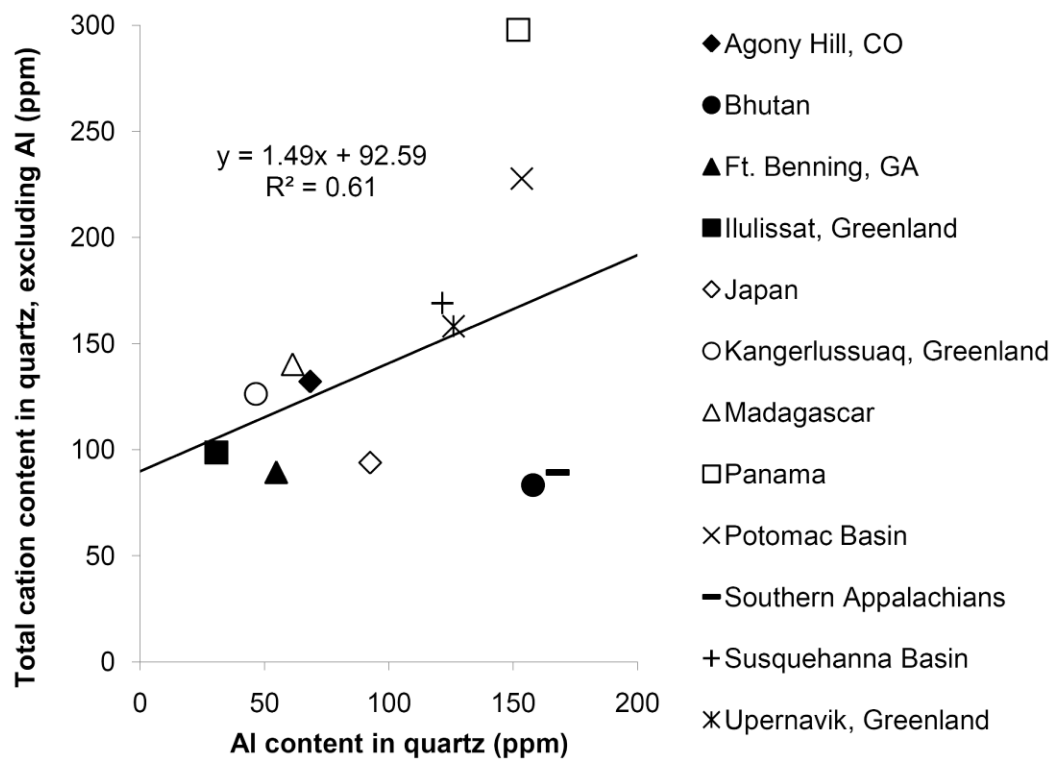
Figure 3.
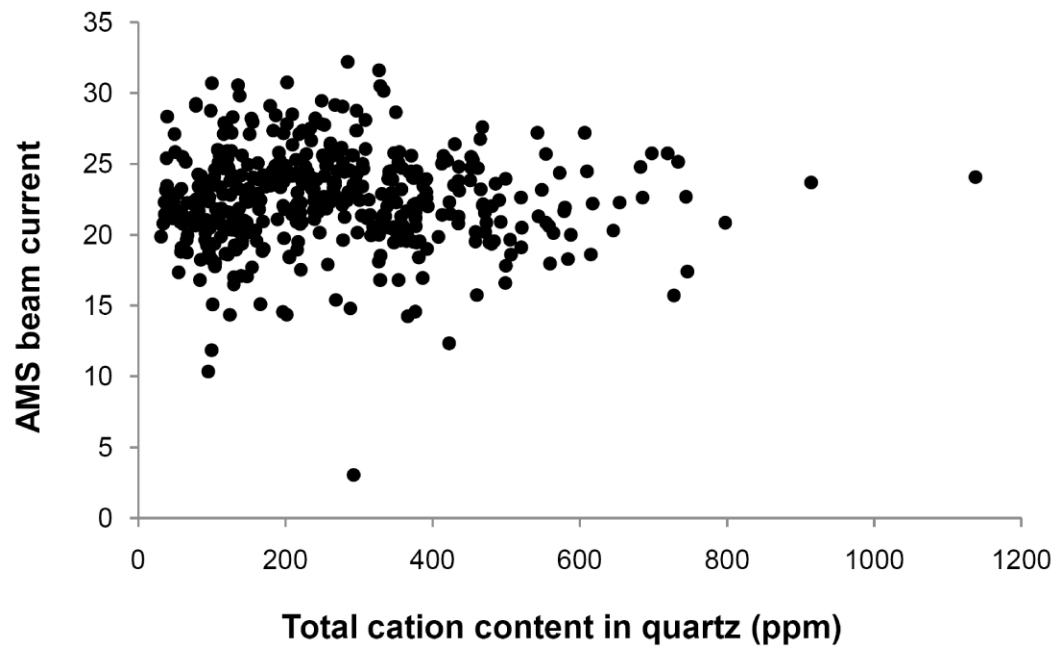
Figure 4.
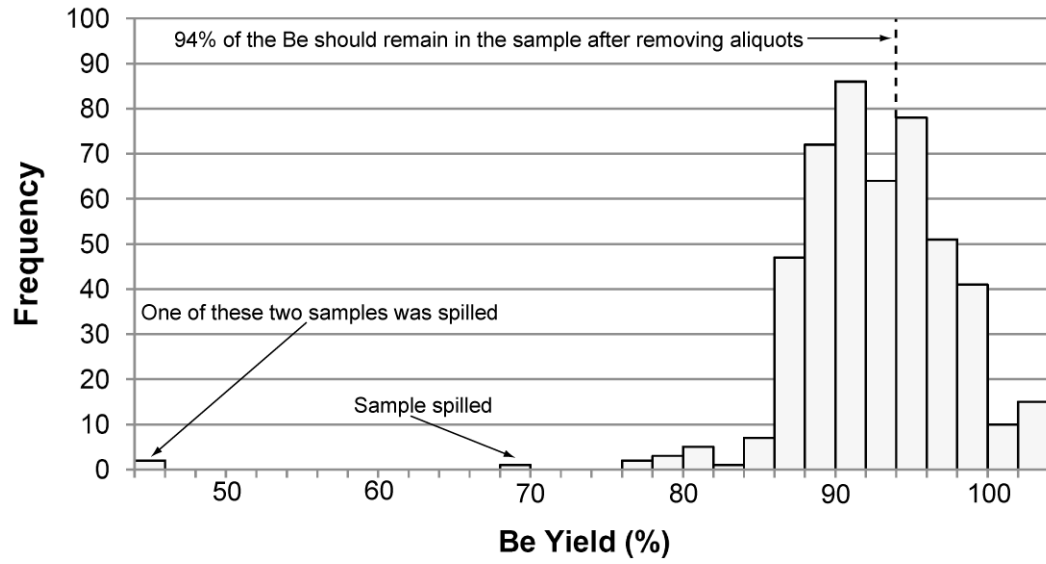
Figure 5.
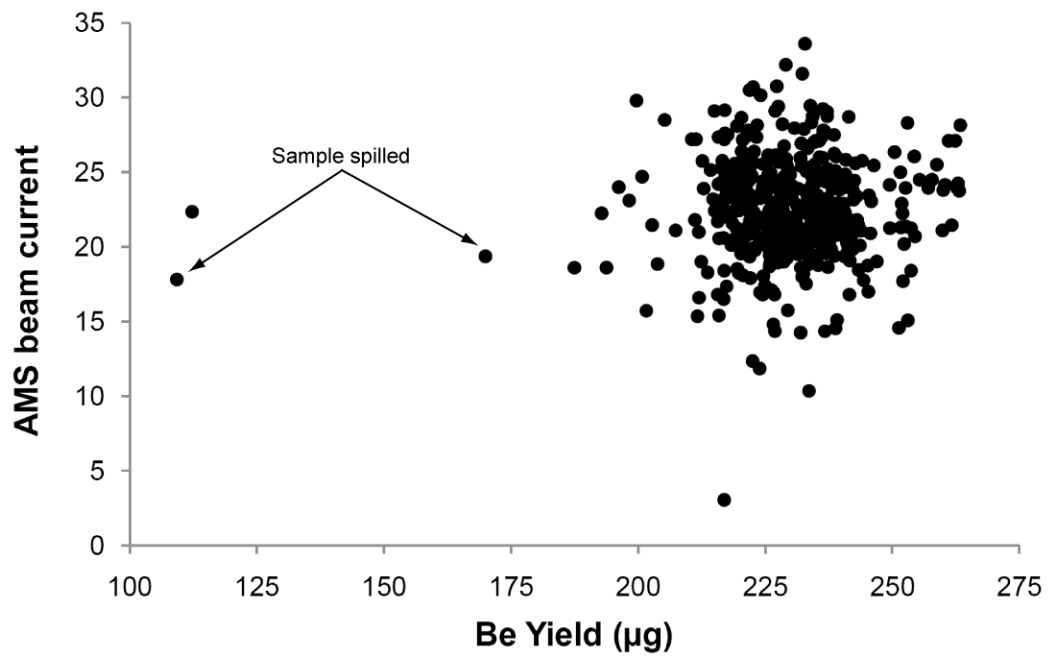
Figure 6.
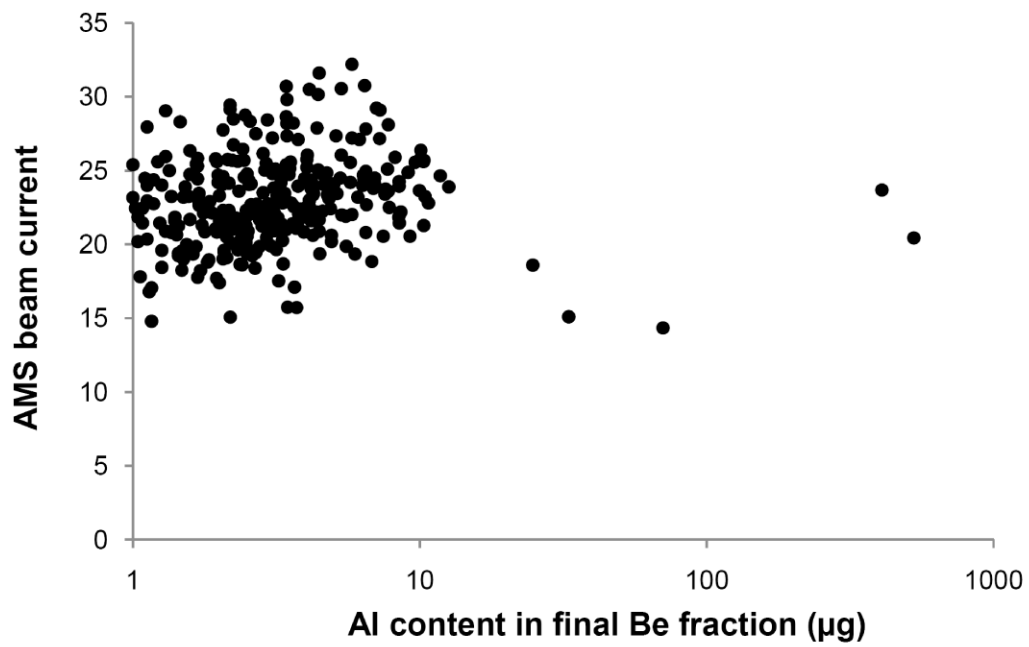
Figure 7.
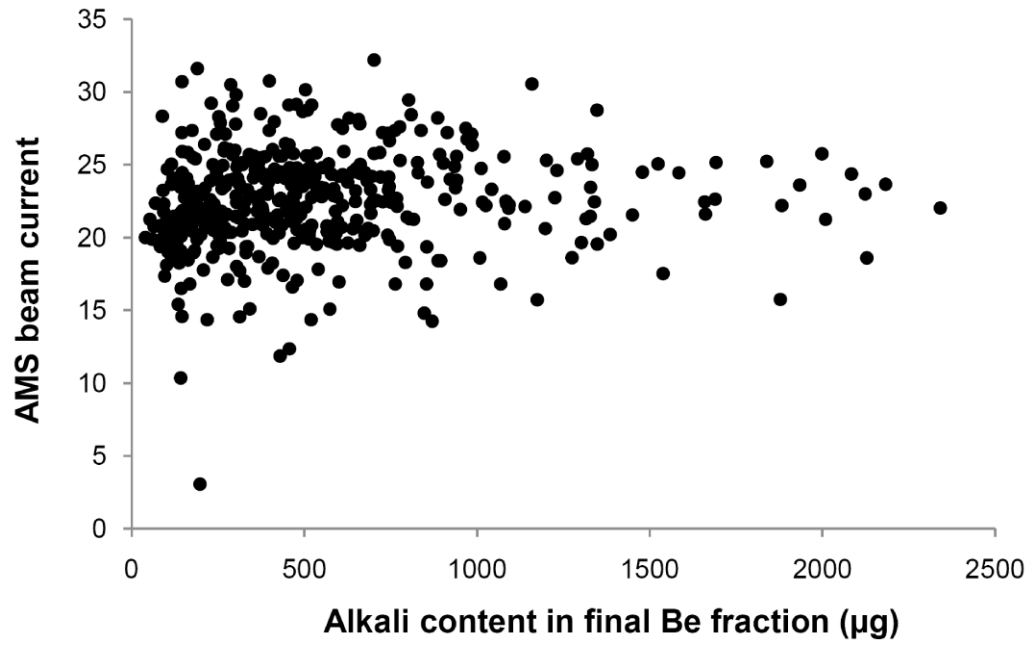
Figure 8.

Figure 9.

Figure 10.
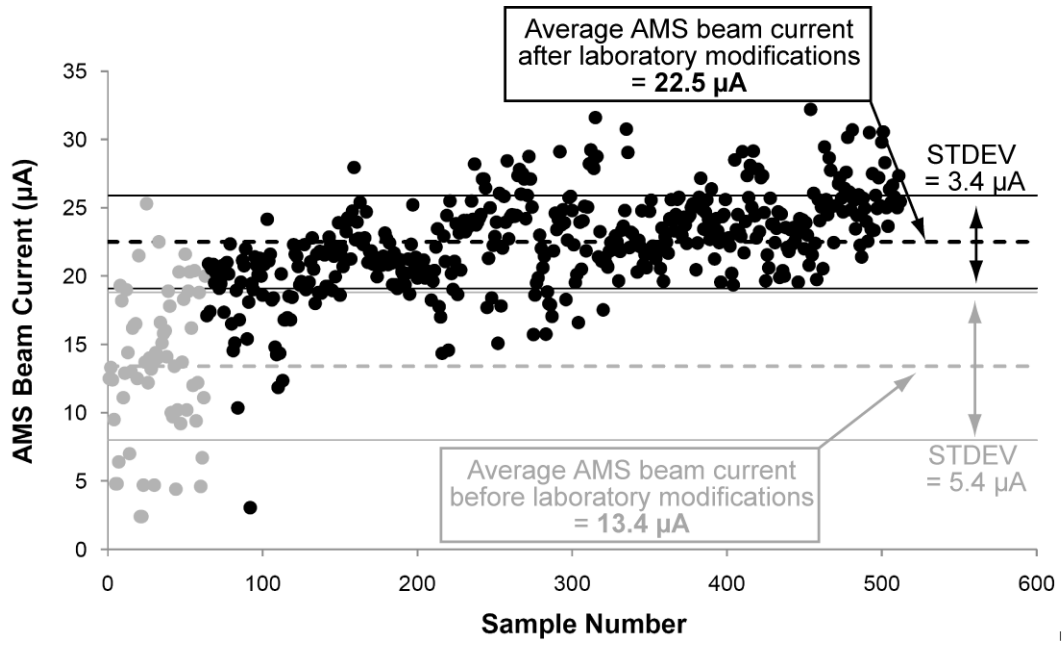
Figure 11.

Figure Legends

Figure 1. Flow chart of Be isotopic sample preparation. The first portion of the work (left) aims to process clean quartz from a rock or sediment sample. The second portion of the work (right) aims to isolate pure Be from the quartz. This flow chart describes the path each sample takes to be readied for AMS analysis. Arrows designate the direction of sample progression, and gray font indicates sample fractions that have been removed from the flow.

Figure 2. Schematic diagram of a column. We implemented a double-fritted column for both anion and cation column chromatography.

Figure 3. Cation column elution data from a column test performed on an artificial sample with a total cation load of 7000 µg. This correctly-calibrated column cleanly separated Ti, Be, and Al, shown in light gray, medium gray, and dark gray, respectively.

Figure 4. Average quartz analyzed during 2009-2010 (n = 762). Bars show average cation contents, and error bars show ± one standard deviation.

Figure 5. Quartz purity levels by site. Not all quartz reaches the same purity levels, despite repeated etches in acid. The black line is the trendline showing the relationship between Al content and total non-Al cation content between quartz from different sites.

Figure 6. Quartz cation contents and AMS beam currents for samples analyzed during 2009-2010 (n = 446).

Figure 7. Final Be yields for samples processed during 2009-2010 (n = 486). The aliquoting process following quartz digestion removes 6% of the sample volume; therefore, theoretical optimal Be yields should be 94%. Values are approximate because diultions are performed volumetrically and a rapid ICP-OES method is used.

Figure 8. Final Be yields and AMS beam currents for samples analyzed during 2009-2010 (n = 446).

Figure 9. Final Al impurities and AMS beam currents for samples analyzed during 2009-2010 (n = 446).

Figure 10. Final alkali metal impurities and AMS beam currents for samples analyzed during 2009-2010 (n = 446).

Figure 11. AMS beam currents for samples processed before and after laboratory modifications and methodological optimization. Gray dots represent samples processed in the old laboratory (n = 63), which were presented in Hunt et al. (2008). Black dots represent samples processed in the new laboratory, after extensive methodological modifications (n = 446). Gray and black dashed lines show the means of the two sample populations. Thin gray and black lines show ± one standard deviation from the mean.

CHAPTER 3. MANUSCRIPT FOR "QUATERNARY SCIENCE REVIEWS"

PAIRED BEDROCK AND BOULDER ^{10}BE CONCENTRATIONS RESULTING FROM EARLY HOLOCENE ICE RETREAT NEAR JAKOBSHAVN ISFJORD, WESTERN GREENLAND

Lee B. Corbett*[a]
Nicolás E. Young[b]
Paul R. Bierman[a]
Jason P. Briner[b]
Thomas A. Neumann[c]
Dylan H. Rood[d,e]
Joseph A. Graly[a]

[a]Department of Geology, University of Vermont, Burlington, VT 05405
[b]Department of Geology, State University of New York at Buffalo, Buffalo, NY 14260
[c]NASA Goddard Space Flight Center, Greenbelt, MD 20770
[d]Center for Accelerator Mass Spectrometry, Lawrence Livermore National Laboratory, Livermore, CA 94550
[e]Earth Research Institute, University of California, Santa Barbara, CA 93106
Contact Author: Ashley.Corbett@uvm.edu, (802) 656-4411

Abstract

We measured *in situ* cosmogenic [10]Be in 16 bedrock and 14 boulder samples collected along a 40-km transect outside of and normal to the modern ice margin near Sikuijuitsoq Fjord in central-west Greenland (69°N). We use these data to understand better the efficiency of glacial erosion and to infer the timing, pattern, and rate of ice loss after the last glaciation. In general, the ages of paired bedrock and boulder samples are in close agreement ($r^2 = 0.72$). Eleven of the fourteen paired bedrock and boulder samples are indistinguishable at 1σ; this concordance indicates that subglacial erosion rates are sufficient to remove most or all [10]Be accumulated during previous periods of exposure, and that few, if any, nuclides are inherited from pre-Holocene interglaciations. The new data agree well with previously-published landscape chronologies from this area, and suggest that two chronologically-distinct land surfaces exist: one outside the Fjord Stade moraine complex (~10.3 ± 0.4 ka; n = 7) and another inside (~8.0 ± 0.7 ka; n = 21). Six [10]Be ages from directly outside the historic (Little Ice Age) moraine show that the ice margin first reached its present-day position ~7.6 ± 0.4 ka. Early Holocene ice margin retreat rates after the deposition of the Fjord Stade moraine complex were ~100-110 m yr^{-1}. Sikuijuitsoq Fjord is a tributary to the much larger Jakobshavn Isfjord and the deglaciation chronologies of these two fjords are similar. This synchronicity suggests that the ice stream in Jakobshavn Isfjord set the timing and pace of early Holocene deglaciation of the surrounding ice margin.

1. Introduction

The measurement of cosmogenic isotopes in morainal boulders and glacially sculpted bedrock surfaces has provided increasingly widespread control on the chronology of deglaciation (Phillips et al., 1990; Fabel and Harbor, 1999; Balco, 2011). Glaciers and ice sheets are sensitive indicators of climate, and respond to changes in precipitation and temperature by expanding and shrinking (IPCC, 2007; Alley et al., 2010). Improved constraints on the timing and pattern of past deglaciation events provides an important context in which to interpret the dynamics of present-day and future ice loss (Long, 2009).

The dating of glacial events with cosmogenic nuclides depends on the veracity of key methodological assumptions: lack of post-depositional erosion or burial and minimal inheritance of nuclides from prior periods of exposure. In recent years, refined analytical and computational techniques have reduced age uncertainty (Hunt et al., 2008; Rood et al., 2010); however, the accuracy of cosmogenic ages still depends on the aforementioned assumptions (Bierman, 1994; Gosse and Phillips, 2001; Heyman et al., 2010). For older glaciations, surface erosion limits the accuracy of ages and results in age underestimates (Smith et al., 2005). Similar age underestimation also results from burial by till or snow cover (Schildgen et al., 2005). Conversely, inheritance of nuclides from prior periods of exposure can lead to age overestimates (Briner and Swanson, 1998). Because erratic boulders and the striated bedrock that underlies them have different pre-exposure histories and different likelihoods of post-exposure burial, a pair-wise comparison of exposure ages provide a useful means to test the assumption of no inheritance and no burial. However, paired sampling of striated bedrock and erratic boulders has been

conducted in only a few places (Marsella et al., 2000; Pallas et al., 2006; Delmas et al., 2008).

Large ice sheets have a variety of different ice margin types and thus can lose mass and retreat in a variety of ways. In some areas, the ice sheet margin is land-based and loses mass through surface melting or sublimation. In areas where the ice sheet margin is floating (marine-based) rather than grounded, mass is lost primarily through calving. For marine-based ice sheets, debris build-up at the glacier's terminus can create an end moraine, which serves to stabilize the ice against further calving (Alley et al., 2007). In some areas, fast-flowing ice streams channelize regional ice flow and transport large volumes of ice to the sea (Bentley, 1987).

Although the deglaciation dynamics of large ice streams has been relatively well-studied (Weidick et al., 1990; Long and Roberts, 2002, 2003; Lloyd et al., 2005; Long et al., 2006; Weidick and Bennike, 2007; Young et al., 2011), the influence of such fast-flowing systems on the retreat of adjacent ice margins is not well-understood. Western Greenland, where ice streams are juxtaposed with less active ice margins, is an ideal place to study the dynamics of ice retreat in an area adjacent to a major ice stream. Here, we present [10]Be data from 16 sites in Sikuijuitsoq Fjord, a tributary fjord of a large, rapidly moving ice stream (Jakobshavn Isbræ; Figs. 1 & 2). Measurements of *in situ* produced cosmogenic [10]Be in 16 striated bedrock samples and 14 erratic boulders allow us to make inferences about subglacial erosion efficiency and deduce the pattern, timing, and rate of early Holocene ice margin retreat. After understanding these parameters for Sikuijuitsoq Fjord, we draw comparisons with the behavior of Jakobshavn Isbræ and show that the chronologies, rates, and dynamics of deglaciation are similar. Our goal is to

determine if fast flowing ice in Jakobshavn Isbræ exerted control on the neighboring ice margin and thus on the concentration of ^{10}Be in the samples we collected.

2. Study Site and Previous Work

We collected samples near and along the narrow (~3 km) Sikuijuitsoq Fjord located on the western margin of the Greenland Ice Sheet. Just to the south is Jakobshavn Isbræ (Figs. 1 & 2; 50°W, 69°N), one of the largest outlet glaciers in the world. At present, the calving margin of Jakobshavn Isbræ is about 50 km east of the town of Ilulissat. The outlet glacier drains through Jakobshavn Isfjord, which is 6 to 8 km wide, up to 1000 m deep (Holland et al., 2008), and almost entirely choked with icebergs due to a shallow shoal at the fjord mouth. Both fjords have inclined rather than vertical walls and the surrounding topography reaches almost 700 m a.s.l. The ice-free landscape between the coast of Disko Bugt and the present ice margin contains glacially scoured bedrock and ubiquitous erratic boulders, which lie both on moraines and directly on bare bedrock surfaces (Fig. 3).

The prominent Fjord Stade moraines (Fig. 2), which lie between Disko Bugt and the present-day ice margin, were deposited during the early Holocene; these moraines consist of the sometimes overlapping outer "Marrait" and inner "Tasiussaq" moraines (Weidick, 1968; Weidick and Bennike, 2007; Young et al., 2011). The Marrait and Tasiussaq moraines form a single complex, which allows the landscape to be divided into two chronologically-distinct land surfaces: an older surface outside of the moraines and a younger surface inside of the moraines.

2.1. Outer Land Surface

The land surface outside of the Fjord Stade moraine complex contains the oldest terrain surrounding Jakobshavn Isfjord (Fig. 2). During the last glaciation, ice extended across Disko Bugt and onto the continental shelf (Weidick and Bennike, 2007). Radiocarbon ages from marine sediment cores suggest that deglaciation through Disko Bugt took place at or prior to ~10.3 cal ka BP (Long and Roberts, 2003; Lloyd et al., 2005); this represents a maximum limiting age for the outer land surface. Radiocarbon ages from raised marine deposits on this surface provide a minimum estimate of deglaciation at ~9.9 ± 0.1 cal ka BP (n = 4) (Weidick and Bennike, 2007). More recently, [10]Be surface exposure ages suggest that this surface is ~10.2 ± 0.1 ka (n = 5) (Young et al., 2011). The body of previous work discussed above constrains the age of the outer land surface to ~10 ka, and serves as a maximum limiting age for the Fjord Stade moraine complex.

2.2. Inner Land Surface

The land surface inside of the Fjord Stade moraine complex was deglaciated after the abandonment of the Tasiussaq moraine and contains the youngest terrain outside of the historic moraine immediately adjacent to today's ice margin (Fig. 2). Basal radiocarbon ages from a lake sediment core southeast of Disko Bugt suggest a minimum limiting age of ~8.0-7.7 cal ka BP (Long and Roberts, 2002); similarly, basal radiocarbon measurements from two lakes above the marine limit just south of Jakobshavn Isfjord provide minimum limiting ages of ~7.7 and 7.6 cal ka BP (Long et al., 2006). More recently, [10]Be surface exposure ages constrain the age of the inner land surface to 8.0 ±

58

0.1 ka (n = 5), not including an older outlier of 12.0 ± 0.3 ka (Young et al., 2011). The

work discussed above demonstrates that this surface was deglaciated ~8 ka, thereby

providing a minimum limiting age for the Fjord Stade moraine complex.

The inner land surface spans the distance from the Fjord Stade moraine complex

to the historic moraine. Therefore, the exposure age of this surface varies with distance

from the ice sheet margin, reflecting the rate of ice margin retreat. Additional ^{10}Be

surface exposure ages from directly outside of the historic moraine near Jakobshavn

Isbræ suggest that the ice margin at Jakobshavn Isfjord reached its present position ~7.5 ±

0.2 ka (n = 7) (Young et al., 2011), or about 0.5 ka after the abandonment of the

Tasiussaq moraines. Similarly, basal radiocarbon ages from lake sediment cores show

that the ice margin first reached its present position ~7.4-7.2 cal ka BP (Briner et al.,

2010). Radiocarbon ages (n = 15) of marine fauna reworked into the historic moraine

range from 6.1 to 2.2 cal ka BP, indicating that the ice margin retreated behind its

present-day position before 6.1 cal ka BP and re-advanced to its current position after 2.2

cal ka BP (Weidick et al., 1990; Weidick and Bennike, 2007).

3. Methods

3.1. Experimental Design

We collected 16 bedrock and 14 boulder samples for the analysis of *in situ*

cosmogenic ^{10}Be (Gosse and Phillips, 2001). Samples were collected along a 40-km

southwest to northeast transect extending from Disko Bugt to the present-day ice margin,

along Sikuijuitsoq Fjord, a tributary to Jakobshavn Isfjord (Table 1; Fig. 2). The sampling

scheme used in this study, known as "dipstick sampling" (Stone et al., 2003), involves

collecting bedrock and boulder pairs at a variety of elevations at several locations along a transect normal to the ice margin. Samples were collected at elevations ranging from 50 to 620 m a.s.l. and included high-, medium-, and low-elevation bedrock/boulder pairs at each "dipstick" wherever possible. This sampling scheme provides a three-dimensional pattern of exposure ages, yielding information about both the vertical and horizontal timing of ice retreat. Measuring ^{10}Be in paired bedrock and boulder samples provides information about the efficiency of subglacial erosion and the likelihood of post depositional burial. If a bedrock sample is appreciably older than a paired boulder sample, inheritance of ^{10}Be from prior periods of exposure is likely (Bierman et al., 1999). If a bedrock sample is appreciably younger than a paired boulder sample, localized shielding by till or snow cover is possible. If the two ages agree, the likelihood of complex exposure histories is low, and both ages are more likely to be accurate.

The relationships among the sample dipsticks, the Fjord Stade moraines, and thus the inner and outer land surface vary by location. Since the fjord walls are sloped rather than vertical, sampled dipsticks span several km of horizontal distance in order to capture the full extent of local vertical relief. The two dipsticks closest to the coastline (numbers 5 and 4) have their low-elevation samples on the edge of Jakobshavn Isfjord, while the next three (numbers 3, 2, and 1) have their low-elevation samples on the edge of the Sikuijuitsoq tributary fjord. The two dipsticks closest to the coastline (numbers 5 and 4) span the Fjord Stade moraine complex; thus, their low-elevation samples are from the inner land surface, and their high-elevation samples are from the outer land surface. The three dipsticks closest to the present-day ice margin (numbers 3, 2, and 1) are entirely inboard of the Fjord Stade moraine complex.

3.2 Field Methods

Using a chisel and hammer, we collected the top several cm of material from flat-lying, glacially-scoured bedrock surfaces and erratic boulders (Table 1). To avoid complex cosmic-ray exposure geometries, we did not collect samples from areas that were sheltered by steep hillsides, cliffs, or large boulders. Wherever possible, we sampled bedrock and boulder pairs in close proximity, usually less than 5 m apart. Latitude/longitude and elevation data were collected with a handheld Garmin 12 GPS that has a positional uncertainty of <10 m; elevation uncertainty is <25 m.

3.3. Quartz and Beryllium Isolation

Samples for ^{10}Be analysis were prepared using mineral separation procedures modified from Kohl and Nishiizumi (1992). Rocks were crushed, ground, and sieved to isolate grains between 250 and 850 μm, then magnetically separated to remove mafic minerals. Samples were ultrasonically etched twice in hot 6N HCl to remove grain coatings, and then three more times in hot, dilute (1%) HF-HNO$_3$ to preferentially dissolve all grains except quartz. If needed, we performed a heavy-liquid density separation. Quartz was tested for purity by inductively coupled plasma optical emission spectrometry, and subsequent HF-HNO$_3$ etches were performed until desired purity levels were reached (usually less than 100 ppm Al and less than 200 ppm total cations).

Beryllium was isolated in the University of Vermont Cosmogenic Laboratory (see www.uvm.edu/cosmolab, Table 1). For each sample, between ~5 and 20 g of purified quartz was used for analysis. Samples were prepared in batches of 12, including either 1 or 2 process blanks. Just over 1 g of low-level ^{9}Be carrier (245 ppm concentration) made

61

from beryl at the University of Vermont was added to each sample, equating to an addition of ~250 µg of ^{9}Be. Complete dissolution took place with 100 g of hot, concentrated HF. After dissolution and drydown, samples were treated with four additions of $HClO_4$, and then converted to chloride form with two additions of HCl. Samples were passed through anion exchange columns to remove Fe, converted to sulfate form with two additions of H_2SO_4, and passed through cation exchange columns primarily to separate Ti, Be, and Al, and to remove B. Average Be recovery for these samples was $96.2 \pm 5.7\%$ (1σ, n = 30). The Be fraction was precipitated at pH 8 as hydroxide gel, dried, ignited to produce BeO, and packed into stainless steel cathodes with Nb powder at a 1:1 molar ratio for accelerator mass spectrometry (AMS) measurements.

3.4. Isotopic Analysis

^{10}Be/^{9}Be ratios were measured by AMS at Lawrence Livermore National Laboratory. All samples were normalized to standard 07KNSTD3110, with a reported ratio of $2850 \cdot 10^{-15}$ (Nishiizumi et al., 2007). Measured sample ratios ranged from $2.3 \cdot 10^{-14}$ to $8.2 \cdot 10^{-14}$, and AMS measurement precisions, including propagated blank corrections, ranged from 1.9 to 3.0% (1σ, Table 1). Samples were prepared in three separate batches, and the process blanks for these three batches contained $1.7 \cdot 10^4$ (n = 1), $7.3 \cdot 10^3$ (average, n = 2), and $1.5 \cdot 10^4$ (n = 1) ^{10}Be atoms, respectively. The blank ^{10}Be/^{9}Be ratios were $1.0 \cdot 10^{-15}$ (n = 1), $4.4 \cdot 10^{-16}$ (average, n = 2), and $9.3 \cdot 10^{-16}$ (n = 1); these blanks were inconsequential as they amounted to only 1-3% of the total sample ratios.

3.5. Exposure Age Calculations

[10]Be exposure ages were calculated with the CRONUS Earth online exposure age calculator developmental version 2.2, constants version 2.2 (Balco et al., 2008). We used the regionally-calibrated northeastern North American production rate of 3.93 ± 0.19 atoms g^{-1} yr^{-1} (Balco et al., 2009) and the Lal/Stone constant production rate model and scaling scheme (Lal, 1991; Stone, 2000) under standard atmosphere. We chose to use the northeastern North American production rate because [10]Be ages calculated this way correlated closely with the independent chronology deduced from other dating methods (e.g. radiocarbon; section 2). Calculated [10]Be ages can vary by as much as 14% based on the chosen production rate, and as much as 4% based on the chosen scaling scheme. In CRONUS, corrections were made for latitude, elevation, sample thickness (1-5 cm), and sample density (2.7 g cm^{-3}; Table 1).

No corrections were made for snow cover. Shielding by snow cover would lead to [10]Be age underestimates (Schildgen et al., 2005); however, snow cover effects at our sample sites are likely minimal. Using contemporary data from a weather station on the southern side of Disko Bugt (www.weather-and-climate.com, Egedesminde station), we determined that mean temperatures are below freezing for eight months of the year (October through May) and that ~180 mm of snow (water equivalent) falls during this time at a rate of ~15-30 mm per month. To assess the significance of potential snow shielding, we assumed that precipitation was added in monthly increments, and that no melting or sublimation occurred until May. Shielding calculated according to Gosse and Phillips (2001) suggests that reported exposure ages could underestimate the true age by no more than 7%. This calculation is likely a significant overestimate because we did not

63

account for snow loss during the winter and because the areas we sampled are likely windswept and exposed during winter months. However, this calculation was performed with only modern snowfall data; if snowfall was different over the course of the Holocene, shielding values may have been lesser or greater than modern data suggest.

No corrections were made for erosion, till cover, or isostatic rebound. Bedrock and boulder erosion can also cause ^{10}Be concentrations to underestimate exposure ages; however, all of the outcrops and boulders we sampled had fresh surfaces and some preserved striations, leading us to conclude that erosion of rock during the Holocene was negligible. The field area contains little till; boulders lie directly on bare bedrock surfaces. Thus, we consider shielding by now-eroded till unlikely. We did not correct sample elevations for post-glacial isostatic rebound because corrections calculated by Young et al. (2011) in the same area all fall within our vertical GPS uncertainty, and amount to less than 1-2% of calculated exposure ages.

Reported age uncertainties reflect AMS errors only, which we refer to as "internal". We use internal uncertainties in our data analysis because we are interested in how the sample ages within this data set relate to each other. This approach allows us to investigate relationships between samples, e.g. testing for inheritance with paired bedrock and boulder samples. We acknowledge that there are additional age uncertainties related to production rate calibration as well as elevation and latitude corrections that would reflect better the precision of our ages when making comparison to other dating methods and cosmogenic ages from other locations. However, because our samples come from a geographically limited region and a restricted elevation range, errors in calibration and correction are correlated and thus affect all samples similarly.

4. Results

All 30 cosmogenic ^{10}Be exposure ages are indicative of Holocene exposure. Bedrock and boulder samples had measured ^{10}Be concentrations of $7.3 \cdot 10^4$ to $3.5 \cdot 10^4$ atoms g^{-1}, yielding ^{10}Be ages of 10.8 ± 0.2 to 6.9 ± 0.2 ka ($n = 30$; Table 1 & Fig. 2). Corresponding bedrock and boulder sample pairs have similar ^{10}Be ages ($r^2 = 0.72$, Fig. 4); a repeated measures t-test verifies that there is no statistically significant difference when boulders and bedrock ages are considered in a paired comparison ($p = 0.980$). Similarly, considering bedrock and boulder samples in two distinct populations results in nearly identical population distributions (Fig. 5); an independent samples t-test indicates that there is no statistical difference between populations ($p = 0.973$).

Eleven of the 14 bedrock/boulder pairs have indistinguishable ^{10}Be ages; only three of the 14 pairs have ^{10}Be ages that differ by more than the 1σ AMS uncertainties. In one of these cases, the boulder sample (GL094, 9.3 ± 0.2 ka) is older than the bedrock sample (GL095, 7.9 ± 0.2 ka) by 1.4 ka (3σ). One low-elevation bedrock sample (GL090, 8.6 ± 0.2 ka) is 0.8 ka (2σ) older than its corresponding boulder (GL091, 7.8 ± 0.2 ka), and one high-elevation bedrock sample (GL096, 10.8 ± 0.2 ka) is 1.1 ka (2σ) older than its corresponding boulder sample (GL097, 9.7 ± 0.3 ka). The reason for bedrock/boulder discordance in these three sample pairs is unknown.

Sample ^{10}Be ages differ according to the location on the landscape that the samples were collected (Fig. 6). Samples from the land surface outside of the Fjord Stade moraine complex have an average age of 10.3 ± 0.4 ka ($n = 7$). Samples from the land surface inside of the Fjord Stade moraine complex have an average age of 8.0 ± 0.7 ka (n

= 21). An independent samples t-test indicates that these are separable populations ($p < 0.001$).

There is a scatter of [10]Be ages within each dipstick (Fig. 7). There is more scatter in the two outboard dipsticks (numbers 5 and 4), which span the Fjord Stade moraines (relative standard deviations = 11.3 and 10.9%). The three dipsticks closest to the present-day ice margin (numbers 3, 2, and 1) are entirely inboard of the Fjord Stade moraine complex and have less scatter (relative standard deviations = 6.0, 2.4, and 4.9%). Within these three inner dipsticks, there is no significant difference between high-, middle-, and low-elevation samples at 1σ. However, sample [10]Be ages decrease towards the present-day ice margin (Figs. 7 & 8); the average ages (1σ) of dipstick numbers 3, 2, and 1 are 8.3 ± 0.5 ka (n = 6), 7.7 ± 0.2 ka (n = 6), and 7.6 ± 0.4 ka (n = 6). A one-way ANOVA shows that the ages of these three dipsticks are separable ($p = 0.006$, Fig. 8). Subsequent independent samples t-tests show that the age of dipstick 3 is separable from both the age of dipstick 1 ($p = 0.014$) and the age of dipstick 2 ($p = 0.011$), but the age of dipstick 1 is not separable from the age of dipstick 2 ($p = 0.591$).

5. Discussion

Cosmogenic analysis of paired bedrock/boulder samples provides a powerful means by which to understand the dynamics of bedrock erosion by ice, improve the accuracy of deglaciation chronologies, estimate rates of ice retreat, and test the influence of large ice streams on adjacent but less dynamic ice margins.

5.1. Cosmogenic Nuclide Inheritance and Last Glaciation Erosion Rates

The Holocene ages of all samples from Sikuijuitsoq Fjord and the robust correlation of paired bedrock and boulder ages (Figs. 4 & 5) both argue that inheritance of cosmogenic nuclides from exposure before the last glaciation is unlikely in this field area. Such exposure could have occurred during the Eemian period when ice extent was much reduced (Letréguilly et al., 1991; Cuffey and Marshall, 2000; Otto-Bliesner et al., 2006), and during many previous interglaciations throughout the Quaternary when global ice volume was low (Lisiecki and Raymo, 2005). The observed lack of inheritance indicates that glacial ice near Ilulissat was highly erosive during the last glaciation, likely removing at least ~2 m of material from bedrock outcrops. Our results are consistent with the abundance of fresh-appearing glacially-scoured bedrock at all elevations visited in the field (Roberts and Long, 2005).

This result differs notably from findings in some other high-latitude areas, where subglacial erosion rates are insufficient to remove ^{10}Be inherited from previous periods of exposure. In these cases, bedrock samples have old exposure ages even though they were overrun by ice during the last glaciation. Such inheritance has been documented in Greenland (Håkansson et al., 2008; Kelly et al., 2008; Corbett et al., 2009), the Canadian Arctic (Bierman et al., 1999; Briner et al., 2003; Marquette et al., 2004), Scandinavia (Stroeven et al., 2002; Harbor et al., 2006), and Antarctica (Sugden et al., 2005; Lilly et al., 2010). The lack of inheritance around Sikuijuitsoq Fjord is likely due to the presence of thick, fast-flowing ice surrounding Jakobshavn Isbræ, creating an ideal environment for the removal of previously exposed bedrock and boulders (Bougamont and Tulaczyk, 2003; Roberts and Long, 2005; Smith et al., 2007). These results suggest that bedrock

67

and boulder samples adjacent to large ice streams are less likely than samples from other geomorphic settings to contain inherited nuclides. In settings such as this, both sculpted bedrock and erratic boulders provide similarly accurate deglaciation chronologies.

5.2. Comparison to Existing Land Surface Chronology

Data from Sikuijuitsoq Fjord agree well with previous estimates of land surface age and confirm the existence of two chronologically-distinct land surfaces (Fig. 6). Samples collected from the land surface outside of the Fjord Stade moraine complex provide an average ^{10}Be age of 10.3 ± 0.4 ka (n = 7). This age is in close agreement with previous limiting age constraints discussed in section 2.1, and is indistinguishable from the ^{10}Be age of ~10.2 ± 0.1 ka (n = 5) from Young et al. (2011).

Samples from the land surface inside of the Fjord Stade moraine complex provide an average ^{10}Be age of 8.0 ± 0.7 ka (n = 21), integrated over a wide geographic area. Samples from directly inside the moraine complex give an average age of 8.2 ± 0.1 ka (n = 2), in close agreement with previous work from Jakobshavn Isfjord discussed above (Young et al., 2011), and provide a minimum limiting age for abandonment of the Tasiussaq moraine. Some of the samples from this land surface were collected from directly outside the historic moraine, and provide an average ^{10}Be age of 7.6 ± 0.4 ka (n = 6). These samples provide an estimate of when the ice margin near Sikuijuitsoq Fjord retreated behind the position of the historic moraine, and are again in close agreement with previous findings (7.5 ± 0.2 ka, n = 7) for samples from the same landscape position but in Jakobshavn Isfjord (Young et al., 2011).

Two samples from the inner land surface have older-than-expected ^{10}Be ages.

Previous work has suggested that the inner (Tasiussaq) moraine was deposited ~8.2 ka

(Long and Roberts, 2002; Weidick and Bennike, 2007; Young et al., 2011), consistent

with the average age we measure for the inner land surface 8.0 ± 0.7 ka (n = 21).

However, two bedrock samples (GL098 and GL103) from just inboard of the Fjord Stade

moraine are more than 1σ above the average. Bedrock sample GL098 (10.0 ± 0.2 ka) is

indistinguishable from the age of the outer land surface (~10 ka, Fig. 6). Bedrock sample

GL103 (9.0 ± 0.2 ka) is 500 years older than its paired boulder and 1000 years older than

the average age of the inner land surface. These differences are best explained by

inheritance of nuclides resulting from early Holocene exposure. The ice margin retreated

inboard of the GL098 and GL103 sample locations ~10 ka, exposing the entire outer land

surface and some of the more distal portions of the inner land surface. Then, the ice re-

advanced and deposited the Fjord Stade moraine complex; however, this re-advance was

too short-lived to completely remove ^{10}Be formed in outcrops near the moraine after the

10 ka retreat and before the 8.2 ka advance. Although this inheritance is only shown by

two samples, these data hint that bedrock samples collected just inboard of moraines

created by short-lived re-advances may be more likely to carry inherited nuclides and

could therefore overestimate actual exposure ages. In cases like this, paired

bedrock/boulder samples are particularly useful.

5.3. Ice Surface Lowering

There is no difference in sample ^{10}Be age with elevation (within 1σ uncertainties)

at the three dipsticks contained within the inner land surface. This differs from other

high-latitude studies, which have documented measurable ice downwasting rates in both Greenland and Antarctica. Ice surface lowering rates in the early Holocene were ~6 cm yr^{-1} near Sisimiut Fjord, western Greenland (Rinterknecht et al., 2009), and ~2.5-9 cm yr^{-1} in Marie Byrd Land, Antarctica (Stone et al., 2003). The lack of a measurable downwasting rate does not imply that ice surface lowering did not occur; rather, the data suggest that any vertical change in ice position at each dipstick took place more rapidly than the resolution of the ^{10}Be chronometer, probably within several decades to at most a few centuries. The rapid change in ice thickness we infer for deglaciation near Sikuijuitsoq Fjord may be unique to areas with marine-terminating glaciers. Given that the glacier in Sikuijuitsoq Fjord was predominately marine-terminating, the ice margin was likely near-vertical, as seen at other calving fronts. This steep geometry would have exposed each dipstick more rapidly than a lower-slope margin more characteristic of terrestrial ice fronts.

5.4. Lateral Ice Margin Retreat

Ice margin retreat through Sikuijuitsoq Fjord occurred rapidly after the abandonment of the inner Fjord Stade moraine. Abundant previous work demonstrates that the Tasiussaq moraine was deposited during a re-advance ~8.2 ka (section 2.2), and Young et al. (2011) suggest that the ice margin left the moraine ~8.0 ka (n = 5). The ice margin went behind the position of the historic moraine only ~400 years later (~7.6 ka, n = 6, this study), after retreating 40 to 45 km.

Since it is unclear when ice flow separation between the two fjords occurred, we cannot determine whether the direction of ice flow was regionally dictated (by the

presence of a large ice stream flowing through Jakobshavn Isfjord) or locally dictated (by

the orientation of Sikuijuitsoq Fjord). Therefore, we calculate ice margin retreat rates in

two ways: assuming that ice retreat was west to east, parallel to Jakobshavn Isfjord (a

distance of ~40 km), and assuming that ice retreat was southwest to northeast, parallel to

Sikuijuitsoq Fjord (a distance of ~45 km). Assuming that retreat began after the

abandonment of the Tasiussaq moraine at 8.0 ka, and ended when the ice margin

retreated behind the historic moraine at 7.6 ka, we calculate integrated retreat rates of

~100 and ~110 m yr^{-1}.

5.5. Sikuijuitsoq Fjord and Jakobshavn Isfjord: Deglaciation Dynamics

The deglaciation chronologies at Sikuijuitsoq Fjord and Jakobshavn Isfjord match

closely (section 5.2), most likely because the two fjords were not separated for most of

the early Holocene. The height of land that divides the two fjords has a maximum

elevation of ~300 m. The inner land surface to the north of Sikuijuitsoq Fjord extends to

a much higher elevation (~500-600 m), as shown by the highest-elevation samples in

dipstick numbers 1-3, which are still inboard of the Fjord Stade moraine complex. This

relationship implies that, at the time of deposition of the inner Fjord Stade moraine, the

two fjords had not yet become divided at the surface. Up until this point, and for a short

time after, they both would have fed into a single outlet glacier. During retreat from the

Fiord Stade moraines to the location of the historic moraine, the ice surface downwasted;

rapid ice flow would have continued to occur in the fjords, but the flow over the dividing

land surface would have slowed and eventually stagnated. The ice stream then must have

71

separated into two distinct tongues; however, with retreat through this area lasting only 400 years, this configuration was not long-lived.

It is possible the retreat of Jakobshavn Isbræ through the main fjord set the pace for retreat of the ice margin in Sikuijuitsoq Fjord. Initially, Jakobshavn Isfjord was filled with glacial ice, preventing sea water from coming in contact with the ice margin in Sikuijuitsoq Fjord. However, as the grounding line progressed up Jakobshavn Isfjord and past the intersection with the tributary, sea water would have entered the mouth of Sikuijuitsoq Fjord, causing the ice margin to float. This conversion to a marine-based ice margin may have initiated fast retreat in Sikuijuitsoq Fjord, which continued at least until the margin reached its present-day position.

The data from this study imply that a major reorganization of Jakobshavn Isbræ ice flow occurred over a very short time period in the early Holocene. Between the time of deposition of the inner Fjord Stade moraine and the time when the ice retreated behind the position of the historic moraine, the vertical and horizontal extent of ice changed significantly. The ice margin retreated several tens of km horizontally at rates of ~100 m yr^{-1}, and lowered at rates too rapid to be measured using ^{10}Be. During this period, the retreating margin exposed two distinct fjords, each containing tongues of ice that flowed independently as they do today.

5.6. Paleoclimatic Context

Retreat of the ice margin at Sikuijuitsoq Fjord was likely driven by external climate forcing and occurred simultaneously with ice retreat elsewhere in Greenland and around the world. Retreat of the ice margin through Disko Bugt and onto land ~10.3-10.2

ka coincided with rising mean annual temperatures in central Greenland (Dahl-Jensen et al., 1998; Vinther et al., 2009). Summer temperatures may have been as much as 5°C warmer than today on Baffin Island (Axford et al., 2009). [10]Be ages inboard of the Fjord Stade moraine complex constrain the deposition of the moraines to before 8.2 ± 0.1 ka. Although the age constraint is a minimum, it is likely a close constraint on deposition of the inner (Tasiussaq) Fjord Stade moraine (Young et al., 2011), and suggests that the Tasiussaq moraine in this region may represent a response of the ice sheet margin to the 8.2 ka event (Alley et al., 1997; Young et al., 2011). Retreat of the Sikuijuitsoq ice margin between ~8.2 and ~7.6 ka to a location behind the historic moraine corresponded to increasing regional temperatures inferred from boreholes at the GRIP and DYE-3 ice core sites (Dahl-Jensen et al., 1998). A local temperature reconstruction depicts summers that were 2°C warmer than modern between ~6 and 4.5 cal yr BP (Young et al., 2011), indicating that ice cover may have been substantially more reduced than today during this time period (Weidick et al., 1990). The [10]Be ages presented in this study and in Young et al. (2011) demonstrate that the Sikuijuitsoq and Jakobshavn ice margins retreated from the Tasiussaq moraine, through their fjords, and behind the historic moraine in unison. This synchroneity suggests a common climatic forcing mechanism that dictated ice margin fluctuations in the Jakobshavn region during the Holocene.

5.7. Ice Margin Retreat Rate Comparisons

The rate of ice margin retreat (~100 m yr^{-1}) at Sikuijuitsoq Fjord (after the abandonment of the Tasiussaq moraine at 8.0 ka, and before the ice margin retreated behind the historic moraine ~7.6 ka) is similar to other estimated retreat rates in the area

for the same time period. At ~10.3 ka, before ice retreat began in Jakobshavn Isfjord and Sikuijuitsoq Fjord, the margin retreated across Disko Bugt primarily via calving at ~110 m yr^{-1} (Long and Roberts, 2003; Long et al., 2006). In Jakobshavn Isfjord itself, [10]Be ages indicate that Jakobshavn Isbræ retreated through the entire length of the fjord between ~8.0 and 7.5 ka, at a rate of ~100 m yr^{-1} (Young et al., 2011).

Modern retreat rates (since the Little Ice Age) in Jakobshavn Isfjord have been more rapid and variable. Retreat rates of the floating tongue of Jakobshavn Isbræ have been erratic over the past ~150 years, and have been punctuated by several episodes of rapid ice loss (Csatho et al., 2008). Significant retreat (~20-25 km) occurred between 1850 and 1946 (Csatho et al., 2008), yielding integrated retreat rates of ~200-250 m yr^{-1}. After a period of stability between 1946 and 1998, the floating tongue retreated another ~20 km between 1999 and 2004 (Csatho et al., 2008), yielding retreat rates over an order of magnitude faster than between 1850 and 1946. However, comparison between geologic and modern rates can be misleading, as the duration of observation at least in part controls the inferred rate of retreat (Gardner et al., 1987). It is possible that, in the early Holocene, Sikuijuitsoq Fjord behaved in a similar fashion to Jakobshavn Isfjord today, alternating between rapid and slow retreat, and yielding longer-term integrated rates of ~100 m yr^{-1}.

The retreat rate we calculate for the ice margin in Sikuijuitsoq Fjord falls in the mid-range of ice margin retreat rates that have been documented for large, high-latitude bodies of ice both in Greenland and elsewhere (Fig. 9). In Sisimiut Fjord (central western Greenland; Fig. 1), retreat rates were ~48 m yr^{-1} between 12.4 and 8.3 ka, and ~18 m yr^{-1} between 8.3 and 4.5 ka (Rinterknecht et al., 2009). During the collapse of the Laurentide

Ice Sheet between 12.0 and 7.0 ka, retreat rates calculated from reduction in ice sheet area are ~260 m yr^{-1}, although these rates range from 80 to 360 m yr^{-1} (Andrews, 1973). While numerous explanations exist for rapid retreat of the Laurentide Ice Sheet margin, it is likely that mass loss through calving of a marine-based margin played an important role, since ~56% of the former ice-covered area had become proglacial lake or sea (Andrews, 1973). On Baffin Island, a marine-based ice margin retreated at a minimum rate of ~58 m yr^{-1} through Sam Ford Fjord ~9.5 ka, and then slowed to ~5 m yr^{-1} when it became grounded at head of the fjord (Briner et al., 2009). Large, calving-dominated outlet glaciers in Alaska have exhibited very rapid retreat rates over the past 100 years, including 350 m yr^{-1} for the McCarthy Glacier (Wiles and Calkin, 1993) and 500 m yr^{-1} for the Icy Bay glacier system (Porter, 1989). However, comparison with these modern-day Alaskan glaciers may suffer from the same duration of observation bias described above.

The variability in ice margin retreat rates discussed above cannot be attributed to a single factor. This variability may be caused by retreat style (e.g. surface ablation versus calving), fjord geometry, ice flow patterns (e.g. influence from nearby ice streams), external forcings (e.g. warm ocean currents), or the duration of observation. The large temporal gap in between the two populations of data (Fig. 9) is likely because global ice cover was not rapidly declining in the middle and late Holocene, and ice margin retreat rates from this time period are underrepresented in the literature. Modern rates of ice margin retreat are appreciably higher than those in the early Holocene; however, it is not possible to determine whether this difference is due to the duration of observation bias or to real differences in climate forcings.

6. Conclusions

^{10}Be concentrations in bedrock and boulders near Sikuijuitsoq Fjord reflect erosion efficiency over the last glaciation as well as the timing and process of deglaciation. Paired bedrock and boulder samples indicate that nuclides inherited from prior periods of cosmic ray exposure are only present in bedrock exposed in the early Holocene and covered for too short a period later in the Holocene to erode the surface effectively. Otherwise, the large number of concordant bedrock and boulder ages indicate clearly that this area has been subjected to subglacial erosion rates sufficiently high to remove at least several meters of rock between major interglaciations. Deglaciation in this region was punctuated by episodes of re-advance, resulting in a complex distribution of ^{10}Be concentrations; an initial episode of retreat exposed the outer land surface and some of the inner land surface ~10.3 ± 0.4 ka (n = 7); a subsequent episode of retreat exposed the inner land surface ~8.0 ± 0.7 ka (n = 21), after the deposition of the Fjord Stade moraine complex. The ice margin ultimately retreated behind the position of the historic moraine ~7.6 ka. Data from this study, as well as the spatial and altitudinal distribution of landscape features, suggest that ice surface lowering at each individual dipstick took place too rapidly to measure with ^{10}Be, likely within several hundred years. Lateral ice margin retreat was also rapid, at rates of ~100 m yr^{-1}. The data indicate that a rapid reorganization of the Jakobshavn Isbræ drainage took place during the early Holocene, following the abandonment of the Fjord Stade moraine complex. Comparison of data from Sikuijuitsoq Fjord and Jakobshavn Isfjord suggests that retreat of Jakobshavn Isbræ set the timing and pace of deglaciation of the surrounding ice margin.

Acknowledgements

References

Alley, R., Anandakrishnan, S., Dupont, T., Parizek, B., Pollard, D., 2007. Effect of sedimentation on ice-sheet grounding-line stability. Science 315, 1838-1841.

Alley, R., Andrews, J., Brigham-Grette, J., Clarke, G., Cuffey, K., Fitzpatrick, J., Funder, S., Marshall, S., Miller, G., Mitrovica, J., 2010. History of the Greenland Ice Sheet: paleoclimatic insights. Quaternary Science Reviews 29, 1728-1756.

Alley, R., Mayewski, P., Sowers, T., Stuiver, M., Taylor, K., Clark, P., 1997. Holocene climatic instability: a prominent, widespread event 8200 yr ago. Geology 25, 483-486.

Andrews, J., 1973. The Wisconsin Laurentide ice sheet: dispersal centers, problems of rates of retreat, and climatic implications. Arctic and Alpine Research 5, 185-199.

Axford, Y., Briner, J., Miller, G., Francis, D., 2009. Paleoecological evidence for abrupt cold reversals during peak Holocene warmth on Baffin Island, Arctic Canada. Quaternary Research 71, 142-149.

Balco, G., 2011. Contributions and unrealized potential contributions of cosmogenic-nuclide exposure dating to glacier chronology, 1990-2010. Quaternary Science Reviews 30, 3-27.

Balco, G., Briner, J., Finkel, R., Rayburn, J., Ridge, J., Schaefer, J., 2009. Regional beryllium-10 production rate calibration for late-glacial northeastern North America. Quaternary Geochronology 4, 93-107.

Balco, G., Stone, J., Lifton, N., Dunai, T., 2008. A complete and easily accessible means of calculating surface exposure ages or erosion rates from ^{10}Be and ^{26}Al measurements. Quaternary Geochronology 3, 174-195.

Bentley, C., 1987. Antarctic ice streams: a review. Journal of Geophysical Research 92, 8843-8858.

Bierman, P., 1994. Using in situ produced cosmogenic isotopes to estimate rates of landscape evolution: A review from the geomorphic perspective. Journal of Geophysical Research 99, 13885-13896.

Bierman, P., Marsella, K., Patterson, C., Davis, P., Caffee, M., 1999. Mid-Pleistocene cosmogenic minimum-age limits for pre-Wisconsinan glacial surfaces in southwestern Minnesota and southern Baffin Island: a multiple nuclide approach. Geomorphology 27, 25-39.

Bougamont, M., Tulaczyk, S., 2003. Glacial erosion beneath ice streams and ice stream tributaries: constraints on temporal and spatial distribution of erosion from numerical simulations of a West Antarctic ice stream. Boreas 32, 178-190.

Briner, J., Bini, A., Anderson, R., 2009. Rapid early Holocene retreat of a Laurentide outlet glacier through an Arctic fjord. Nature Geoscience 2, 496-499.

Briner, J., Miller, G., Davis, P., Bierman, P., Caffee, M., 2003. Last Glacial Maximum ice sheet dynamics in Arctic Canada inferred from young erratics perched on ancient tors. Quaternary Science Reviews 22, 437-444.

Briner, J., Stewart, H., Young, N., Phillips, W., Losee, S., 2010. Using proglacial-threshold lakes to constrain fluctuations of the Jakobshavn Isbræ ice margin, western Greenland, during the Holocene. Quaternary Science Reviews 29, 3861-3874.

Briner, J., Swanson, T., 1998. Using inherited cosmogenic ^{36}Cl to constrain glacial erosion rates of the Cordilleran ice sheet. Geology 26, 3-6.

Corbett, L., Bierman, P., Graly, J., Neumann, T., Rood, D., Finkel, R., 2009. In situ cosmogenic ^{10}Be estimates of deglaciation timing and glacial erosion efficiency, western Greenland. Geological Society of America Abstracts with Programs 41, 621.

Csatho, B., Schenk, T., Van der Veen, C., Krabill, W., 2008. Intermittent thinning of Jakobshavn Isbræ, West Greenland, since the Little Ice Age. Journal of Glaciology 54, 131-144.

Cuffey, K., Marshall, S., 2000. Substantial contribution to sea-level rise during the last interglacial from the Greenland ice sheet. Nature 404, 591-594.

Dahl-Jensen, D., Mosegaard, K., Gundestrup, N., Clow, G., Johnsen, S., Hansen, A., Balling, N., 1998. Past temperatures directly from the Greenland Ice Sheet. Science 282, 268-271.

Delmas, M., Gunnell, Y., Braucher, R., Calvet, M., Bourles, D., 2008. Exposure age chronology of the last glaciation in the eastern Pyrenees. Quaternary Research 69, 231-241.

Fabel, D., Harbor, J., 1999. The use of in-situ produced cosmogenic radionuclides in glaciology and glacial geomorphology. Annals of Glaciology 28, 103-110.

Gardner, T., Jorgensen, D., Shuman, C., Lemieux, C., 1987. Geomorphic and tectonic process rates: Effects of measured time interval. Geology 15, 259-261.

Gosse, J., Phillips, F., 2001. Terrestrial in situ cosmogenic nuclides: theory and application. Quaternary Science Reviews 20, 1475-1560.

Håkansson, L., Alexanderson, H., Hjort, C., Moller, P., Briner, J., Aldahan, A., Possnert, G., 2008. Late Pleistocene glacial history of Jameson Land, central East Greenland, derived from cosmogenic ^{10}Be and ^{26}Al exposure dating. Boreas 38, 244-260.

Harbor, J., Stroeven, A., Fabel, D., Clarhäll, A., Kleman, J., Li, Y., Elmore, D., Fink, D., 2006. Cosmogenic nuclide evidence for minimal erosion across two subglacial sliding boundaries of the late glacial Fennoscandian ice sheet. Geomorphology 75, 90-99.

Heyman, J., Stroeven, A., Harbor, J., Caffee, M., 2010. Too young or too old: Evaluating cosmogenic exposure dating based on an analysis of compiled boulder exposure ages. Earth and Planetary Science Letters 302, 71-80.

Holland, D., Thomas, R., De Young, B., Ribergaard, M., Lyberth, B., 2008. Acceleration of Jakobshavn Isbræ triggered by warm subsurface ocean waters. Nature Geoscience 1, 659-664.

Hunt, A., Larsen, J., Bierman, P., Petrucci, G., 2008. Investigation of factors that affect the sensitivity of accelerator mass spectrometry for cosmogenic ^{10}Be and ^{26}Al isotope analysis. Analytical Chemistry 80, 1656-1663.

IPCC, 2007. Climate Change 2007: The Physical Science Basis. Contribution of Working Group I to the Fourth Assessment Report of the Intergovernmental Panel on Climate Change. Cambridge University Press.

Kelly, M., Lowell, T., Hall, B., Schaefer, J., Finkel, R., Goehring, B., Alley, R., Denton, G., 2008. A [10]Be chronology of lateglacial and Holocene mountain glaciation in the Scoresby Sund region, east Greenland: implications for seasonality during lateglacial time. Quaternary Science Reviews 27, 2273-2282.

Kohl, C., Nishiizumi, K., 1992. Chemical isolation of quartz for measurement of in-situ-produced cosmogenic nuclides. Geochimica et Cosmochimica Acta 56, 3583-3587.

Lal, D., 1991. Cosmic ray labeling of erosion surfaces: in situ nuclide production rates and erosion models. Earth and Planetary Science Letters 104, 424-439.

Letréguilly, A., Reeh, N., Huybrechts, P., 1991. The Greenland ice sheet through the last glacial-interglacial cycle. Global and Planetary Change 4, 385-394.

Lilly, K., Fink, D., Fabel, D., Lambeck, K., 2010. Pleistocene dynamics of the interior of the East Antarctic ice sheet. Geology 38, 703-706.

Lisiecki, L., Raymo, M., 2005. A Plio-Pleistocene stack of 57 globally distributed benthic [18]O records. Paleoceanography 20, 522–533.

Lloyd, J., Park, L., Kuijpers, A., Moros, M., 2005. Early Holocene palaeoceanography and deglacial chronology of Disko Bugt, West Greenland. Quaternary Science Reviews 24, 1741-1755.

Long, A., 2009. Back to the future: Greenland's contribution to sea-level change. GSA Today 19, 4-10.

Long, A., Roberts, D., 2002. A revised chronology for the 'Fjord Stade' moraine in Disko Bugt, West Greenland. Journal of Quaternary Science 17, 561-579.

Long, A., Roberts, D., 2003. Late Weichselian deglacial history of Disko Bugt, West Greenland, and the dynamics of the Jakobshavns Isbrae ice stream. Boreas 32, 208-226.

Long, A., Roberts, D., Dawson, S., 2006. Early Holocene history of the West Greenland Ice Sheet and the GH-8.2 event. Quaternary Science Reviews 25, 904-922.

Marquette, G., Gray, J., Gosse, J., Courchesne, F., Stockli, L., Macpherson, G., Finkel, R., 2004. Felsenmeer persistence under non-erosive ice in the Torngat and Kaumajet mountains, Quebec and Labrador, as determined by soil weathering and cosmogenic nuclide exposure dating. Canadian Journal of Earth Sciences 41, 19-38.

Marsella, K., Bierman, P., Davis, P., Caffee, M., 2000. Cosmogenic [10]Be and [26]Al ages for the last glacial maximum, eastern Baffin Island, Arctic Canada. Geological Society of America Bulletin 112, 1296-1312.

Nishiizumi, K., Imamura, M., Caffee, M., Southon, J., Finkel, R., McAninch, J., 2007. Absolute calibration of [10]Be AMS standards. Nuclear Instruments and Methods in Physics Research Section B: Beam Interactions with Materials and Atoms 258, 403-413.

Otto-Bliesner, B., Marshall, S., Overpeck, J., Miller, G., Hu, A., 2006. Simulating Arctic climate warmth and icefield retreat in the last interglaciation. Science 311, 1751-1753.

Pallas, R., Rodes, A., Braucher, R., Carcaillet, J., Ortuno, M., Bordonau, J., Bourles, D., Vilaplana, J., Masana, E., Santanach, P., 2006. Late Pleistocene and Holocene glaciation in the Pyrenees: a critical review and new evidence from [10]Be exposure ages, south-central Pyrenees. Quaternary Science Reviews 25, 2937-2963.

Phillips, F., Zreda, M., Smith, S., Elmore, D., Kubik, P., Sharma, P., 1990. Cosmogenic chlorine-36 chronology for glacial deposits at Bloody Canyon, eastern Sierra Nevada. Science 248, 1529-1532.

Porter, S., 1989. Late Holocene fluctuations of the fiord glacier system in Icy Bay, Alaska, USA. Arctic and Alpine Research 21, 364-379.

Rinterknecht, V., Gorokhovich, Y., Schaefer, J., Caffee, M., 2009. Preliminary [10]Be chronology for the last deglaciation of the western margin of the Greenland Ice Sheet. Journal of Quaternary Science 24, 270-278.

Roberts, D., Long, A., 2005. Streamlined bedrock terrain and fast ice flow, Jakobshavns Isbrae, West Greenland: implications for ice stream and ice sheet dynamics. Boreas 34, 25-42.

Rood, D., Hall, S., Guilderson, T., Finkel, R., Brown, T., 2010. Challenges and opportunities in high-precision Be-10 measurements at CAMS. Nuclear Instruments and Methods in Physics Research Section B: Beam Interactions with Materials and Atoms 268, 730-732.

Schildgen, T., Phillips, W., Purves, R., 2005. Simulation of snow shielding corrections for cosmogenic nuclide surface exposure studies. Geomorphology 64, 67-85.

Smith, A., Murray, T., Nicholls, K., Makinson, K., Adalgeirsdottir, G., Behar, A., Vaughan, D., 2007. Rapid erosion, drumlin formation, and changing hydrology beneath an Antarctic ice stream. Geology 35, 127-130.

Smith, J., Finkel, R., Farber, D., Rodbell, D., Seltzer, G., 2005. Moraine preservation and boulder erosion in the tropical Andes: interpreting old surface exposure ages in glaciated valleys. Journal of Quaternary Science 20, 735-758.

Stone, J., 2000. Air pressure and cosmogenic isotope production. Journal of Geophysical Research 105, 23753-23759.

Stone, J., Balco, G., Sugden, D., Caffee, M., Sass III, L., Cowdery, S., Siddoway, C., 2003. Holocene deglaciation of Marie Byrd Land, West Antarctica. Science 299, 99-102.

Stroeven, A., Fabel, D., Hättestrand, C., Harbor, J., 2002. A relict landscape in the centre of Fennoscandian glaciation: cosmogenic radionuclide evidence of tors preserved through multiple glacial cycles. Geomorphology 44, 145-154.

Sugden, D., Balco, G., Cowdery, S., Stone, J., Sass III, L., 2005. Selective glacial erosion and weathering zones in the coastal mountains of Marie Byrd Land, Antarctica. Geomorphology 67, 317-334.

Vinther, B., Buchardt, S., Clausen, H., Dahl-Jensen, D., Johnsen, S., Fisher, D., Koerner, R., Raynaud, D., Lipenkov, V., Andersen, K., 2009. Holocene thinning of the Greenland ice sheet. Nature 461, 385-388.

Weidick, A., 1968. Observations on some Holocene glacier fluctuations in West Greenland. *Medd. om Gronland* 165(6), 194 pp.

Weidick, A., Bennike, O., 2007. Quaternary glaciation history and glaciology of Jakobshavn Isbræ and the Disko Bugt region, west Greenland: a review. Geologic Survey of Denmark and Greenland Bulletin 14, 1-13.

Weidick, A., Oerter, H., Reeh, N., Thomsen, H., Thorning, L., 1990. The recession of the Inland Ice margin during the Holocene climatic optimum in the Jakobshavn Isfjord area of West Greenland. Global and Planetary Change 2, 389-399.

Wiles, G., Calkin, P., 1993. Neoglacial fluctuations and sedimentation of an iceberg-calving glacier resolved with tree rings (Kenai Fjords National Park, Alaska). Quaternary International 18, 35-42.

Young, N., Briner, J., Stewart, H., Axford, Y., Csatho, B., Rood, D., Finkel, R., 2011. Response of Jakobshavn Isbrae, Greenland, to Holocene climate change. Geology 39, 131-134.

Sample Name	Sample Type	Dipstick Number	Land Surface	Elevation (m)	Latitude (°N)[a]	Longitude (°E)[a]	Thickness (cm)	Quartz (g)	9Be (ug)[b]	10Be/9Be Ratio[c]	Uncertainty[d]	10Be Conc (atoms/g)	Exposure Age (ka)[e]	Uncertainty (ka)[d]
GL022	Bedrock	1	Inner	515	69.432	-50.289	5	20.60	247	6.90×10^{-14}	1.28×10^{-15}	5.54×10^{4}	8.0	0.1
GL023	Boulder	1	Inner	511	69.433	-50.289	3	19.86	248	6.41×10^{-14}	1.41×10^{-15}	5.35×10^{4}	7.6	0.2
GL001	Bedrock	1	Inner	434	69.433	-50.272	1	19.39	247	5.43×10^{-14}	1.58×10^{-15}	4.62×10^{4}	6.9	0.2
GL002	Boulder	1	Inner	432	69.433	-50.273	2	19.90	247	5.85×10^{-14}	1.37×10^{-15}	4.86×10^{4}	7.4	0.2
GL003	Bedrock	1	Inner	395	69.434	-50.266	3	19.86	248	5.67×10^{-14}	1.43×10^{-15}	4.73×10^{4}	7.5	0.2
GL004	Boulder	1	Inner	392	69.434	-50.266	2	20.46	248	6.16×10^{-14}	1.47×10^{-15}	4.99×10^{4}	7.9	0.2
GL080	Bedrock	2	Inner	621	69.395	-50.416	3	17.58	247	6.58×10^{-14}	1.47×10^{-15}	6.18×10^{4}	7.9	0.2
GL081	Boulder	2	Inner	618	69.395	-50.416	1.5	18.96	247	6.90×10^{-14}	1.30×10^{-15}	6.01×10^{4}	7.6	0.1
GL086	Bedrock	2	Inner	304	69.374	-50.458	2.5	20.26	247	5.26×10^{-14}	1.35×10^{-15}	4.28×10^{4}	7.4	0.2
GL087	Boulder	2	Inner	303	69.374	-50.458	2	19.99	248	5.38×10^{-14}	1.16×10^{-15}	4.45×10^{4}	7.7	0.2
GL088	Bedrock	2	Inner	95	69.344	-50.429	2.5	16.59	249	4.38×10^{-14}	1.05×10^{-15}	3.49×10^{4}	7.5	0.2
GL089	Boulder	2	Inner	93	69.344	-50.429	2.5	19.22	247	4.20×10^{-14}	9.41×10^{-16}	3.61×10^{4}	7.8	0.2
GL103	Bedrock	3	Inner	578	69.318	-50.640	1	19.63	247	8.19×10^{-14}	2.04×10^{-15}	6.89×10^{4}	9.0	0.2
GL104	Boulder	3	Inner	578	69.318	-50.640	5	19.89	247	7.54×10^{-14}	1.44×10^{-15}	6.26×10^{4}	8.5	0.2
GL105	Bedrock	3	Inner	300	69.293	-50.602	1	17.00	246	4.81×10^{-14}	1.11×10^{-15}	4.65×10^{4}	8.0	0.2
GL106	Boulder	3	Inner	300	69.293	-50.602	2	20.63	247	5.71×10^{-14}	1.18×10^{-15}	4.58×10^{4}	7.9	0.2
GL090	Bedrock	3	Inner	93	69.269	-50.581	2	20.64	252	4.92×10^{-14}	1.03×10^{-15}	4.02×10^{4}	8.6	0.2
GL091	Boulder	3	Inner	91	69.269	-50.582	2	10.65	248	2.32×10^{-14}	6.41×10^{-16}	3.61×10^{4}	7.8	0.2
GL096	Bedrock	4	Outer	468	69.250	-50.823	3	15.28	247	6.72×10^{-14}	1.29×10^{-15}	7.27×10^{4}	10.8	0.2
GL097	Boulder	4	Outer	470	69.251	-50.822	2	16.35	247	6.54×10^{-14}	1.70×10^{-15}	6.62×10^{4}	9.7	0.3
GL094	Boulder	4	N/A[f]	308	69.229	-50.810	1	13.33	247	4.43×10^{-14}	1.16×10^{-15}	5.49×10^{4}	9.3	0.2
GL095	Bedrock	4	N/A[f]	308	69.229	-50.810	2.5	21.49	247	6.00×10^{-14}	1.68×10^{-15}	4.61×10^{4}	7.9	0.2
GL098	Bedrock	4	Inner	163	69.199	-50.791	3	16.76	248	5.04×10^{-14}	1.08×10^{-15}	4.97×10^{4}	10.0	0.2
GL092	Boulder	5	Outer	397	69.230	-50.902	1	20.14	248	8.01×10^{-14}	1.59×10^{-15}	6.59×10^{4}	10.3	0.2
GL093	Bedrock	5	Outer	397	69.230	-50.902	2	18.94	246	7.71×10^{-14}	1.94×10^{-15}	6.69×10^{4}	10.5	0.3
GL100	Boulder	5	Outer	292	69.227	-50.930	2	15.53	247	5.60×10^{-14}	1.22×10^{-15}	5.95×10^{4}	10.4	0.2
GL101	Bedrock	5	Outer	295	69.227	-50.929	3.5	20.19	247	6.87×10^{-14}	1.30×10^{-15}	5.62×10^{4}	9.9	0.2
GL107	Bedrock	5	Inner	53	69.180	-50.891	1	20.68	248	4.57×10^{-14}	1.01×10^{-15}	3.66×10^{4}	8.1	0.2
GL108	Boulder	5	Inner	53	69.180	-50.891	1	15.14	249	3.39×10^{-14}	9.32×10^{-16}	3.73×10^{4}	8.3	0.2
GL102	Bedrock	6	Outer	85	69.207	-51.134	1	19.65	247	5.70×10^{-14}	1.27×10^{-15}	4.79×10^{4}	10.3	0.2

[a] Locations and elevations were recorded in the field with a Garmin GPS-12.

[b] Samples were prepared with a low-level beryl carrier of 245 ppm concentration.

[c] Ratios were measured at the Lawrence Livermore National Laboratory and were normalized to the standard 07KNSTD3110 (Nishiizumi et al., 2007). Reported ratios have already been blank-corrected (the blank ratios ranged from 4.4×10^{-16} to 1.0×10^{-15}, or 1-3% of the samples).

[d] Reported uncertainties are internal AMS uncertainties.

[e] Ages were calculated using the northeastern North American production rate and the Lal (1991)/Stone (2000) scaling scheme in the CRONUS Earth online calculator. Ages have been scaled for elevation, sample density, sample thickness, latitude, and longitude.

[f] This sample pair was collected in between the two Fjord Stade moraines, on neither the inner nor the outer land surface.

Table 1.

83

Figure 1.

Figure 2.

85
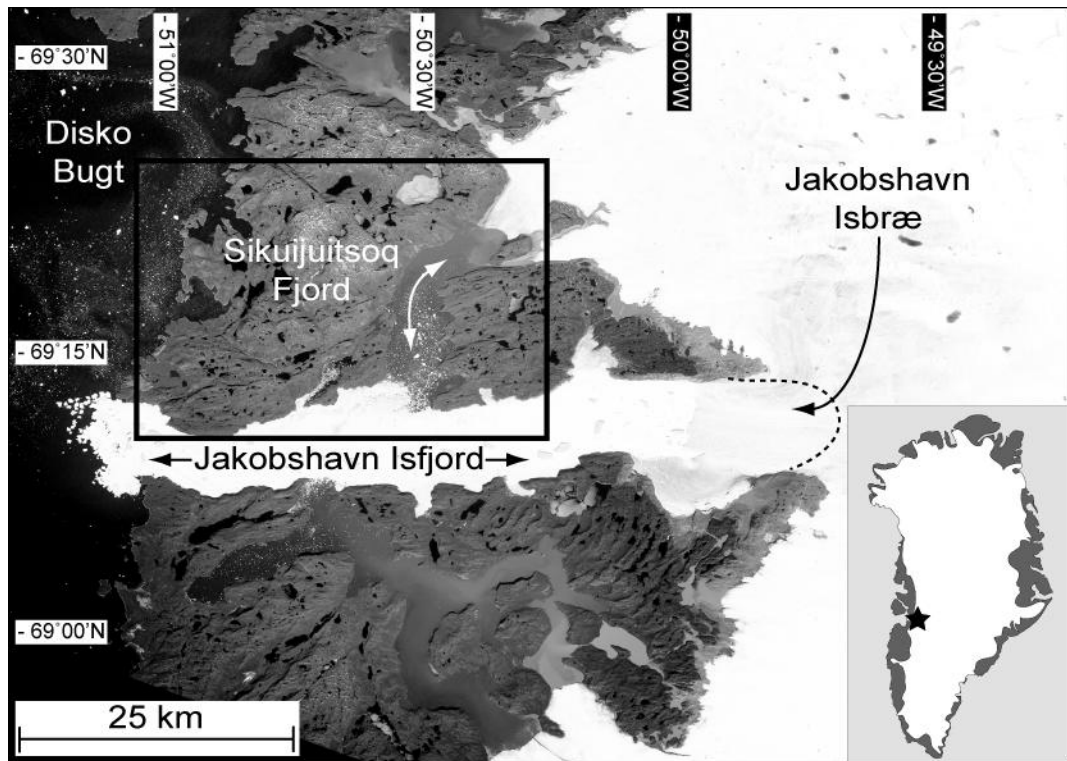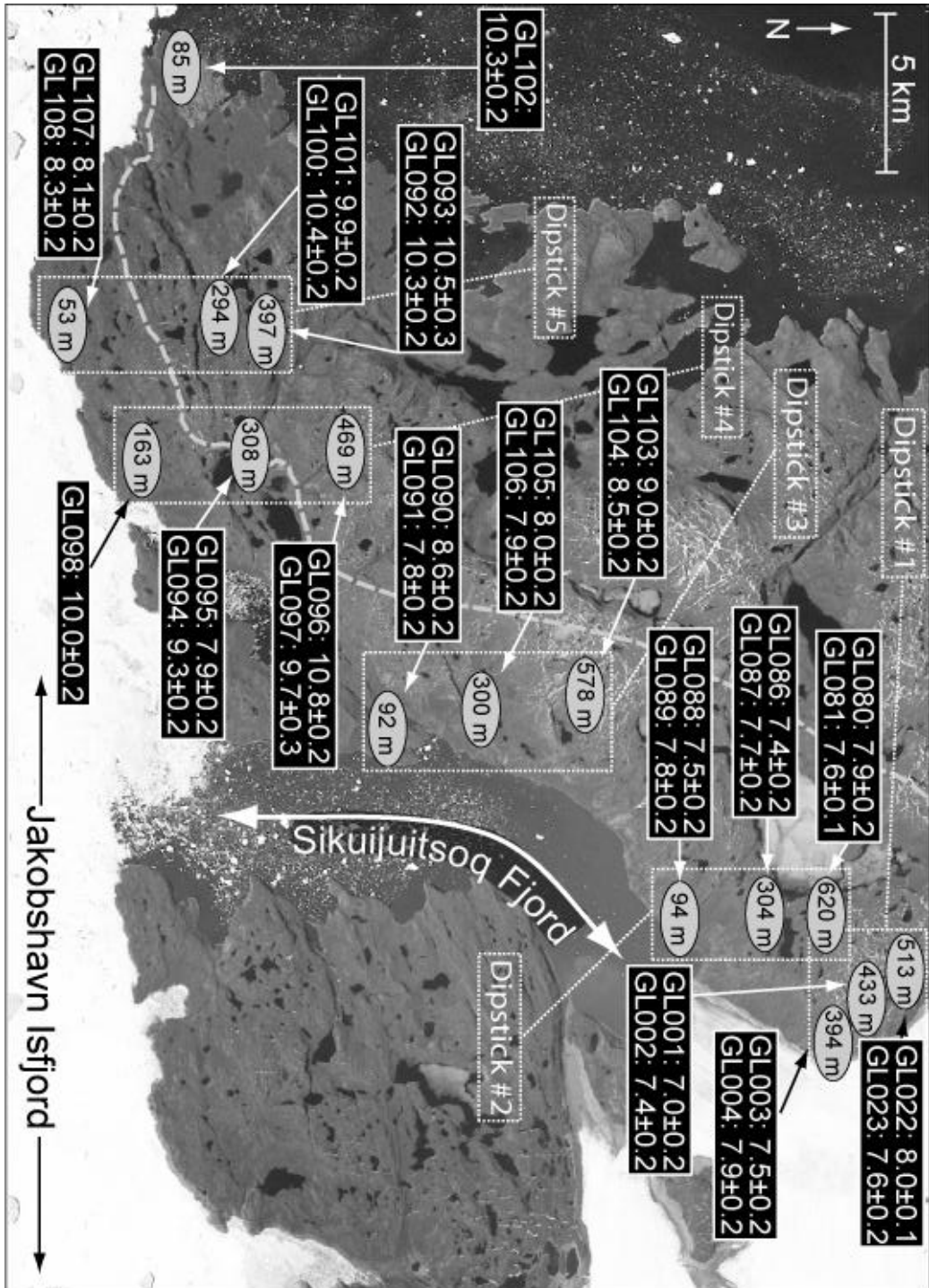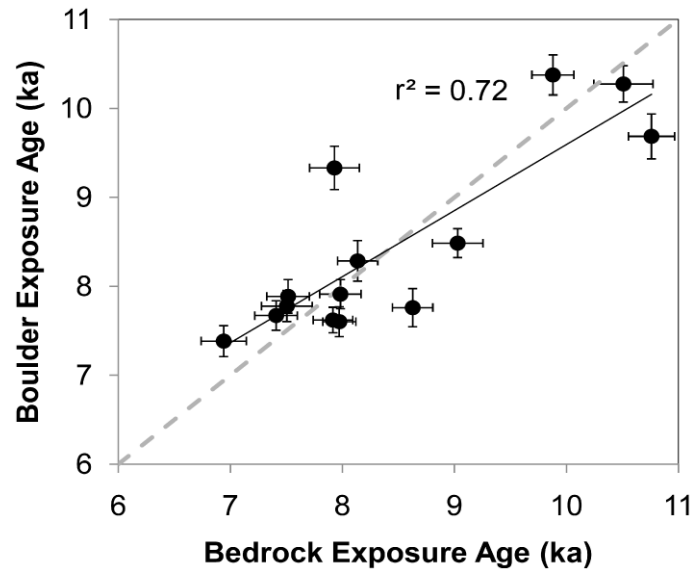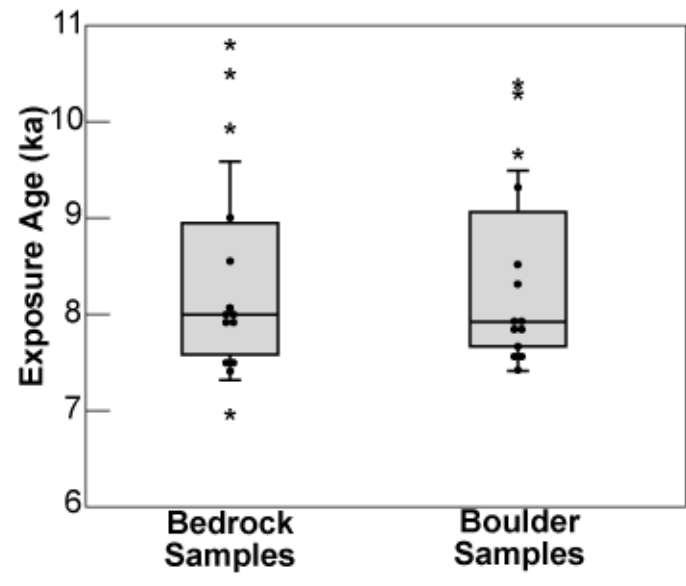
Figure 3.
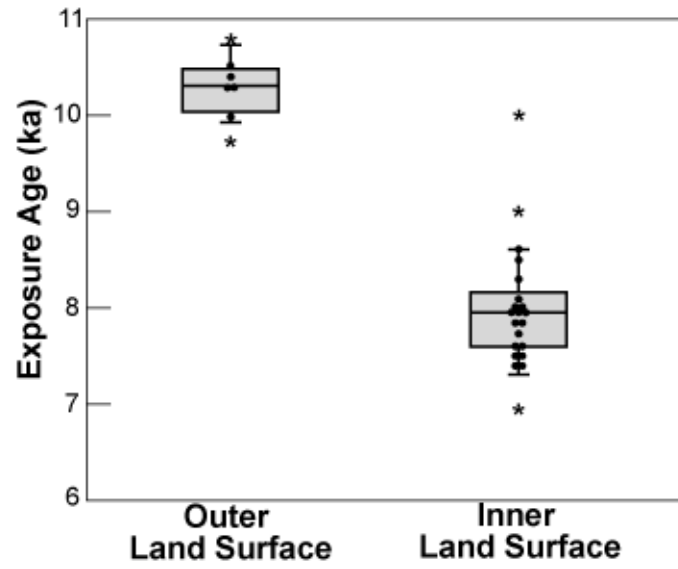
Figure 4.

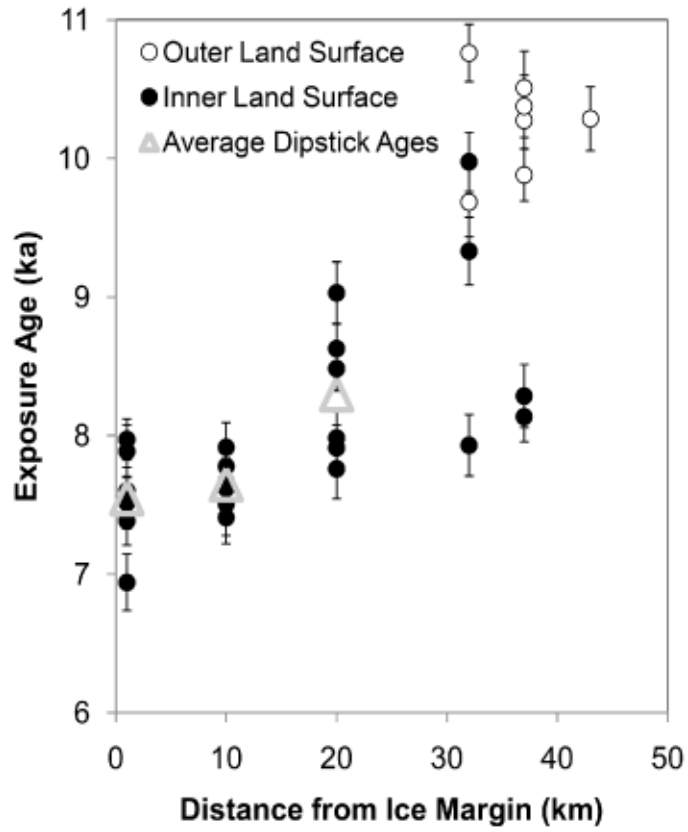**Figure 5.**
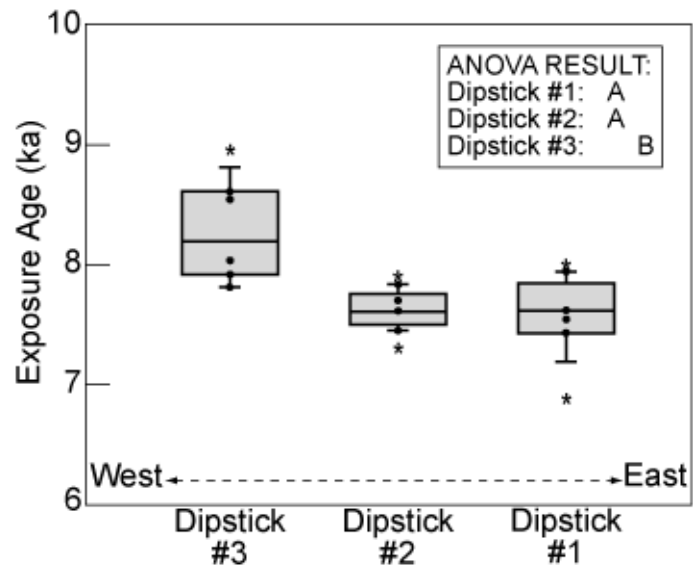
Figure 6.
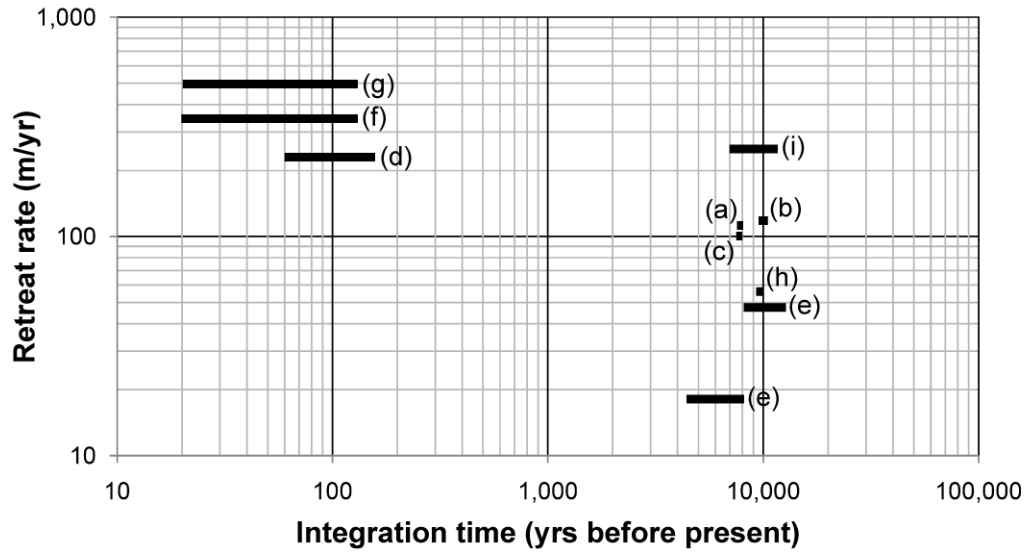
Figure 7.

Figure 8.

Figure 9.

Table Legends

Table 1. Sample collection and laboratory information for 16 bedrock samples and 14 boulder samples at Sikuijuitsoq Fjord. Samples were collected in six "dipsticks" at a range of elevations along a 40-km transect normal to the ice margin.

Figure Legends

Figure 1. Sikuijuitsoq Fjord is a northerly tributary of Jakobshavn Isfjord, located on the western margin of the Greenland Ice Sheet. Inset: Location of study area is shown by the star. Main image: Aerial imagery of Sikuijuitsoq Fjord, Jakobshavn Isfjord, and Jakobshavn Isbræ. The box indicates the area covered by Figure 2, and the black dashed line shows the approximate modern location of the calving margin of Jakobshavn Isbræ (Csatho et al., 2008). Image courtesy of the National Survey and Cadastre of Denmark.

Figure 2. Bedrock and boulder samples were collected along a 40-km transect north of Jakobshavn Isfjord, parallel to the northern tributary Sikuijuitsoq Fjord. Wherever possible, bedrock/boulder pairs were taken from high, medium, and low elevations shown by gray ovals. At each sampling location, model ^{10}Be ages are shown (expressed in ka, with 1σ internal error), with the bedrock sample listed first and the boulder sample listed second; in the two instances where boulders were not available, only the bedrock ^{10}Be ages are listed. The gray dashed line shows the approximate location of the Fjord Stade moraine complex. Image courtesy of the National Survey and Cadastre of Denmark.

Figure 3. The land surface surrounding Sikuijuitsoq Fjord is characterized by striated, sculpted bedrock outcrops and ubiquitous erratic boulders. There is negligible till cover. Here, a sample (GL091) is collected from a large boulder lying directly on ice-sculpted bedrock.

Figure 4. Bedrock and boulder ages at sample sites are correlated with a slope of 0.74 ($r^2 = 0.72$). The dashed gray line represents a 1:1 ratio between bedrock and boulder sample ages, and the solid line is the linear regression. Error bars show 1σ internal error.

Figure 5. Box and whisker plots of bedrock and boulder age populations. The box encloses the area between the first and third quartiles, and the horizontal line represents the median. Whiskers show one standard deviation. Samples that lie outside one standard deviation from the mean are shown with an asterisk; all other samples are shown with dots.

Figure 6. Box and whisker plots of sample age populations from the land surfaces outside and inside of the Fjord Stade moraine complex. The box encloses the area between the first and third quartiles, and the horizontal line represents the median. Whiskers show one standard deviation. Samples that lie outside one standard deviation from the mean are shown with an asterisk; all other samples are shown with dots.

Figure 7. ^{10}Be ages of bedrock and boulder samples plotted against distance from the present-day ice sheet margin. Bars show 1σ internal error. Sample ^{10}Be ages show an overall decreasing trend towards the present-day ice sheet margin. Average dipstick ages have been calculated for the three inner-most dipsticks, which do not cross-cut the Fjord Stade moraine complex.

Figure 8. Box and whisker plots of sample age populations from the three eastern-most dipsticks, which do not crosscut the Fjord Stade moraine complex. The box encloses the area between the first and third quartiles, and the horizontal line represents the median. Whiskers show one standard deviation. Samples that lie outside one standard deviation from the mean are shown with an asterisk; all other samples are shown with dots. ANOVA results are shown in the upper right.

Figure 9. Compilation of lateral ice margin retreat rates from studies that investigated large bodies of ice at high latitudes (see section 5.6), including: (a) Sikuijuitsoq Fjord, West Greenland (this study); (b) Disko Bugt, West Greenland (Long and Roberts, 2003); (c) Jakobshavn Isfjord, West Greenland (Young et al., 2011); (d) Jakobshavn Isfjord, West Greenland (Csatho et al., 2008); (e) Sisimiut Fjord, West Greenland (Rinterknecht et al., 2009); (f) McCarthy Glacier, Alaska, USA (Wiles and Calkin, 1993); (g) Icy Bay Glacier System, Alaska, USA (Porter, 1989); (h) Sam Ford Fjord, Baffin, Canada (Briner et al., 2009); and (i) Laurentide Ice Sheet, USA (Andrews, 1973).

CONSTRAINING LANDSCAPE HISTORY WITH [10]BE AND [26]AL IN PAIRED BEDROCK AND BOULDER SAMPLES, UPERNAVIK, CENTRAL-WESTERN GREENLAND

Lee B. Corbett*[1]
Paul R. Bierman[1]
Joseph A. Graly[1]
Thomas A. Neumann[2]
Dylan H. Rood[3,4]
Robert C. Finkel[3]

[1]Department of Geology, University of Vermont, Burlington, VT 05405
[2]NASA Goddard Space Flight Center, Cryospheric Sciences Branch, Greenbelt, MD 20770
[3]Center for Accelerator Mass Spectrometry, Lawrence Livermore National Laboratory, Livermore, CA 94550
[4]Earth Research Institute, University of California, Santa Barbara CA 93106
*Contact Author: Ashley.Corbett@uvm.edu, (802) 656-4411

Abstract

In order to investigate landscape history near Upernavik, northwest Greenland, we collected 33 paired bedrock and boulder samples for the analysis of *in situ* cosmogenic ^{10}Be and ^{26}Al. Samples were collected along a 100-km transect stretching from the present-day ice margin to the coast, at elevations up to 1000 m a.s.l. Minimum limiting single nuclide ages range from ~11 to 104 ka. Bedrock samples are significantly older than their corresponding boulder samples, and sample ages tend to increase with elevation. The prevalence of ^{10}Be inherited from previous periods of exposure, especially in bedrock samples at high elevation, indicates that these areas record long surface exposure histories. They were likely preserved beneath non-erosive cold-based ice or perennial snowfields after periods of near surface exposure to cosmic radiation. Minimum limiting two-isotope exposure durations range from 0.01 to 0.12 Ma, and minimum limiting burial durations range from 0 to 0.70 Ma. Minimum limiting total histories are as high as 0.8 Ma. The old total histories suggest that high-elevation surfaces have persisted at least since marine oxygen isotope stage 12. Because of high degrees of inheritance, few samples in this data set are useful for dating the latest Pleistocene deglaciation; only the six youngest boulder samples have overlapping ages at 1σ and appear to accurately record the timing of ice loss. These six samples provide an estimated deglaciation age of 11.3 ± 0.5 ka for the Upernavik coast. There appears to be little trend in deglaciation age along the length of the 100-km sample transect, and statistical simulations suggest that deglaciation took place rapidly at ~ 170 m yr^{-1}.

1. Introduction

Global ice volume and the extent of the Greenland Ice Sheet fluctuate greatly over glacial-interglacial cycles (Bintanja and Van De Wal, 2008; Lisiecki and Raymo, 2005); over the duration of the Quaternary, glacial ice may have come and gone from Greenland's coastal areas at least two dozen times. However, modeling results indicate that fluctuations in ice margin position were likely not uniform over space (Cuffey and Marshall, 2000; Letréguilly et al., 1991; Otto-Bliesner et al., 2006). Certain areas of the Greenland Ice Sheet are thought to have experienced significant reductions in volume during interglacial periods, while other areas, including near Upernavik (~73°N; Fig. 1), are thought to have lost less ice. Here, we use *in situ* produced terrestrial cosmogenic nuclides to study the glacial history of the Upernavik area in order to determine whether pronounced fluctuations in ice margin position occurred there during the past, to develop a chronology of deglaciation, and to make inferences about subglacial erosion efficiency.

Measurement of *in situ* produced cosmogenic nuclides can be employed to answer a wide array of questions about glacial geology and geomorphology (Balco, 2011; Fabel and Harbor, 1999). Cosmogenic nuclides, including ^{10}Be, ^{26}Al, and ^{36}Cl, can be used to determine the age of glacial moraine boulders, thereby constraining the timing of glaciation episodes (Phillips et al., 1990). Similar determination of exposure ages can also be applied to glacially sculpted bedrock, yielding information about landscape chronology and the timing of ice margin retreat (Nishiizumi et al., 1991). In areas where trimlines exist or the ice surface was lower than the highest topography, cosmogenic nuclides can provide information about ice surface elevation (Stone et al., 2003; Stone et al., 1998). In areas of non-erosive glacial ice, cosmogenic nuclides can be used to

determine the amount of inheritance, thereby constraining subglacial erosion rates (Briner and Swanson, 1998). Finally, employing two or more nuclides together can help to understand surfaces with complex exposure histories, which have been alternately exposed and buried beneath weakly erosive glacial ice (Bierman et al., 1999; Nishiizumi et al., 1991; Roberts et al., 2009).

Comparison of previous work conducted in various areas along Greenland's coast demonstrates that ice characteristics and behavior vary greatly over space, even though all of these areas are fed from the same body of ice. Certain areas, including regions near the large outlet glacier Jakobshavn Isbræ in central west Greenland (Corbett et al., 2011; Roberts and Long, 2005; Weidick and Bennike, 2007) and near Sisimiut Fjord in southwest Greenland (Roberts et al., 2009), are characterized by ice that efficiently eroded the landscape during the last glacial period. Other areas, such as those near Scoresby Sund in central east Greenland, experienced less aggressive erosion and preserve terrains with significantly longer histories (Håkansson et al., 2008). Certain areas of the Greenland Ice Sheet margin retreated relatively slowly at several tens of m yr^{-1} at the end of the last glacial period (Rinterknecht et al., 2009), while others retreated relatively rapidly at ~100 m yr^{-1} (Corbett et al., 2011; Long and Roberts, 2003; Young et al., 2011). Deglaciation took place at different times across Greenland, with coastal areas becoming ice-free as early as ~13 and as late as ~6 cal ka BP (Bennike and Björck, 2002). These contrasts suggest that subglacial erosion rates, ice dynamics, and ice retreat patterns are strongly controlled by regional and local factors.

Here, we make use of paired bedrock and boulder samples, paired ^{10}Be and ^{26}Al analyses, and a three-dimensional layout of samples; this allows us to make inferences

about ice thickness, subglacial erosion rates, and the timing of ice margin retreat during the most recent deglaciation. We compare our results from the Upernavik area with results from elsewhere on the Greenland Ice Sheet in order to make inferences about how ice characteristics vary over space.

2. Study Site and Previous Work

The Upernavik region (~73°N, Fig. 1) is characterized by dissected terrain that encompasses table-top shaped islands up to 1 km in elevation separated by deep fjords, including the large Upernaviks Isfjord to the north. It has been suggested that the water depth in Upernaviks Isfjord is ~700 m (Peterson, 2003). The present-day ice margin lies ~100 km to the southeast of the outboard islands. The bedrock in the Upernavik area is predominately granite or granite pegmatite, some of which is weakly foliated; however, younger, layered basalts cover the granite towards the southeastern end of the sample transect (Escher and Pulvertaft, 1995).

A pronounced contrast exists between the low-elevation and high-elevation landscapes. Many of the low-elevation bedrock forms retain a sculpted shape (Fig. 2), although striations and glacial polish were not observed in the locations we visited. Conversely, many of the high-elevation bedrock forms exhibit pronounced surface weathering features (Fig. 3) including pedestals up to 10 cm in height, weathering pits, and pervasive frost shattering. At high elevations, much of the bedrock erodes by breaking into sheets that range from several centimeters to several tens of centimeters thick, and in many cases the surfaces are mantled with grus. Both low- and high-elevation surfaces are covered with erratic boulders.

Previous dating constraints on deglaciation of the Upernavik region have been derived from radiocarbon chronology (Fig. 1); however, data from this region are relatively sparse in relation to the rest of Greenland's coast (Bennike and Björck, 2002). A basal radiocarbon age from a lake on Svartenhuk Halvø, the large peninsula of land ~1° south of Upernavik, provided a minimum deglaciation age of 10.4 to 10.2 cal ka BP (Bennike, 2000). Farther away in Melville Bugt, ~2° north of Upernavik, a whale vertebra found on recently-deglaciated terrain yielded a radiocarbon age of ~9.3 to 9.0 cal ka BP (Bennike, 2008), using a marine reservoir correction of 400 years. The vertebra was likely deposited on the ocean floor after the whale's death, and incorporated into the ice sheet during the neoglaciation (~4.0 to 0.1 ka). Bennike (2008) infers that, by ~9.3 to 9.0 ka, the ice sheet margin at Melville Bugt was similar to or behind its present-day position, indicating that the coast had been deglaciated by the early Holocene. Also near Melville Bugt, a basal radiocarbon age from a lake sediment core yielded a minimum deglaciation age of ~9.9 to 9.3 cal ka BP (Bennike, 2008; Fredskild, 1985) and a radiocarbon age from shell fragments in marine material gave an age of ~9.0 to 8.5 cal ka BP (Bennike, 2008; Kelly, 1980), also with a marine reservoir correction of 400 years.

3. Using cosmogenic nuclides to understand glacial exposure and erosion

Measurement of *in situ* produced cosmogenic nuclides is a useful technique for understanding the timing of surface exposure and burial, as well as the efficiency of subglacial erosion. Because cosmogenic radionuclides, such as ^{10}Be and ^{26}Al, form in minerals at known rates through bombardment of cosmogenic radiation (Lal, 1988), quantifying the nuclide concentration in a sample allows inferences to be made about that

sample's exposure history (Phillips et al., 1990). Cosmogenic radionuclide formation in quartz is the most commonly-used system. In simple cases, a surface is exposed from beneath a geologic material sufficiently thick to block cosmic-ray penetration (e.g., glacial ice), and the concentration of cosmogenic nuclides can be used to determine when exposure occurred (Phillips et al., 1990). In other cases, a surface is exposed and then buried, perhaps multiple times, yielding nuclide concentrations indicative of a complicated sample history (Granger and Muzikar, 2001).

A two-isotope system, known as burial dating, can be used to understand complex exposure and burial histories (Granger and Muzikar, 2001; Nishiizumi et al., 1991; Nishiizumi et al., 1989). If two cosmogenic nuclides are used, the ratio of their concentrations can be correlated to the minimum amount of time the surface spent exposed and the minimum amount of time the surface spent shielded from radiation. Sample ^{26}Al/^{10}Be ratios may fall along a constant exposure path, within an erosion envelope, or along burial paths, indicating different sample histories (see Figure 8 in Bierman et al., 1999).

The two-isotope approach has proven to be illustrative in areas where the glacial history of a surface is unknown, and where surfaces at high elevation appear to be significantly more weathered than surfaces at low elevation (Dyke, 1979; Sugden, 1977, 1978). However, this weathering discrepancy can be caused by different mechanisms. It is possible that the ice surface was lower than the uplands, and thus the uplands have been continuously exposed (Dyke, 1979). This scenario has been documented in southwestern Greenland (Roberts et al., 2009) and Scotland (Stone et al., 1998), where high-elevation samples had old single nuclide minimum limiting exposure ages and ratios

indistinguishable from constant exposure; these surfaces would have been nunataks protruding from above the ice sheet, allowing inferences to be made about last glacial period ice surface elevation. Conversely, it is also possible that the ice surface was higher than the uplands, and the uplands were covered by cold-based, non-erosive ice (Sugden, 1977, 1978; Sugden and Watts, 1977). This was the case in Baffin Island, Canada (Bierman et al., 1999; Briner et al., 2003; Sugden and Watts, 1977) and Newfoundland, Canada (Gosse et al., 1993; Gosse et al., 1995), where high-elevation samples had old single nuclide minimum limiting exposure ages and ratios indicative of burial. Episodes of burial were likely caused by cold-based, non-erosive glacial ice which would have been incapable of removing sufficient material to create fresh surfaces after glaciation. Either of the above scenarios could be complicated by perennial snowfields, which could exist at high elevations during either glacial periods or interglacial periods. Prolonged snow cover would shield, but not erode, the underlying bedrock surface (Bierman et al., 1999).

Since the uplands in Upernavik exhibit more significant weathering than the lowlands, we consider the aforementioned scenarios using paired ^{10}Be and ^{26}Al data (Fig. 4). Any combination of the above factors would lead to cosmogenic ages significantly older than the local deglaciation age established by radiocarbon chronology (see Section 2). However, the first would lead to matched bedrock/boulder ages, while the second would lead to discordant bedrock/boulder ages. Although perennial snowfields could lead to the appearance of burial, snowfields alone could not lead to a bedrock/boulder age mismatch because thick snow would cover the surfaces evenly and would not transport

new, fresh boulders. Therefore, burial by cold-based ice at least one time is needed to explain bedrock/boulder discordance (Fig. 4).

4. Methods

4.1. Experimental design

In the Upernavik area, we collected 20 bedrock and 13 boulder samples for the analysis of *in situ* cosmogenic ^{10}Be and ^{26}Al (Granger and Muzikar, 2001). Samples were collected along a 100-km northwest to southeast transect extending from the farthest outboard island to a nunatak ~2 km within the present-day ice margin (Table 1; Fig. 5). This transect is parallel to large fjords immediately to the north (Upernaviks Isfjord) and south (Laksefjorden). The sampling scheme used in this study, known as "dipstick sampling" (Stone et al., 2003), involves collecting bedrock and boulder pairs at a variety of elevations at several locations along a transect normal to the ice margin. Paired bedrock and boulder samples were collected from a range of elevations (~20-1000 m a.s.l.) at each "dipstick". This sampling scheme yields information about both vertical and horizontal variability in nuclide concentrations, allowing us to make inferences about exposure time and ice behavior.

Measuring ^{10}Be in paired bedrock and boulder samples provides information about the efficiency of subglacial erosion and the occurrence of post-depositional burial by glacial ice or snowfields. If the two ages agree, the likelihood of complex exposure histories is low, and both ages are more likely to report an accurate exposure age. If a bedrock sample is appreciably older than a paired boulder sample, inheritance of ^{10}Be from prior periods of exposure is likely (Bierman et al., 1999).

104

4.2. Field methods

Wherever possible, we sampled bedrock and boulder pairs in close proximity, usually less than 10 m apart. We collected the top several cm of material from the flat-lying surfaces of bedrock forms and erratic boulders using a chisel and hammer (Table 1), and avoided sampling in sheltered areas to minimize complex exposure geomotreis. Latitude/longitude and elevation data were collected with a handheld Garmin 12 GPS that has a positional uncertainty of <10 m and an elevation uncertainty of <25 m.

4.3. Laboratory methods

Samples were prepared as outlined in Corbett et al. (2011). Quartz was isolated from the rock using a series of both physical and chemical processes, and Be and Al were isolated from the quartz through a series of chemical processes (Table 2). Two different [9]Be carriers were used in the preparation of these samples: a commercial (SPEX) carrier of 1000 ppm concentration was used on six samples in the early stages of processing, and a low-level beryl carrier of 245 ppm concentration made at the University of Vermont was used on all subsequent samples. Enough carrier was added to each sample to achieve a Be load of ~250 µg (Table 2).

In order to ensure that enough Al was present in the sample for isotopic analysis (2000 µg), we added commercial Al carrier (SPEX, 1000 ppm concentration) when necessary. Immediately after quartz dissolution, two aliquots representing ~6% of the material were removed from each sample. We used these replicate aliquots to quantify the Al load within each sample through inductively coupled plasma optical emission spectrometry (ICP-OES) by using internal standardization and by measuring two

105

different emission lines. The two measurements of sample Al concentration derived from these two aliquots were usually within 1%, and always within 3.5%, of each other. Measured Al concentrations of blanks were within 1% of expected Al concentrations based on the mass of ^{27}Al carrier that was added.

4.4. Isotopic analysis

Isotopic ratios were measured by accelerator mass spectrometry (AMS) at Lawrence Livermore National Laboratory (Table 3). All 33 samples were analyzed for ^{10}Be. Samples were normalized to standard 07KNSTD3110, with a reported ratio of $2850 \cdot 10^{-15}$ (Nishiizumi et al., 2007). Measured sample ratios ranged from $2.6 \cdot 10^{-14}$ to $1.0 \cdot 10^{-12}$, and AMS measurement precisions, including propagated blank uncertainties, ranged from 1.9 to 5.4% (1σ, Table 3). Samples were processed in five separate batches, two of which were prepared with SPEX Be carrier and three of which were prepared with beryl carrier. The process blanks for these five batches contained $2.1 \cdot 10^5$ (average, n = 2, SPEX carrier), $3.3 \cdot 10^5$ (n = 1, SPEX carrier), $4.0 \cdot 10^3$ (average, n = 2, beryl carrier), $4.7 \cdot 10^3$ (n = 1, beryl carrier), and $5.2 \cdot 10^3$ (n = 1, beryl carrier) ^{10}Be atoms, respectively. The blank ^{10}Be/^{9}Be ratios were $1.2 \pm 0.2 \cdot 10^{-14}$ (average, 1SD, n = 2), $2.0 \pm 0.7 \cdot 10^{-14}$ (1σ, n = 1), $2.4 \pm 1.2 \cdot 10^{-16}$ (average, 1SD, n = 2), $2.9 \pm 1.1 \cdot 10^{-16}$ (1σ, n = 1), and $3.2 \pm 1.1 \cdot 10^{-16}$ (1σ, n = 1). For the first two batches, processed with commercial Be carrier, we applied a long-term average blank correction equal to a ratio of $1.2 \pm 0.2 \cdot 10^{-14}$ (1SD, n = 19 batches). For the remaining three batches, processed with beryl carrier, we applied the average blank for the three batches, equal to a ratio of $2.71 \pm 0.76 \cdot 10^{-16}$ (1SD, n = 4). For samples prepared with the commercial carrier, blanks amounted to 1 to 24% of the total

sample ratios. For samples prepared with the beryl carrier, blanks amounted to <1% of the total sample ratios. Blank ratios were subtracted from sample ratios, and blank uncertainties were propagated in quadrature.

After determining ^{10}Be concentrations and modeling exposure ages, we chose 20 samples to analyze for ^{26}Al. Sixteen of these 20 samples were chosen because of their high minimum limiting ^{10}Be ages ($\geq$20 ka). Independent chronology from radiocarbon dating suggests that the Upernavik region was deglaciated ~10 cal ka BP (Section 2). Therefore, we inferred that samples with modeled ^{10}Be ages appreciably above ~10 ka do not have simple exposure histories and necessitated further investigation with ^{26}Al. The remaining four samples analyzed were the two youngest bedrock samples (GU001 and GU098) and the two youngest boulder samples (GU002 and GU104). These four samples served as a test for constant exposure in young samples.

For ^{26}Al analysis, all samples were normalized to standard KNSTD10650, with a reported ratio of $1065 \cdot 10^{-14}$ (Nishiizumi, 2004). Measured sample ratios ranged from $1.3 \cdot 10^{-13}$ to $1.7 \cdot 10^{-12}$, and AMS measurement precisions ranged from 2.4 to 12.8% (1σ, Table 3). Samples were processed in five separate batches. The process blanks for these five batches contained $6.9 \cdot 10^4$ (n = 1), $6.9 \cdot 10^4$ (n = 1), $2.7 \cdot 10^4$ (average, n = 2), $7.8 \cdot 10^4$ (n = 1), and $2.9 \cdot 10^4$ (n = 1) ^{26}Al atoms, respectively. The blank ^{26}Al/^{27}Al ratios were $1.6 \cdot 10^{-15}$ (n = 1), $1.5 \cdot 10^{-15}$ (n = 1), $6.0 \cdot 10^{-16}$ (average, n = 2), $1.8 \cdot 10^{-15}$ (n = 1), and $6.6 \cdot 10^{-16}$ (n = 1). Blank corrections were performed with the average blank for the five batches (equal to a ratio of $1.1 \pm 0.6 \cdot 10^{-15}$, 1SD) because all batches were prepared with the same carrier and a long-term ^{26}Al blank has not been well-constrained for the new University of Vermont laboratory. Blanks amounted to <0.5% of the total sample ratios.

4.5. Age calculations

Minimum limiting ^{10}Be and ^{26}Al exposure ages (Table 3) were calculated with the CRONUS Earth online exposure age calculator developmental version 2.2, constants version 2.2 (Balco et al., 2008), under standard atmosphere. We used the regionally-calibrated northeastern North American sea-level production rates of 3.93 ± 0.19 atoms g^{-1} yr^{-1} for ^{10}Be, and 26.54 ± 1.27 atoms g^{-1} yr^{-1} for ^{26}Al (Balco et al., 2009) and the Lal/Stone constant production rate model and scaling scheme (Lal, 1991; Stone, 2000). In CRONUS, corrections were made for latitude, elevation, sample thickness (ranged from 1 to 7 cm), and sample density (2.7 g cm^{-3}; Table 1). Calculated exposure ages can vary by as much as 14% based on the chosen production rate, and as much as 4% based on the chosen scaling scheme.

No corrections were made for snow cover or till cover. Shielding by snow cover would lead to ^{10}Be or ^{26}Al age underestimates (Schildgen et al., 2005), and the appearance of burial on a two-isotope plot; however, seasonal snow cover effects at our sample sites are likely minimal. Using data from a weather station in the town of Upernavik (www.weather-and-climate.com), we determined that mean temperatures are below freezing for 8 months of the year (October through May) and that ~140 mm of snow (water equivalent) falls during this time at a rate of ~7 to 35 mm per month. We assumed that precipitation was added in monthly increments, and that no melting or sublimation occurred until June. Shielding calculations (Gosse and Phillips, 2001) suggest that reported exposure ages could underestimate the true age by no more than 5%. However, this calculation is likely a significant overestimate because the areas we

sampled are windswept and exposed during winter months and because we did not account for snow loss during the winter.

Bedrock and boulder erosion can also cause [10]Be and [26]Al concentrations to underestimate exposure ages. While field observations suggest that subaerial erosion has removed mass from rock surfaces at high-elevations (Fig. 3), post glacial erosion is less evident at low elevations (Fig. 2). Although samples from low elevations did not preserve striations, they had glacially sculpted surfaces. For low-elevation samples, especially boulders, we can conclude that little erosion has taken place since the end of the last glacial period, and we therefore do not correct for erosion when calculating exposure ages for the latest Pleistocene deglaciation.

Reported age uncertainties reflect AMS errors only, which we refer to as "internal". Because we are most interested in investigating relationships between samples within the data set (i.e. a bedrock sample versus its paired boulder), we use internal uncertainties in our data analysis. Additional uncertainties are introduced in relation to the production rate, elevation corrections, and latitude corrections when comparing the ages in this study to ages in other data sets. However, we can expect errors in calibration and correction to be correlated and thus to affect all samples similarly because our samples come from a geographically limited region.

4.6. Data Reduction and Interpretation

Single-nuclide [10]Be and [26]Al exposure ages for each sample are calculated by CRONUS assuming that no burial has occurred, as described in section 2.2.1. of Bierman et al. (1999). We also consider both nuclides together to present minimum-limiting total

109

exposure and burial histories as described in section 2.2.2. of Bierman et al. (1999). In the calculations, we used northeastern North American high latitude, sea-level production rates of 3.93 ± 0.19 atoms g^{-1} yr^{-1} for ^{10}Be and 26.54 ± 1.27 atoms g^{-1} yr^{-1} for ^{26}Al (Balco et al., 2009), scaling the production rate of each sample based on elevation. Scaled production rates ranged from 4.37 to 10.8 atoms g^{-1} yr^{-1} for ^{10}Be and 29.5 to 72.6 atoms g^{-1} yr^{-1} for ^{26}Al. We assume a ^{26}Al/^{10}Be production ratio of 6.75 (Balco et al., 2009). We used decay constants of $5.02 \cdot 10^{7}$ for ^{10}Be and $9.83 \cdot 10^{7}$ for ^{26}Al, corresponding to half-lives of $1.38 \cdot 10^{6}$ yr (Nishiizumi et al., 2007) and $7.05 \cdot 10^{5}$ yr (Nishiizumi, 2004), respectively. Calculations involving burial assumed complete burial with no nuclide production.

4.7. Retreat rate simulations

        To estimate the rate of latest Pleistocene ice sheet retreat along the sample transect, we considered only the youngest, inheritance-free boulder samples. We systematically simulated potential linear retreat patterns taking into account the location and uncertainty of each age measurement. The probability of every linear fit through the ^{10}Be ages was systematically calculated using only the six youngest ^{10}Be measurements. These fits are of the form $Y = B_0 + B_1 \cdot X$, where Y is time, X is distance from the present margin, B_0 is the time at which the present margin was reached during ice sheet retreat, and B_1 is the rate of ice sheet retreat. B_1 can alternatively be expressed as the total time (years) required for the 100 km ice sheet retreat. For each total time of ice sheet retreat (B_1) between 0 and 3000 years, B_0 was systematically tested between values of 8500 and 12000 years. The probability of each of these simulations was calculated from the normal

110

distributions of the ^{10}Be measurements. By summing the probabilities for each value of B$_1$, the probability distribution over the range of possible B$_1$ values was constructed. The maximum of this normal distribution is the statistical most likely retreat rate.

5. Results

5.1. Data overview and exposure ages

Cosmogenic nuclide abundances vary within the 33 samples in the data set (Table 3). Measured ^{10}Be concentrations range from $5.0 \cdot 10^4$ to $9.1 \cdot 10^5$ atoms g^{-1}; ^{26}Al concentrations range from $4.3 \cdot 10^5$ to $5.2 \cdot 10^6$ atoms g^{-1}. Single-nuclide minimum limiting exposure ages range from 10.6 to 104 ka for ^{10}Be (Fig. 6), and 10.9 to 89.4 ka for ^{26}Al (Fig. 7). Comparing the two single-isotope concentrations for an individual sample yields a strong correlation ($r^2 = 0.99$; Fig. 8). In general, ^{10}Be and ^{26}Al single-nuclide concentrations are more similar for samples with shorter exposure times, but samples with longer exposure times have greater ^{10}Be concentrations than ^{26}Al concentrations.

^{26}Al/^{10}Be ratios range from ~4.7 to 7.2 (Fig. 9). The four "control" samples used to test the production ratio (GU001, GU002, GU098, and GU104) all have ^{26}Al/^{10}Be ratios indistinguishable from 6.75 at 1σ, and fall along the constant exposure path (Section 3). The average ratio of these four "control" samples is 6.9 ± 0.2 (average, 1SD). Of the remaining 16 samples, four (GU097, GU100, GU106, and GU112) have ratios that overlap the constant exposure path with 1σ uncertainties. The other 12 samples fall below the erosion envelope; their ratios can be explained by varying lengths of burial time after at least one period of surface exposure.

5.2. Bedrock/boulder comparisons

There is a pronounced contrast between bedrock and boulder sample ages. Within all 13 sample pairs, the bedrock sample has a higher concentration of ^{10}Be than the boulder sample by more than 1σ. Bedrock samples contain, on average, ~2.3 times as much ^{10}Be as their corresponding boulder samples, although this value varies from ~1.1 to 5.1 times. This contrast between bedrock and boulder sample ages is evident at the scale of each individual bedrock/boulder pair as well as at the scale of whole sample populations.

Corresponding bedrock and boulder sample pairs have dissimilar minimum limiting ^{10}Be exposure ages and do not have a 1:1 relationship ($r^2 = 0.41$, Fig. 10). A repeated measures t-test verifies that there is a statistically significant difference when bedrock and boulder ages are considered in a paired comparison ($p = 0.007$). Considering bedrock and boulder samples in two distinct populations also results in non-overlapping population distributions (Fig. 11); an independent samples t-test indicates that there is a statistical difference between populations ($p = 0.022$).

5.3. Spatial variability

Minimum limiting cosmogenic exposure ages vary appreciably over space. This variation is pronounced in the vertical dimension, where both bedrock ($r^2 = 0.43$; n = 20) and boulder ($r^2 = 0.41$; n = 13) sample ages increase with elevation (Fig. 12). A one-way ANOVA shows that bedrock sample ^{10}Be age has a weakly significant relationship with elevation ($p = 0.051$), using the categorical elevation designations in Table 1. The same test performed on boulder samples shows that ^{10}Be age has a significant relationship with

elevation (p < 0.01). Spatial variability is less pronounced in the horizontal dimension, where there is no relationship between bedrock sample age or boulder sample age and distance along the 100-km sample transect (Fig. 13).

Five bedrock samples from the nunatak yielded minimum limiting ^{10}Be ages of 43.3 to 80.9 ka, and minimum limiting ^{26}Al ages of 35.6 to 67.6 ka. Calculated ^{26}Al/^{10}Be ratios range from 5.6 to 6.3, overlap at 1σ, and all fall below the constant exposure path. The lowest-elevation nunatak sample shows the least exposure for both isotopes; conversely, the highest-elevation nunatak sample shows the most exposure for both isotopes.

6. Discussion

The Upernavik landscape has a long and complex glacial history. The presence of some young, Holocene ages suggests that certain areas were efficiently eroded during the last glacial period. In these areas, all at low elevation, nuclide concentrations reflect exposure ages. However, the majority of the data set has pre-Holocene ^{10}Be and ^{26}Al ages, and therefore does not provide insight about the latest Pleistocene deglaciation. Using dual isotope analysis, calculated minimum limiting exposure durations range from 0.01 to 0.12 Ma, and minimum limiting burial durations are as high as 0.7 Ma (Table 3). Minimum limiting total histories are as high as 0.8 Ma.

6.1. Glacial period ice extent and thickness

Field observations and ^{10}Be and ^{26}Al data demonstrate that glacial period ice in the Upernavik region was horizontally extensive and covered peaks ~1 km in elevation.

Latest Pleistocene deglacial ages of the farthest outboard samples show that ice extended at least that far during the last glacial period. The farthest west samples lie ~100 km northwest of the present-day ice sheet margin, providing a minimum estimate for the horizontal dimension of ice cover that was lost during deglaciation.

This data set also demonstrates that glacial period ice has, at some point during the Quaternary, covered the highest-elevation land surfaces. The existence of large, erratic boulders that do not match the local bedrock type (e.g. GU102, boulder, foliated granite; and GU103, bedrock, unfoliated granite) suggests that these areas were once covered by the main ice sheet rather than just by local ice caps or ice fields. Flowing glacial ice would have transported erratics from farther inland, leading to mismatched bedrock/boulder lithologies. Such erratics at high elevations were also observed in Melville Bugt to the north (Kelly, 1980).

Cosmogenic data also demonstrates that these high-elevation surfaces have been buried. The highest-elevation bedrock samples (GU096, 778 m; GU103, 998 m; and GU110, 745 m) all yielded ^{26}Al/^{10}Be ratios less than ~5.75, indicating that burial has occurred at least once. Modeled two-isotope burial durations are several hundred ka; because glacial periods last roughly ~100 ka, these long burial durations demonstrate that high elevation surfaces have been buried repeatedly. The boulders that correspond to these bedrock samples (GU097 and GU102) have younger minimum limiting ^{10}Be ages of 19.7 and 45.7 ka, indicating that the boulders were emplaced at some point after the initial exposure of the bedrock; the most likely explanation for mismatched bedrock/boulder ages is burial by cold-based ice at least once (Fig. 4). It is not possible to determine how much of this burial was caused by cold-based ice and how much was

caused by perennial snowfields. However, this evidence does show that cold-based ice covered the uplands at least once, thus providing a minimum ice thickness estimate of ~1 km (the elevation difference between the fiord bottoms and our highest sample site).

6.2. Isotope inheritance and subglacial erosion efficiency

This data set demonstrates that cosmogenic isotopes inherited from prior periods of exposure are present in most of the bedrock and boulders near Upernavik. The old minimum limiting [10]Be ages, leftward skew of the data (Fig. 6), disagreement between bedrock and boulder sample ages (Figs. 9 & 10), and long modeled two-isotope exposure durations (Table 3) suggest that many of the samples contain more [10]Be than could have accumulated during the Holocene. Instead, this excess [10]Be is inherited from former periods of exposure, when the climate warmed and upland surfaces were exposed from beneath cold-based glaciers or snowfields. Such exposure could have occurred during many previous interglacial periods throughout the Quaternary when global ice volume was as low or lower than today (Lisiecki and Raymo, 2005). While modeling has suggested that the ice margin near Upernavik is more static than the ice margin elsewhere in Greenland (Cuffey and Marshall, 2000; Letréguilly et al., 1991; Otto-Bliesner et al., 2006; Overpeck et al., 2006), the presence of inherited [10]Be demonstrates that ice retreat during previous interglacial periods caused the ice margin to retreat at least as far inland as it has during the Holocene.

The presence of inherited [10]Be indicates that subglacial erosion rates during previous glacial periods were low, and that glacial ice was not capable of removing [10]Be inherited from preceding interglacial periods. Furthermore, the relationship between

sample age and elevation (Fig. 12) suggests that glacial ice removed more material from low elevations than it did from high elevations. This trend is reinforced with field observations; low-elevation areas tended to preserve sculpted landforms indicative of glacial erosion (Fig. 2), while high-elevation areas showed evidence of long-lived surface weathering (Fig. 3). Elevation-related erosion intensity is likely caused by the relationship between ice thickness and subglacial temperatures (Sugden, 1977). During glacial periods, low-lying areas were covered by thick, warm-based ice (> 1 km, see Section 6.1) capable of performing significant erosion. Conversely, higher areas were covered by thin, cold-based ice capable of performing little erosion (Sugden, 1977; Sugden and Watts, 1977). It is also possible that the uplands experienced burial by perennial snowfields; however, as described in Section 6.2, cold-based ice covered these areas at least once (Fig. 4).

The low subglacial erosion rates we infer in Upernavik are similar to findings in other high-latitude areas. Inheritance has been documented in Greenland (Håkansson et al., 2008; Kelly et al., 2008), the Canadian Arctic (Bierman et al., 1999; Briner et al., 2003; Marquette et al., 2004), Scandinavia (Harbor et al., 2006; Stroeven et al., 2002), and Antarctica (Lilly et al., 2010; Sugden et al., 2005). This result differs notably from the Jakobshavn Isbræ region, 500 km away. There, no inheritance of cosmogenic isotopes from prior periods of exposure was detected, regardless of sample type or elevation (Corbett et al., 2011). This is likely because thick, fast-flowing ice in Jakobshavn Isbræ may have eroded material from bedrock outcrops with a high degree of efficiency.

The overwhelming presence of inheritance in this data set suggests that neither bedrock samples nor boulder samples in areas of thin, cold-based ice provide accurate

116

exposure ages or deglaciation chronologies. This is even true in the fjord bottoms, where erosion has evidently taken place to shape the fjords, but inherited [10]Be is still present. Even the fjord-bottom bedrock samples have minimum limiting [10]Be ages of ≥~14 ka, which contrasts with the young, fresh, striated fjord-bottoms in Baffin Island (Briner et al., 2003). The origin of these fjords, therefore, may be tectonic as well as glacial (England, 1987; Glasser and Ghiglione, 2009; Swift et al., 2008).

6.3. Landscape Longevity

Certain parts of the landscape in the Upernavik region have been preserved through multiple glacial-interglacial cycles. High elevation bedrock surfaces have minimum limiting total histories of hundreds of ka, suggesting that these locations remained relatively unchanged by the coming and going of glacial ice. Six of these samples, or about one third of the data set, have minimum limiting total histories of ~0.4 Ma, roughly coincident with marine oxygen isotope stage 12, one of the largest global ice volumes during the Quaternary (Lisiecki and Raymo, 2005). It is possible that this glacial period led to the build-up of thicker ice in Upernavik, which served to erode high-elevation land surfaces and "reset" the cosmogenic clock. Progressive smaller glacial periods only allowed for the build-up of thinner ice or snowfields, which would have been unable to perform significant erosion and therefore would have preserved these old landscapes. Most high-elevation surfaces have minimum limiting burial durations of ~0.3-0.4 Ma and total minimum limiting histories of ~0.4-0.5 Ma, suggesting that these surfaces have been buried by cold-based ice and/or perennial snowfields ~75-80% of the time since marine oxygen isotope stage 12. These minimum burial durations are slightly

shorter than those recorded in the high elevations of Baffin Island (~0.4 Ma) by Bierman et al. (1999), and longer than those recorded from elsewhere on Baffin Island (~0.2 Ma) by Briner et al. (2003).

6.4. Post-glacial ice retreat

Determining the timing of ice retreat after the last glacial period is difficult due to ubiquitous inheritance in the data set; only a small subset of the samples appear to have simple exposure histories, allowing us to investigate the timing and pattern of ice retreat in the deep fjords. The six youngest boulder samples have overlapping ^{10}Be ages of 11.3 ± 0.5 ka (average, 1SD), and we interpret this to be the best estimate for the deglaciation of the Upernavik coast. These samples show little trend in age along the 100-km sample transect (Fig. 13). While we are unable to constrain the exact directions of Pleistocene ice flow, our sample transect likely approximates ice flow because it parallels two pronounced fjords directly to the north and south (Fig. 5). The data suggest that significant lateral retreat of the ice margin (~100 km) took place rapidly. This retreat likely occurred within several hundred, and certainly not more than a thousand, years. The statistical maximum likelihood ice retreat rate was ~170 m yr^{-1}, with possible rates as low as 110 m yr^{-1} and as high as 330 m yr^{-1} (1SD). The data imply that the statistical maximum likelihood duration of ice retreat was 600 years, and may have ranged between 300 and 900 years (1SD).

The rapid rate of ice loss in Upernavik is higher than many estimates of retreat rates of large bodies of ice from the same time period (see Figure 9 in Corbett et al., 2011). In Ilulissat, 500 km to the south, calculated rates of ice margin retreat were ~100-

110 m yr^{-1} through Jakobshavn Isfjord, its tributary fjord, and its adjacent bay (Corbett et al., 2011; Long and Roberts, 2003; Long et al., 2006; Young et al., 2011). In Sisimiut Fjord, central western Greenland, retreat rates were ~20-50 m yr^{-1} (Rinterknecht et al., 2009). On North America, retreat rates of ~260 m yr^{-1} were calculated for the Laurentide Ice Sheet as a whole (Andrews, 1973) and ~60 m yr^{-1} for Sam Ford Fjord on Baffin Island (Briner et al., 2009).

Rapid retreat of glacial ice in the Upernavik area was likely driven by multiple factors. Ice in the Upernavik region would have been largely marine-based due to local topography (Fig. 5); mass would have been lost through calving, as well as through ablation, thus accelerating the rate of ice loss. Additionally, abundant cosmogenic inheritance caused by low subglacial erosion rates suggests the presence of cold-based ice, likely resulting from a thinner ice sheet. Therefore, when the ice sheet began to break up, disintegration would have happened rapidly due to the presence of thin ice.

6.5. Paleoclimatic Context

Rapid ice loss from the Upernavik area ~11.3 ± 0.5 ka was likely driven by external climate forcings (Fig. 14). Oxygen isotope ratios from the GISP2 ice core (Stuiver and Grootes, 2000) and from the GRIP and Dye3 ices cores (Dahl-Jensen et al., 1998) show that this time period was characterized by rapid warming. This warming may have coincided with the end of the Younger Dryas cold reversal, which is thought to have occurred abruptly ~11.6 ka (Alley, 2000; Taylor et al., 1993; Taylor et al., 1997); however, this relationship is speculative because only a small subset of the samples

investigated in this study were viable recorders of deglaciation age, and because the average deglaciation age of the Upernavik fjords has an uncertainty of 500 years (1SD).

7. Conclusions

Analysis of ^{10}Be and ^{26}Al in paired bedrock and boulder samples near Upernavik, Greenland, reveals a complex landscape history. Bedrock and boulder samples have discordant ages, suggesting that ^{10}Be inherited from previous periods of exposure is present. High-elevation surfaces have old single nuclide minimum limiting exposure ages and long modeled durations of burial after initial exposure. These surfaces, which exhibit pronounced surface weathering features, have likely been preserved under non-erosive, cold-based ice or perennial snowfields over the course of numerous glacial cycles. Many of these high-elevation surfaces have modeled total histories of 0.4 Ma, suggesting that they may have been preserved since marine oxygen isotope stage 12. Low-elevation surfaces have younger ages, although bedrock samples still preserve inheritance and evidence of burial. Boulders at low elevations suggest that deglaciation along the 100-km sample transect took place rapidly at a rate of ~170 m yr^{-1} at ~11.3 ± 0.5 ka.

Acknowledgements

References

Alley, R., 2000, The Younger Dryas cold interval as viewed from central Greenland: Quaternary Science Reviews, v. 19, p. 213-226.

Andrews, J., 1973, The Wisconsin Laurentide ice sheet: dispersal centers, problems of rates of retreat, and climatic implications: Arctic and Alpine Research, v. 5, p. 185-199.

Balco, G., 2011, Contributions and unrealized potential contributions of cosmogenic-nuclide exposure dating to glacier chronology, 1990-2010: Quaternary Science Reviews, v. 30, p. 3-27.

Balco, G., Briner, J., Finkel, R., Rayburn, J., Ridge, J., and Schaefer, J., 2009, Regional beryllium-10 production rate calibration for late-glacial northeastern North America: Quaternary Geochronology, v. 4, p. 93-107.

Balco, G., Stone, J., Lifton, N., and Dunai, T., 2008, A complete and easily accessible means of calculating surface exposure ages or erosion rates from ^{10}Be and ^{26}Al measurements: Quaternary Geochronology, v. 3, p. 174-195.

Bennike, O., 2000, Palaeoecological studies of Holocene lake sediments from west Greenland: Palaeogeography, Palaeoclimatology, Palaeoecology, v. 155, p. 285-304.

—, 2008, An early Holocene Greenland whale from Melville Bugt, Greenland: Quaternary Research, v. 69, p. 72-76.

Bennike, O., and Björck, S., 2002, Chronology of the last recession of the Greenland Ice Sheet: Journal of Quaternary Science, v. 17, p. 211-219.

Bierman, P., Marsella, K., Patterson, C., Davis, P., and Caffee, M., 1999, Mid-Pleistocene cosmogenic minimum-age limits for pre-Wisconsinan glacial surfaces in southwestern Minnesota and southern Baffin Island: a multiple nuclide approach: Geomorphology, v. 27, p. 25-39.

Bintanja, R., and Van De Wal, R., 2008, North American ice-sheet dynamics and the onset of 100,000-year glacial cycles: Nature, v. 454, p. 869-872.

Briner, J., Bini, A., and Anderson, R., 2009, Rapid early Holocene retreat of a Laurentide outlet glacier through an Arctic fjord: Nature Geoscience, v. 2, p. 496-499.

Briner, J., Miller, G., Davis, P., Bierman, P., and Caffee, M., 2003, Last Glacial Maximum ice sheet dynamics in Arctic Canada inferred from young erratics perched on ancient tors: Quaternary Science Reviews, v. 22, p. 437-444.

Briner, J., and Swanson, T., 1998, Using inherited cosmogenic ^{36}Cl to constrain glacial erosion rates of the Cordilleran ice sheet: Geology, v. 26, p. 3-6.

Corbett, L., Young, N., Bierman, P., Briner, J., Neumann, T., Graly, J., and Rood, D., 2011, ^{10}Be concentrations in bedrock and boulder samples resulting from early Holocene ice retreat near Jakobshavn Isfjord, western Greenland: Quaternary Science Reviews, v. DOI 10.1016/j.quascirev.2011.04.001.

Cuffey, K., and Marshall, S., 2000, Substantial contribution to sea-level rise during the last interglacial from the Greenland ice sheet: Nature, v. 404, p. 591-594.

Dahl-Jensen, D., Mosegaard, K., Gundestrup, N., Clow, G., Johnsen, S., Hansen, A., and Balling, N., 1998, Past temperatures directly from the Greenland Ice Sheet: Science, v. 282, p. 268-271.

Dyke, A., 1979, Quaternary geomorphology, glacial chronology, and climatic and sea-level history of southwestern Cumberland Peninsula, Baffin Island, Northwest Territories, Canada: Arctic and Alpine Research, v. 11, p. 179-202.

England, J., 1987, Glaciation and the evolution of the Canadian high arctic landscape: Geology, v. 15, p. 419-423.

Escher, J., and Pulvertaft, T., 1995, Geological Map of Greenland 1:2,500,000, Geologic Survey of Greenland, Copenhagen.

Fabel, D., and Harbor, J., 1999, The use of in-situ produced cosmogenic radionuclides in glaciology and glacial geomorphology: Annals of Glaciology, v. 28, p. 103-110.

Fredskild, B., 1985, The Holocene vegetational development of Tugtuligssuaq and Qeqertat, northwest Greenland, Museum Tusculanum Press, 20 p.

Glasser, N., and Ghiglione, M., 2009, Structural, tectonic and glaciological controls on the evolution of fjord landscapes: Geomorphology, v. 105, p. 291-302.

Gosse, J., Grant, D., Klein, J., Klassen, R., Evenson, E., Lawn, B., and Middleton, R., 1993, Significance of altitudinal weathering zones in Atlantic Canada, inferred from in situ produced cosmogenic radionuclides: Geological Society of America Abstracts with Programs, v. 25, p. A394.

Gosse, J., Grant, D., Klein, J., and Lawn, B., 1995, Cosmogenic ^{10}Be and ^{26}Al constraints on weathering zone genesis, ice cap basal conditions, and Long Range Mountain (Newfoundland) glacial history: CANQUA-CGRG conference abstracts, v. CA19.

Gosse, J., and Phillips, F., 2001, Terrestrial in situ cosmogenic nuclides: theory and application: Quaternary Science Reviews, v. 20, p. 1475-1560.

Granger, D., and Muzikar, P., 2001, Dating sediment burial with in situ-produced cosmogenic nuclides: theory, techniques, and limitations: Earth and Planetary Science Letters, v. 188, p. 269-281.

Håkansson, L., Alexanderson, H., Hjort, C., Moller, P., Briner, J., Aldahan, A., and Possnert, G., 2008, Late Pleistocene glacial history of Jameson Land, central East Greenland, derived from cosmogenic ^{10}Be and ^{26}Al exposure dating: Boreas, v. 38, p. 244-260.

Harbor, J., Stroeven, A., Fabel, D., Clarhäll, A., Kleman, J., Li, Y., Elmore, D., and Fink, D., 2006, Cosmogenic nuclide evidence for minimal erosion across two subglacial sliding boundaries of the late glacial Fennoscandian ice sheet: Geomorphology, v. 75, p. 90-99.

Kelly, M., 1980, Preliminary investigations of the Quaternary of Melville Bugt and Dundas, northwest Greenland: Rapport Gronlands Geologiske Undersogelse, v. 100, p. 33-38.

Kelly, M., Lowell, T., Hall, B., Schaefer, J., Finkel, R., Goehring, B., Alley, R., and Denton, G., 2008, A ^{10}Be chronology of lateglacial and Holocene mountain glaciation in the Scoresby Sund region, east Greenland: implications for seasonality during lateglacial time: Quaternary Science Reviews, v. 27, p. 2273-2282.

Lal, D., 1988, In situ-produced cosmogenic isotopes in terrestrial rocks: Annual Review of Earth and Planetary Sciences, v. 16, p. 355-388.

—, 1991, Cosmic ray labeling of erosion surfaces: in situ nuclide production rates and erosion models: Earth and Planetary Science Letters, v. 104, p. 424-439.

Letréguilly, A., Reeh, N., and Huybrechts, P., 1991, The Greenland ice sheet through the last glacial-interglacial cycle: Global and Planetary Change, v. 4, p. 385-394.

Lilly, K., Fink, D., Fabel, D., and Lambeck, K., 2010, Pleistocene dynamics of the interior of the East Antarctic ice sheet: Geology, v. 38, p. 703-706.

Lisiecki, L., and Raymo, M., 2005, A Plio-Pleistocene stack of 57 globally distributed benthic ^{18}O records: Paleoceanography, v. 20, p. 522–533.

Long, A., and Roberts, D., 2003, Late Weichselian deglacial history of Disko Bugt, West Greenland, and the dynamics of the Jakobshavns Isbrae ice stream: Boreas, v. 32, p. 208-226.

Long, A., Roberts, D., and Dawson, S., 2006, Early Holocene history of the West Greenland Ice Sheet and the GH-8.2 event: Quaternary Science Reviews, v. 25, p. 904-922.

Marquette, G., Gray, J., Gosse, J., Courchesne, F., Stockli, L., Macpherson, G., and Finkel, R., 2004, Felsenmeer persistence under non-erosive ice in the Torngat and Kaumajet mountains, Quebec and Labrador, as determined by soil weathering and cosmogenic nuclide exposure dating: Canadian Journal of Earth Sciences, v. 41, p. 19-38.

Nishiizumi, K., 2004, Preparation of ^{26}Al AMS standards: Nuclear Instruments and Methods in Physics Research Section B: Beam Interactions with Materials and Atoms, v. 223, p. 388-392.

Nishiizumi, K., Imamura, M., Caffee, M., Southon, J., Finkel, R., and McAninch, J., 2007, Absolute calibration of ^{10}Be AMS standards: Nuclear Instruments and Methods in Physics Research Section B: Beam Interactions with Materials and Atoms, v. 258, p. 403-413.

Nishiizumi, K., Kohl, C., Arnold, J., Klein, J., Fink, D., and Middleton, R., 1991, Cosmic ray produced ^{10}Be and ^{26}Al in Antarctic rocks: exposure and erosion history: Earth and Planetary Science Letters, v. 104, p. 440-454.

Nishiizumi, K., Winterer, E., Kohl, C., Klein, J., Middleton, R., Lal, D., and Arnold, J., 1989, Cosmic ray production rates of ^{10}Be and ^{26}Al in quartz from glacially polished rocks: Journal of Geophysical Research, v. 94, p. 17907.

Otto-Bliesner, B., Marshall, S., Overpeck, J., Miller, G., and Hu, A., 2006, Simulating Arctic climate warmth and icefield retreat in the last interglaciation: Science, v. 311, p. 1751-1753.

Overpeck, J., Otto-Bliesner, B., Miller, G., Muhs, D., Alley, R., and Kiehl, J., 2006, Paleoclimatic evidence for future ice-sheet instability and rapid sea-level rise: Science, v. 311, p. 1747-1750.

Peterson, R., 2003, Settlements, kinship and hunting grounds in traditional Greenland, 327 pp. p.

Phillips, F., Zreda, M., Smith, S., Elmore, D., Kubik, P., and Sharma, P., 1990, Cosmogenic chlorine-36 chronology for glacial deposits at Bloody Canyon, eastern Sierra Nevada: Science, v. 248, p. 1529-1532.

Rinterknecht, V., Gorokhovich, Y., Schaefer, J., and Caffee, M., 2009, Preliminary ^{10}Be chronology for the last deglaciation of the western margin of the Greenland Ice Sheet: Journal of Quaternary Science, v. 24, p. 270-278.

Roberts, D., and Long, A., 2005, Streamlined bedrock terrain and fast ice flow, Jakobshavns Isbrae, West Greenland: implications for ice stream and ice sheet dynamics: Boreas, v. 34, p. 25-42.

Roberts, D., Long, A., Schnabel, C., Davies, B., Xu, S., Simpson, M., and Huybrechts, P., 2009, Ice sheet extent and early deglacial history of the southwestern sector of the Greenland Ice Sheet: Quaternary Science Reviews, v. 28, p. 2760-2773.

Schildgen, T., Phillips, W., and Purves, R., 2005, Simulation of snow shielding corrections for cosmogenic nuclide surface exposure studies: Geomorphology, v. 64, p. 67-85.

Stone, J., 2000, Air pressure and cosmogenic isotope production: Journal of Geophysical Research, v. 105, p. 23753-23759.

Stone, J., Balco, G., Sugden, D., Caffee, M., Sass III, L., Cowdery, S., and Siddoway, C., 2003, Holocene deglaciation of Marie Byrd Land, West Antarctica: Science, v. 299, p. 99-102.

Stone, J., Ballantyne, C., and Keith Fifield, L., 1998, Exposure dating and validation of periglacial weathering limits, northwest Scotland: Geology, v. 26, p. 587-590.

Stroeven, A., Fabel, D., Hättestrand, C., and Harbor, J., 2002, A relict landscape in the centre of Fennoscandian glaciation: cosmogenic radionuclide evidence of tors preserved through multiple glacial cycles: Geomorphology, v. 44, p. 145-154.

Stuiver, M., and Grootes, P., 2000, GISP2 oxygen isotope ratios: Quaternary Research, v. 53, p. 277-284.

Sugden, D., 1977, Reconstruction of the morphology, dynamics, and thermal characteristics of the Laurentide Ice Sheet at its maximum: Arctic and Alpine Research, v. 9, p. 21-47.

—, 1978, Glacial erosion by the Laurentide ice sheet: Journal of Glaciology, v. 20, p. 367-391.

Sugden, D., Balco, G., Cowdery, S., Stone, J., and Sass III, L., 2005, Selective glacial erosion and weathering zones in the coastal mountains of Marie Byrd Land, Antarctica: Geomorphology, v. 67, p. 317-334.

Sugden, D., and Watts, S., 1977, Tors, felsenmeer, and glaciation in northern Cumberland Peninsula, Baffin Island: Canadian Journal of Earth Sciences, v. 14, p. 2817-2823.

Swift, D., Persano, C., Stuart, F., Gallagher, K., and Whitham, A., 2008, A reassessment of the role of ice sheet glaciation in the long-term evolution of the East Greenland fjord region: Geomorphology, v. 97, p. 109-125.

Taylor, K., Lamorey, G., Doyle, G., Alley, R., Grootes, P., Mayewski, P., White, J., and Barlow, L., 1993, The 'flickering switch' of late Pleistocene climate change: Nature, v. 361, p. 432-436.

Taylor, K., Mayewski, P., Alley, R., Brook, E., Gow, A., Grootes, P., Meese, D., Saltzman, E., Severinghaus, J., and Twickler, M., 1997, The Holocene-Younger Dryas transition recorded at Summit, Greenland: Science, v. 278, p. 825-827.

Weidick, A., and Bennike, O., 2007, Quaternary glaciation history and glaciology of Jakobshavn Isbrae and the Disko Bugt region, west Greenland: a review: Geologic Survey of Denmark and Greenland Bulletin, v. 14, p. 1-13.

Young, N., Briner, J., Stewart, H., Axford, Y., Csatho, B., Rood, D., and Finkel, R., 2011, Response of Jakobshavn Isbrae, Greenland, to Holocene climate change: Geology, v. 39, p. 131-134.

Dipstick Number	Sample Name	Sample Type	Elevation Designation	Elevation (m a.s.l.)[a]	Latitude (°N)[a]	Longitude (°E)[a]	Rock Type	Thickness (cm)[b]
DIPSTICK #1 *offshore island*	GU091	Bedrock	Low	24	72.782	-56.586	Granite	2
	GU092	Boulder	Low	21	72.782	-56.586	Granite	1.5
DIPSTICK #2 *offshore island*	GU093	Bedrock	High	91	72.740	-56.385	Granite	2.5
	GU094	Boulder	High	90	72.740	-56.386	Granite	2
	GU095	Bedrock	Low	20	72.744	-56.382	Granite	3
DIPSTICK #3 *fjord-dissected terrain*	GU096	Bedrock	High	778	72.754	-55.873	Granite	3
	GU097	Boulder	High	774	72.754	-55.872	Granite	2
	GU098	Bedrock	Mid	372	72.793	-55.932	Granite	3
	GU099	Boulder	Mid	366	72.793	-55.933	Granite	1
	GU100	Bedrock	Low	74	72.812	-55.826	Granite	1
	GU101	Boulder	Low	71	72.812	-55.826	Granite	3
DIPSTICK #4 *fjord-dissected terrain*	GU102	Boulder	High	980	72.718	-55.473	Foliated Granite	2
	GU103	Bedrock	High	998	72.718	-55.475	Granite	2
	GU106	Bedrock	High-Mid	498	72.741	-55.552	Granite	4
	GU107	Boulder	High-Mid	500	72.741	-55.551	Foliated Granite	2
	GU104	Boulder	Low-Mid	253	72.773	-55.503	Granite	2
	GU105	Bedrock	Low-Mid	270	72.774	-55.504	Granite	1
	GU108	Bedrock	Low	33	72.781	-55.443	Granite	2
	GU109	Boulder	Low	27	72.780	-55.442	Granite	2
DIPSTICK #5 *fjord-dissected terrain*	GU110	Bedrock	High	745	72.661	-55.122	Granite	1
	GU111	Bedrock	Mid	325	72.682	-55.025	Granite	1
	GU112	Boulder	Mid	325	72.682	-55.025	Granite	1.5
	GU113	Bedrock	Low	90	72.660	-54.983	Granite	1
	GU114	Boulder	Low	91	72.660	-54.983	Granodiorite	1.5
DIPSTICK #6 *ice-marginal terrain*	GU001	Bedrock	High	603	72.536	-53.733	Granite	3
	GU002	Boulder	High	603	72.536	-53.733	Granite	3
	GU006	Bedrock	Low	539	72.539	-53.732	Granite	3.5
	GU017	Boulder	Low	539	72.539	-53.732	Granite	1
DIPSTICK #7 *nunatak*	GU041	Bedrock	High	898	72.615	-53.589	Granite	4
	GU042	Bedrock	High-Mid	895	72.615	-53.592	Granite	7
	GU043	Bedrock	Mid	857	72.616	-53.596	Granite	3
	GU044	Bedrock	Low-Mid	808	72.617	-53.596	Granite	3
	GU045	Bedrock	Low	776	72.619	-53.597	Granite	3

[a]Elevations and locations were recorded in the field with a Garmin GPS-12.
[b]Refers to the thickness of the slab that was collected for analysis.

Table 1.

Sample Name	Quartz Added (g)	Total Be Load (μg)[a]	Total Al Load (μg)[b]
GU091	21.76	251	----
GU092	17.41	252	----
GU093	22.85	248	----
GU094	11.57	247	----
GU095	22.11	247	----
GU096	16.87	248	2429
GU097	20.49	248	3858
GU098	20.45	248	3257
GU099	20.09	248	----
GU100	20.83	246	3699
GU101	8.75	247	----
GU102	14.85	253	2493
GU103	16.69	252	2229
GU106	18.81	248	3512
GU107	5.43	248	----
GU104	21.03	248	3085
GU105	23.25	247	3484
GU108	17.81	246	----
GU109	17.61	258	----
GU110	17.86	248	11120
GU111	15.65	244	3289
GU112	16.25	248	2764
GU113	21.51	248	4515
GU114	14.60	247	----
GU001	21.16	248	3854
GU002	21.28	248	4214
GU006	11.09	248	----
GU017	8.14	248	----
GU041	21.42	245	2749
GU042	21.04	249	3023
GU043	20.02	248	3535
GU044	20.48	248	3759
GU045	19.33	248	3793

[a]Refers to the Be load added through carrier.

[b]Refers to the cumulative quantified Al load, including both Al added through carrier and native Al in the quartz.
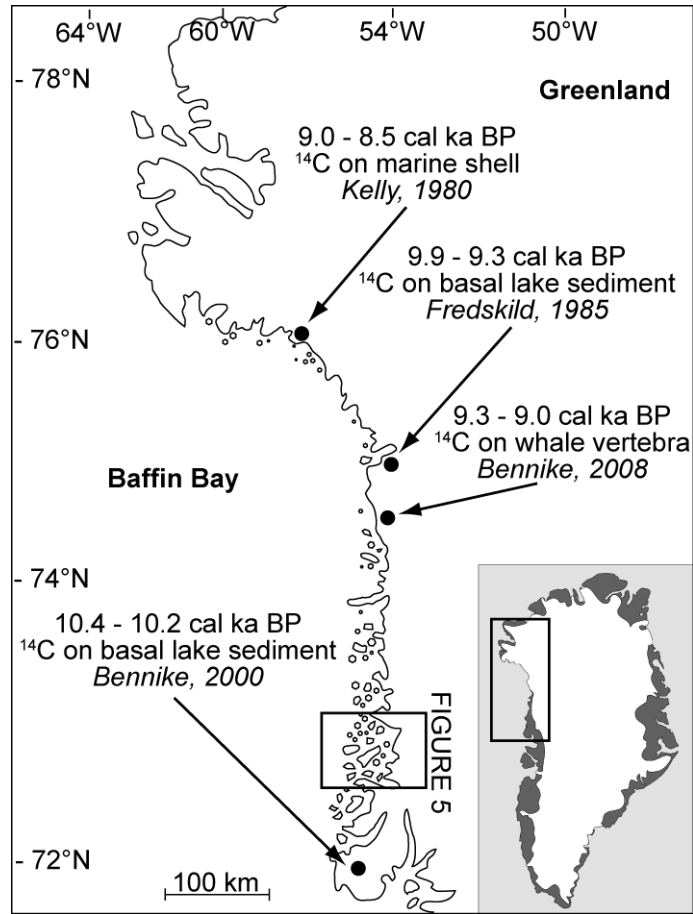
Table 2.

Sample Name	$^{10}Be/^9Be$ Ratio[a]	Ratio Uncertainty[b]	^{10}Be Conc (atoms g^{-1})	$^{26}Al/^{27}Al$ Ratio[a]	Ratio Uncertainty[b]	^{26}Al Conc (atoms g^{-1})	$^{26}Al/^{10}Be$ Ratio	Minimum Limiting ^{10}Be Age[c]	Minimum Limiting ^{26}Al Age[c]	Two-isotope Exposure Time (Ma)	Two-isotope Burial Time (Ma)	Two-isotope total history (Ma)
GU091	7.81 x 10^{-14}	3.08 x 10^{-15}	6.98 x 10^4	----	----	----	----	16.4	----	----	----	----
GU092	5.15 x 10^{-14}	2.76 x 10^{-15}	6.19 x 10^4	----	----	----	----	14.5	----	----	----	----
GU093	1.00 x 10^{-13}	2.99 x 10^{-15}	7.29 x 10^4	----	----	----	----	15.9	----	----	----	----
GU094	3.60 x 10^{-14}	1.30 x 10^{-15}	5.17 x 10^4	----	----	----	----	11.3	----	----	----	----
GU095	8.85 x 10^{-14}	2.03 x 10^{-15}	6.63 x 10^4	----	----	----	----	15.7	----	----	----	----
GU096	9.23 x 10^{-13}	2.09 x 10^{-14}	9.09 x 10^5	1.62 x 10^{-12}	3.89 x 10^{-14}	5.22 x 10^6	5.8 ± 0.2	103.7	89.4	0.12	0.27	0.39
GU097	2.18 x 10^{-13}	4.95 x 10^{-15}	1.77 x 10^5	2.82 x 10^{-13}	1.48 x 10^{-14}	1.19 x 10^6	6.7 ± 0.4	19.7	19.6	0.02	0.00	0.02
GU098	1.03 x 10^{-13}	2.35 x 10^{-15}	8.38 x 10^4	1.65 x 10^{-13}	1.45 x 10^{-14}	5.90 x 10^5	7.0 ± 0.6	13.7	14.3	0.01	0.00	0.01
GU099	8.58 x 10^{-14}	1.95 x 10^{-15}	7.11 x 10^4	----	----	----	----	11.5	----	----	----	----
GU100	1.28 x 10^{-13}	2.92 x 10^{-15}	1.01 x 10^5	1.82 x 10^{-13}	8.17 x 10^{-15}	7.26 x 10^5	7.2 ± 0.4	22.3	23.7	0.02	0.00	0.02
GU101	2.63 x 10^{-14}	1.10 x 10^{-15}	5.03 x 10^4	----	----	----	----	11.3	----	----	----	----
GU102	4.18 x 10^{-13}	1.26 x 10^{-14}	4.90 x 10^5	7.20 x 10^{-13}	6.99 x 10^{-14}	2.70 x 10^6	5.5 ± 0.6	45.7	37.3	0.06	0.39	0.45
GU103	8.84 x 10^{-13}	2.47 x 10^{-14}	9.07 x 10^5	1.73 x 10^{-12}	5.14 x 10^{-14}	5.17 x 10^6	5.7 ± 0.2	83.9	71.5	0.10	0.30	0.40
GU106	2.58 x 10^{-13}	5.86 x 10^{-15}	2.28 x 10^5	3.52 x 10^{-13}	1.22 x 10^{-14}	1.47 x 10^6	6.5 ± 0.3	33.5	32.1	0.04	0.07	0.11
GU107	3.18 x 10^{-14}	1.37 x 10^{-15}	9.79 x 10^4	----	----	----	----	14.1	----	----	----	----
GU104	7.63 x 10^{-14}	1.48 x 10^{-15}	6.03 x 10^4	1.31 x 10^{-13}	1.67 x 10^{-14}	4.31 x 10^5	7.2 ± 0.9	11.1	11.7	0.01	0.00	0.01
GU105	3.32 x 10^{-13}	7.56 x 10^{-15}	2.35 x 10^5	4.48 x 10^{-13}	1.50 x 10^{-14}	1.50 x 10^6	6.4 ± 0.3	42.4	40.2	0.05	0.09	0.14
GU108	8.04 x 10^{-14}	2.83 x 10^{-15}	8.55 x 10^4	----	----	----	----	19.9	----	----	----	----
GU109	5.88 x 10^{-14}	2.85 x 10^{-15}	6.98 x 10^4	----	----	----	----	16.4	----	----	----	----
GU110	6.10 x 10^{-13}	1.60 x 10^{-14}	5.67 x 10^5	1.91 x 10^{-13}	8.37 x 10^{-15}	2.67 x 10^6	4.7 ± 0.2	65.2	45.4	0.10	0.70	0.80
GU111	4.09 x 10^{-13}	9.31 x 10^{-15}	4.26 x 10^5	5.04 x 10^{-13}	1.63 x 10^{-14}	2.37 x 10^6	5.6 ± 0.2	73.3	60.6	0.09	0.36	0.45
GU112	1.18 x 10^{-13}	2.70 x 10^{-15}	1.21 x 10^5	2.03 x 10^{-13}	9.85 x 10^{-15}	7.74 x 10^5	6.4 ± 0.3	20.6	19.5	0.02	0.10	0.12
GU113	3.08 x 10^{-13}	7.04 x 10^{-15}	2.37 x 10^5	3.23 x 10^{-13}	1.16 x 10^{-14}	1.52 x 10^6	6.4 ± 0.3	51.9	49.4	0.06	0.08	0.14
GU114	4.90 x 10^{-14}	1.46 x 10^{-15}	5.58 x 10^4	----	----	----	----	12.1	----	----	----	----
GU001	1.31 x 10^{-13}	3.09 x 10^{-15}	1.03 x 10^5	1.66 x 10^{-13}	7.97 x 10^{-15}	6.79 x 10^5	6.6 ± 0.4	13.6	13.2	0.01	0.04	0.05
GU002	1.03 x 10^{-13}	2.44 x 10^{-15}	8.06 x 10^4	1.25 x 10^{-13}	9.66 x 10^{-15}	5.59 x 10^5	6.9 ± 0.6	10.6	10.9	0.01	0.00	0.01
GU006	7.86 x 10^{-14}	1.87 x 10^{-15}	1.18 x 10^5	----	----	----	----	16.6	----	----	----	----
GU017	4.55 x 10^{-14}	1.40 x 10^{-15}	9.32 x 10^4	----	----	----	----	12.9	----	----	----	----
GU041	1.02 x 10^{-12}	2.41 x 10^{-14}	7.83 x 10^5	1.53 x 10^{-12}	4.06 x 10^{-14}	4.38 x 10^6	5.6 ± 0.2	80.9	67.6	0.10	0.34	0.44
GU042	6.34 x 10^{-13}	1.49 x 10^{-14}	5.02 x 10^5	9.29 x 10^{-13}	2.91 x 10^{-14}	2.98 x 10^6	5.9 ± 0.2	52.9	46.8	0.06	0.23	0.29
GU043	5.96 x 10^{-13}	1.47 x 10^{-14}	4.95 x 10^5	7.92 x 10^{-13}	2.27 x 10^{-14}	3.13 x 10^6	6.3 ± 0.2	52.3	49.2	0.06	0.11	0.17
GU044	7.14 x 10^{-13}	1.62 x 10^{-14}	5.79 x 10^5	8.66 x 10^{-13}	2.77 x 10^{-14}	3.55 x 10^6	6.1 ± 0.2	64.1	58.7	0.07	0.16	0.23
GU045	4.45 x 10^{-13}	1.01 x 10^{-14}	3.82 x 10^5	4.83 x 10^{-13}	1.71 x 10^{-14}	2.12 x 10^6	5.6 ± 0.2	43.3	35.6	0.05	0.38	0.43

[a] Ratios were measured at Lawrence Livermore National Laboratory and have already been blank corrected.

[b] Reported uncertainties are internal AMS uncertainties.

[c] Ages were calculated using the northeastern North American production rate and the Lal (1991)/Stone (2001) scaling schemen in the CRONUS Earth online calculator. Ages have been scaled for elevation, sample density, sample thickness, latitude, and longitude.
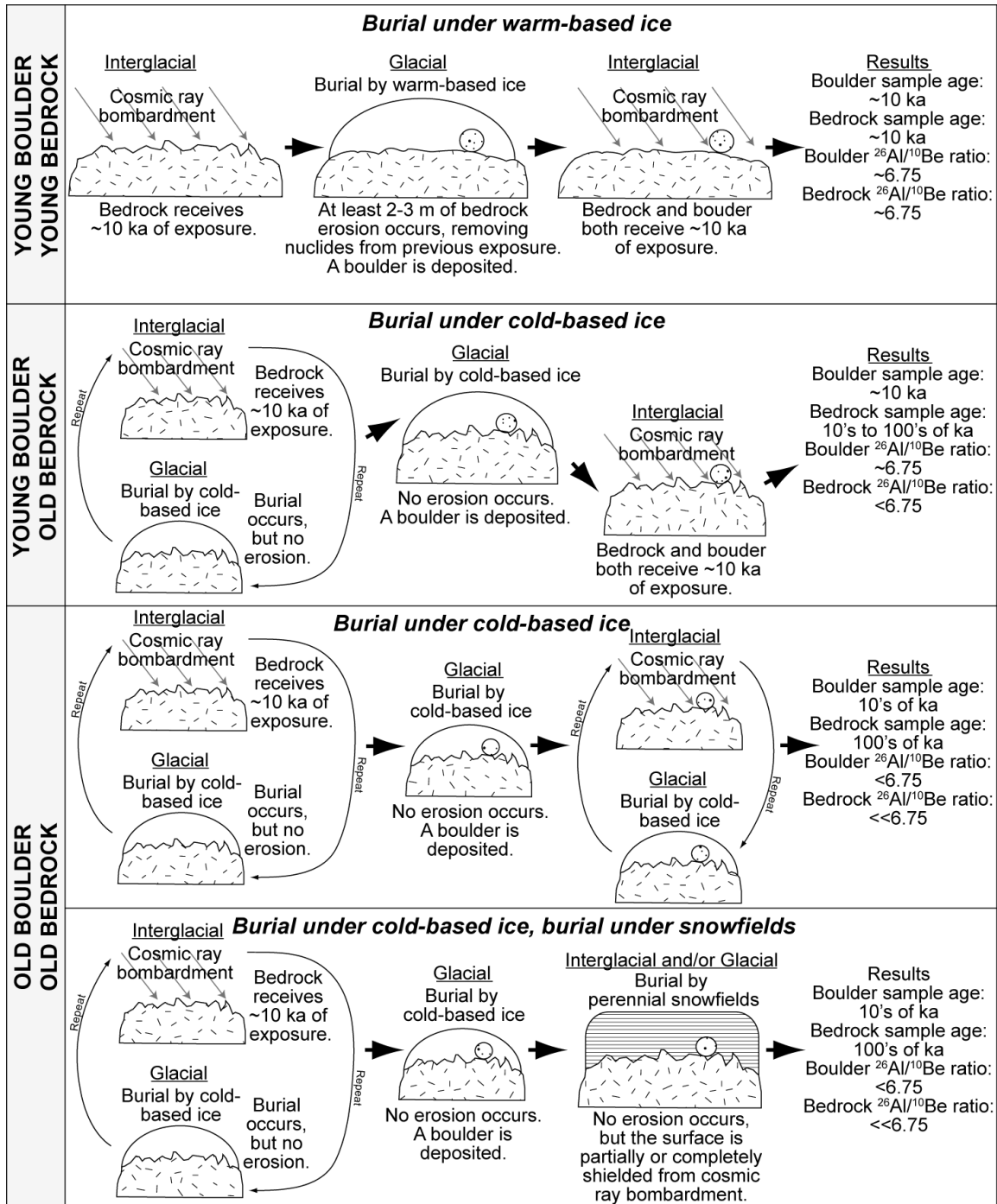
Table 3.

129

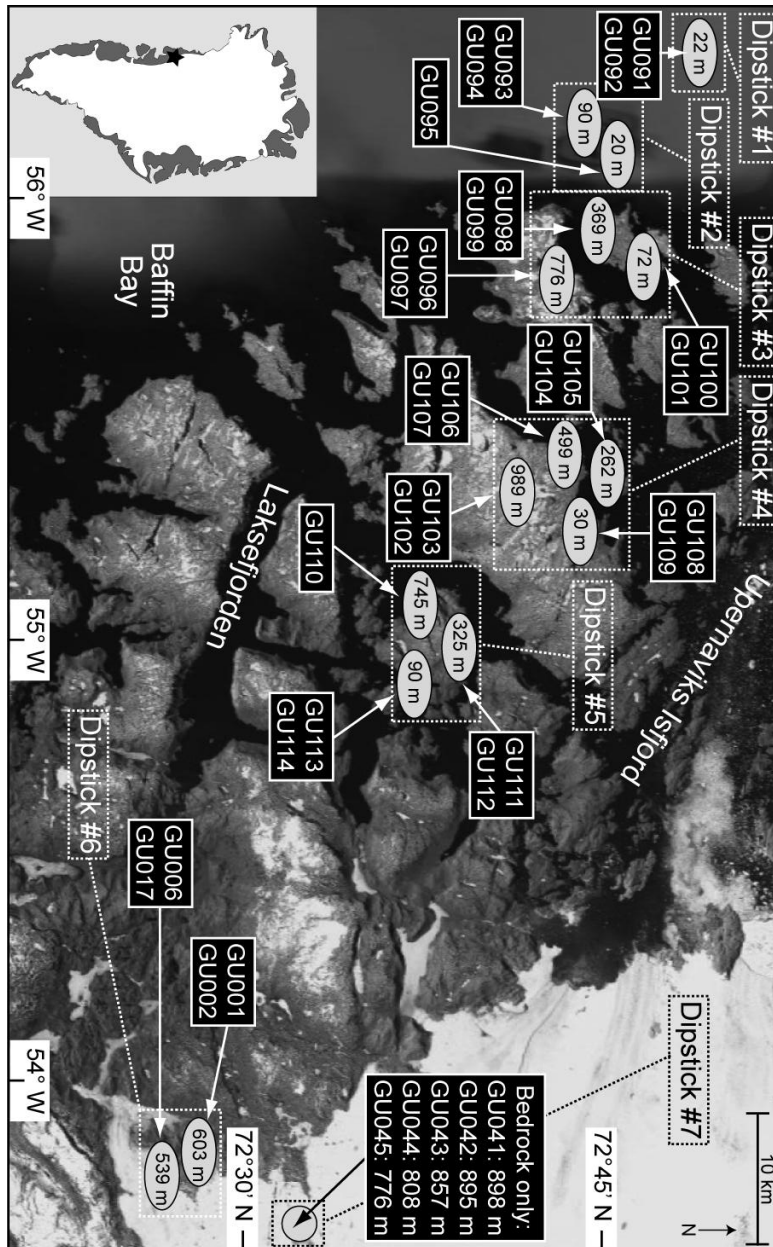**Figure 1.**

Figure 2.

Figure 3.

Figure 4.

Figure 5.

134

Figure 6.

Figure 7.

Figure 8.

137
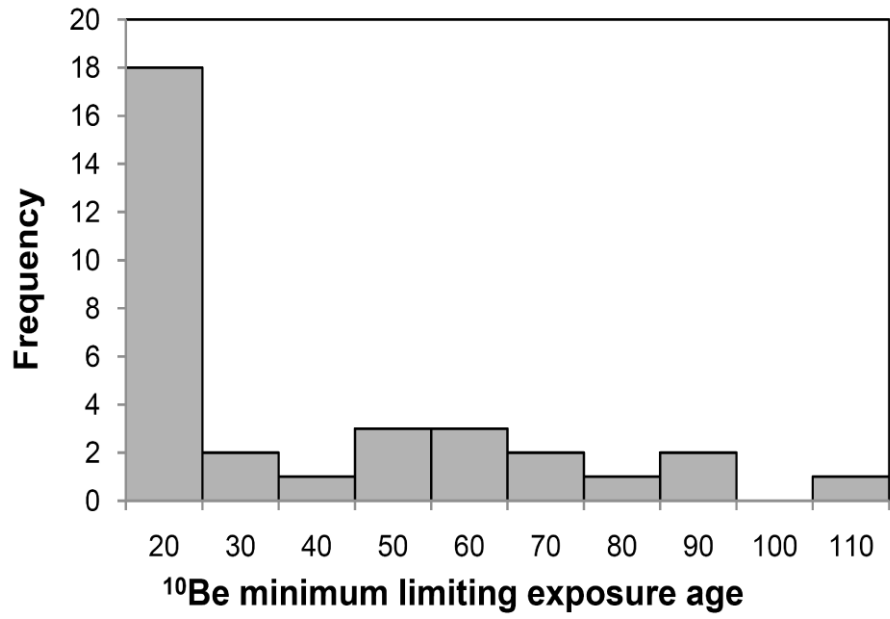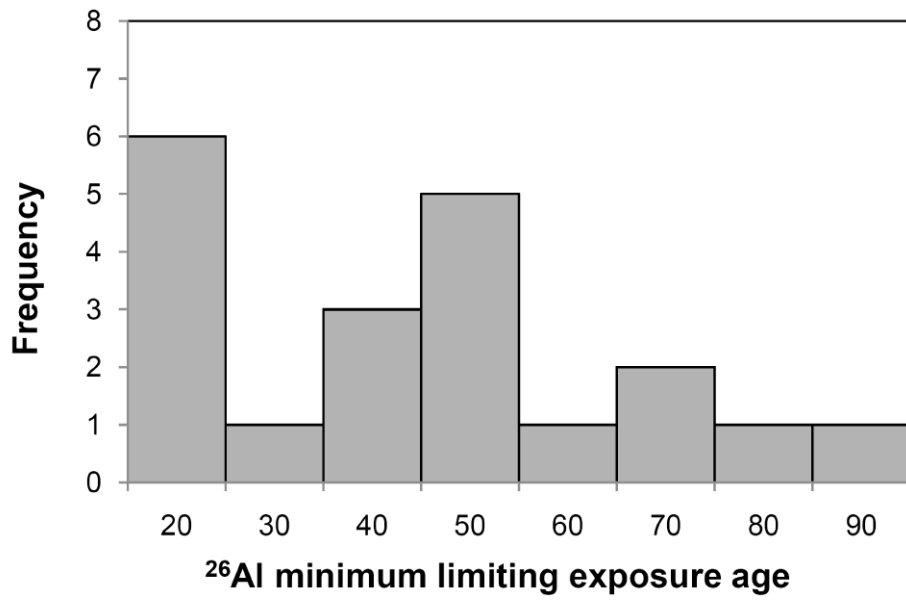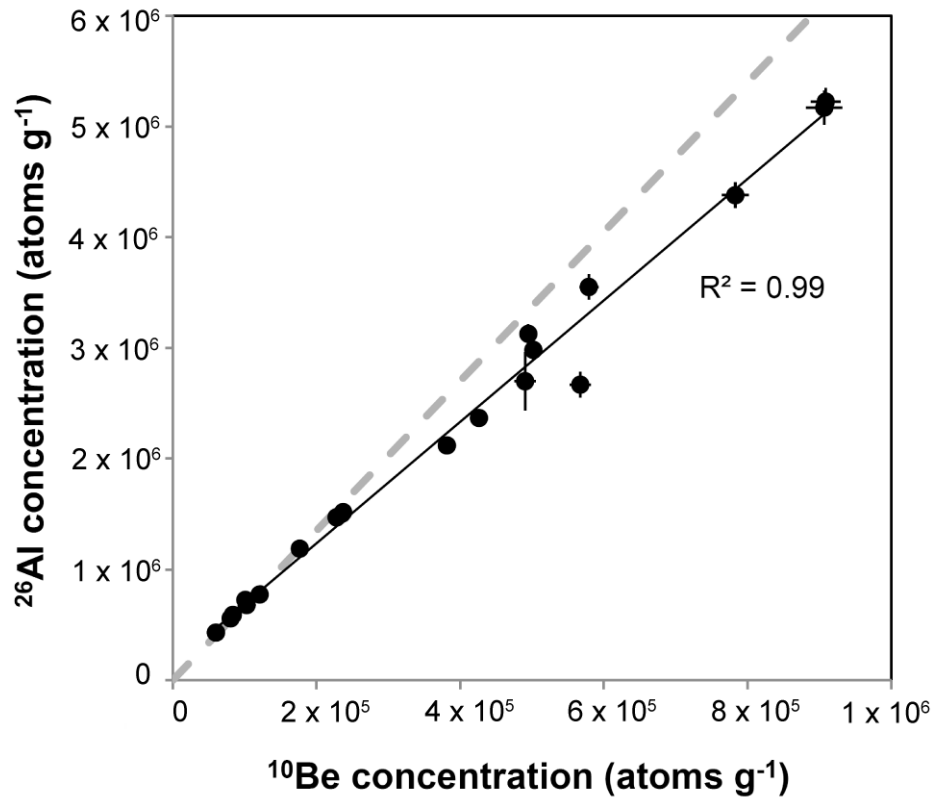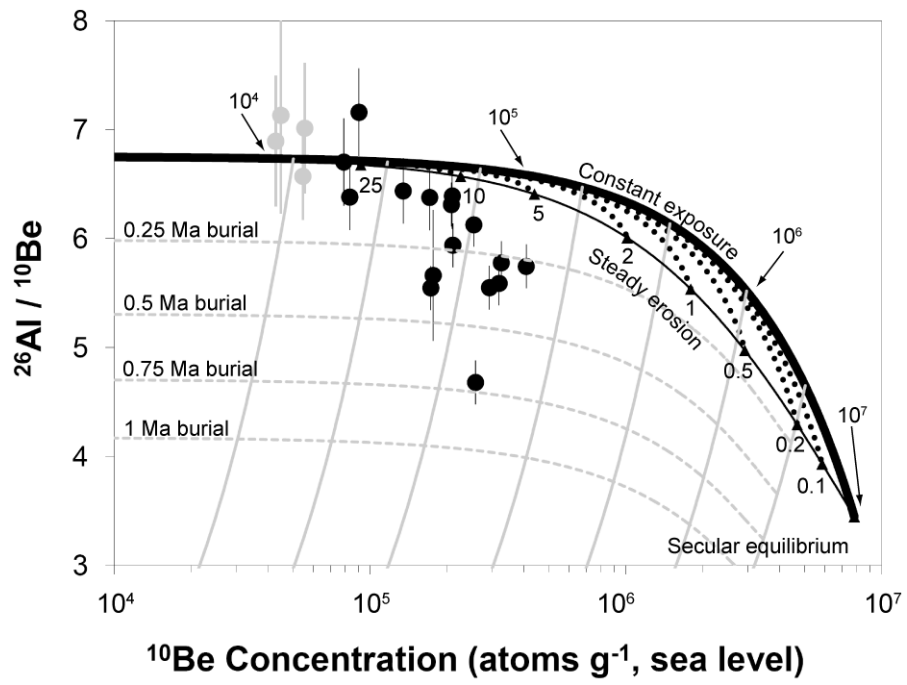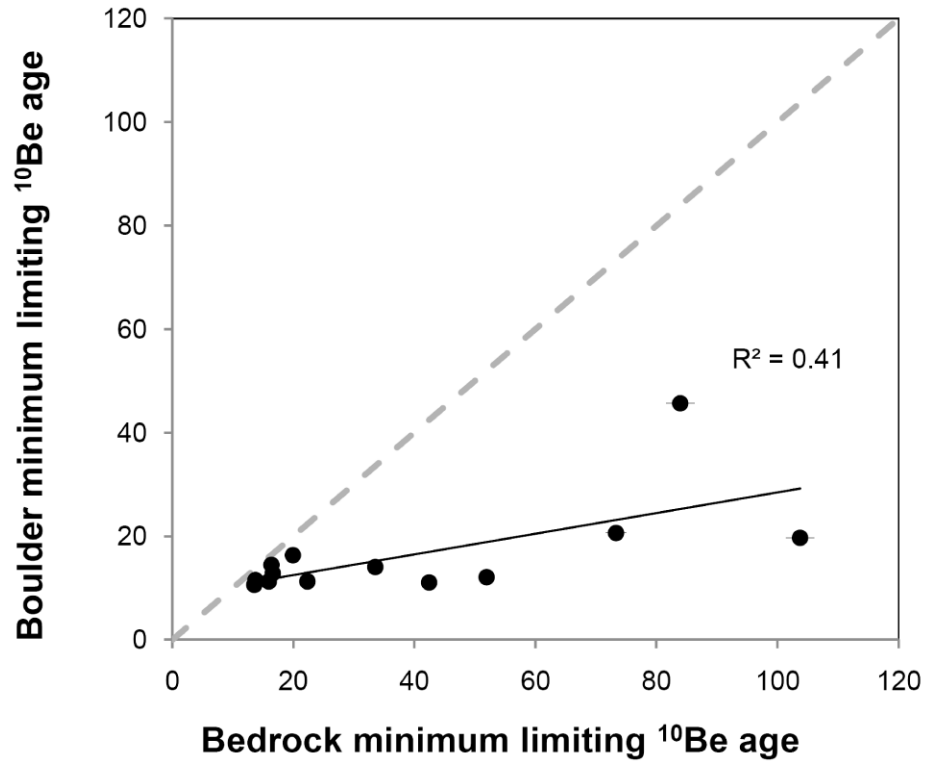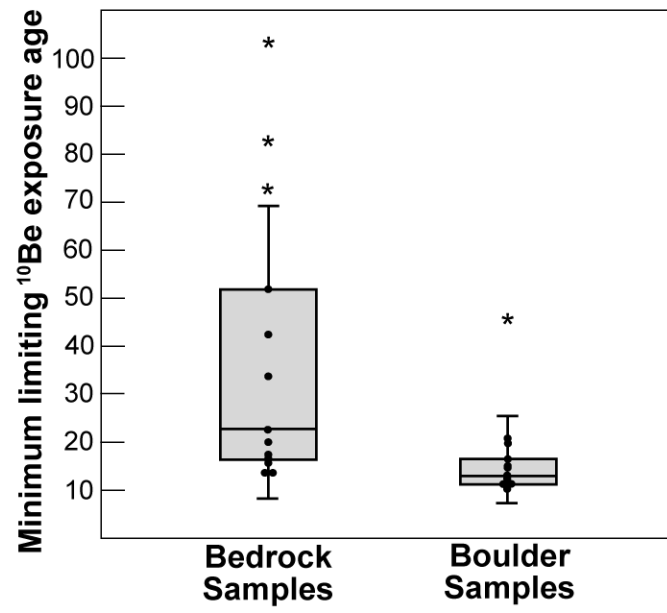
Figure 9.
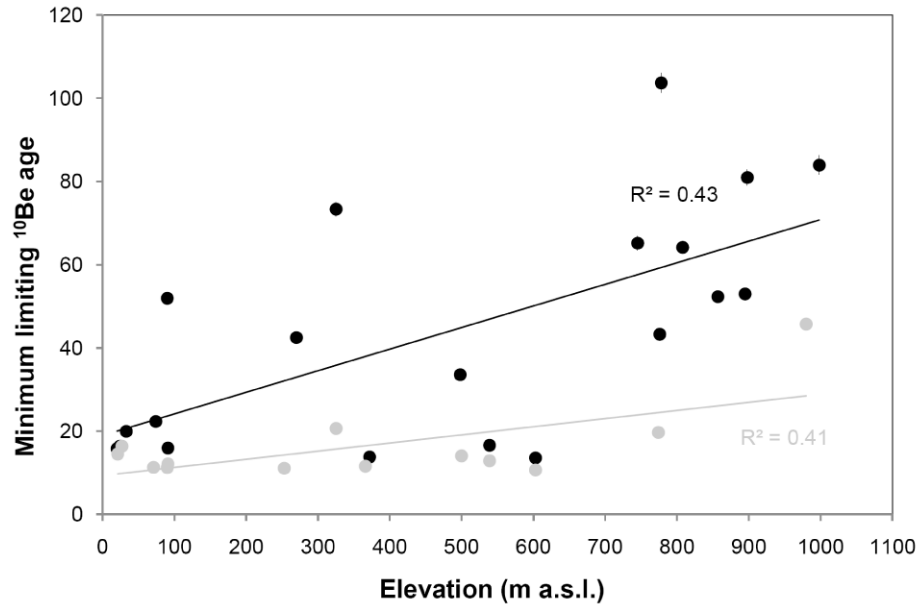
Figure 10.

Figure 11.

Figure 12.
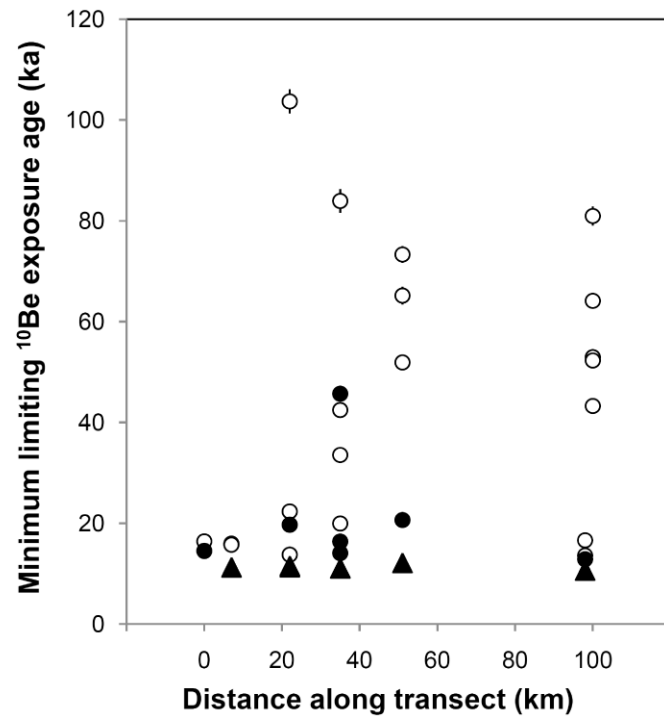
Figure 13.
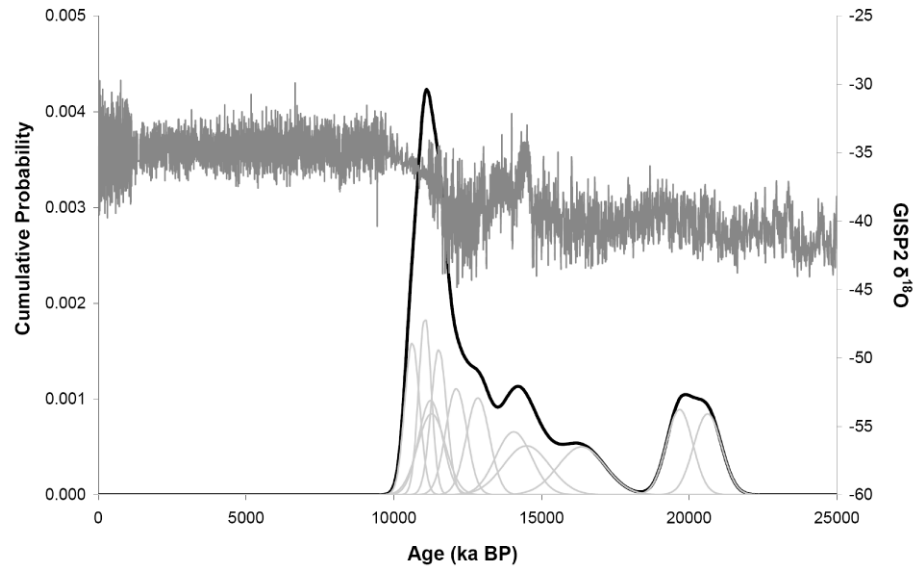
Figure 14.

Table Legends

Table 1. Location information for the 20 bedrock and 13 boulder samples collected near Upernavik, Greenland.

Table 2. Laboratory information from work performed at the cosmogenic nuclide laboratory at the University of Vermont.

Table 3. Isotopic information from work performed at Lawrence Livermore National Laboratory and age calculations conducted with the CRONUS Earth online calculator and numerical modeling.

Figure Legends

Figure 1. Regional map of central-western and northwestern Greenland. The small box shows the location of the study site as shown in Figure 5. Black dots indicate radiocarbon ages as described in the text.

Figure 2. Low-elevation locations were characterized by sculpted bedrock forms and abundant erratic boulders. No glacial striations or polish were observed.

Figure 3. High-elevation locations exhibited evident surface weathering features including pedestals, weathering pits, frost shattering, abundant grus, and sheet weathering.

Figure 4. Illustration of bedrock/boulder age relationships and possible scenarios to explain them.

Figure 5. Study site map. Bedrock and boulder samples were collected along a 100-km northwest-southeast transect near Upernavik, Greenland, at seven different "dipsticks". Wherever possible, bedrock/boulder pairs were taken from a variety of elevations shown by gray ovals. Within each sample pair, the bedrock sample is listed first, followed by the boulder sample. In the few instances where boulders were not available, only the bedrock sample is listed. Image courtesy of Google Earth.

Figure 6. Histogram of minimum limiting ^{10}Be exposure ages for all 20 bedrock and 13 boulder samples.

Figure 7. Histogram of minimum limiting ^{26}Al exposure ages for the 15 bedrock and five boulder samples on which Al analysis was performed.

Figure 8. Correlation ^{10}Be and ^{26}Al concentrations. Error bars show 1σ internal error; in most cases, error bars are smaller than the data points. The gray dashed line represents the 1 to 6.75 (Be to Al) production ratio.

Figure 9. ^{26}Al/^{10}Be ratios plotted against ^{10}Be concentrations for the 15 bedrock and five boulder samples on which both isotopes were analyzed. Exposure durations (in years) are shown along the thick black "constant exposure" path. Erosion rates, in m Ma^{-1}, are shown along the bottom of the "steady erosion" envelope. Individual erosion paths for the erosion rates mentioned are shown with black dotted lines. Burial paths are shown with thin gray lines, and burial isochrones are shown with thin gray dashed lines. Gray dots represent the four "control" samples, and black dots represent the 16 other samples. Error bars show 1σ internal error.

Figure 10. Comparison of bedrock and boulder sample ages shown by a correlation of minimum limiting ^{10}Be ages for 13 sample pairs. Error bars show 1σ internal error; in

most cases, error bars are smaller than the data points. The gray dashed line represents a 1:1 correlation.

Figure 11. Comparison of bedrock and boulder sample age populations shown by box and whisker plots (bedrock, n = 20; boulders n = 13). The box encloses the area between the first and third quartiles, and the horizontal line represents the median. Whiskers show one standard deviation. Samples that lie outside one standard deviation from the mean are shown with an asterisk; all other samples are shown with dots.

Figure 12. Correlation of sample age and elevation. Black dots represent bedrock samples (n = 20) and gray dots represent boulder samples (n = 13). Error bars show 1σ internal error; in most cases, error bars are smaller than the data points.

Figure 13. Spatial variability of ages. Minimum limiting ^{10}Be ages plotted against the distance along the sample transect. The solid symbols represent boulder samples (n = 13) and the hollow symbols represent bedrock samples (n = 20). Solid triangles (n = 6) indicate the boulder samples used to estimate a deglaciation age of 11.3 ± 0.5 ka (see text for more details). Error bars show 1σ internal error; in most cases, error bars are smaller than the data points.

Figure 14. Deglaciation timing and paleoclimate context. Thin gray lines show the probability density functions for each individual boulder sample (the oldest boulder sample, 44.3 ka, has been omitted from this plot for better visibility). The thick black line shows the summed cumulative probability for the entire boulder data set. The dark gray line represents δ^{18}O values from the GISP2 ice core from Greenland's summit; this data, available online at http://depts.washington.edu/qil/datasets/, is courtesy of M. Stuiver and P.M. Grootes at University of Washington. Minimum limiting ^{10}Be ages are plotted against the left axis, while GISP2 δ^{18}O values are plotted against the right axis.

CHAPTER 5. CONCLUSIONS

1. Conclusions

Analysis of ~500 cosmogenic ^{10}Be samples demonstrates that laboratory

modifications and methodological advances have greatly enhanced the quality of samples

produced in University of Vermont's Cosmogenic Laboratory. The success of a ^{10}Be

sample can be measured by the beam current it achieves while being analyzed by

accelerator mass spectrometry. Methodological optimization increased average beam

currents from 13.4 ± 5.4 µA (old laboratory; n = 63) to 22.5 ± 3.4 µA (new laboratory, n

= 446). The data demonstrate that samples processed during 2009-2010 had high Be yield

and few impurities; this has been critical to the success of my work in western Greenland

because the samples from those field sites have low concentrations of ^{10}Be, and are only

able to achieve high-precision measurements with optimal beam currents. None of the

factors explored in this analysis closely explained the variability in beam currents; this is

likely because the impurity levels in the samples were small enough to not depress beam

currents. Instead, this variability is driven by factors not quantified in this analysis, such

as differences in the behavior of the accelerator mass spectrometer over time.

Work near Ilulissat, Greenland (69°N) provided insight about the timing and style

of ice margin retreat at the end of the last glacial period. Ice retreat first exposed coastal

areas about 10,300 years ago, and the ice margin retreated behind its present-day position

about 7,600 years ago. Ice retreat through Sikuijuitsoq Fjord occurred at rates of 100

meters per year, which is consistent with other estimates of ice retreat for the same time

period from Greenland and other glaciated areas. Comparison with neighboring areas suggests that the large ice stream, Jakobshavn Isbræ, set the pace and timing for ice retreat in the Ilulissat area. It is likely that the retreat of Jakobshavn Isbræ beyond the mouth of Sikuijuitsoq Fjord allowed sea water to enter the fjord, thereby initiating a phase of rapid retreat in the study area. The ice in the Ilulissat area had high rates of subglacial erosion, efficiently abrading and sculpting the landscape during the last glacial period. Ice in this region was likely fast-flowing and thick, allowing the base of the ice sheet to be warm enough for meltwater to exist. High rates of subglacial erosion led to the development of the fresh, non-weathered landscape visible today.

A similar study was conducted 500 kilometers to the north, near Upernavik, Greenland (73°N). Ice retreat at the end of the last glacial period occurred rapidly at about 170 meters per year, and this episode of deglaciation took place around 11,300 years ago. Ice may have retreated rapidly from this area because the majority of the ice sheet's base would have been floating, thereby allowing the ice margin to retreat episodically via calving. The ice in the Upernavik area had low rates of subglacial erosion, especially at high elevations, and failed to perform significant erosion. This is likely because the ice sheet was thin, and the base of the ice was too cold to allow meltwater to form. Low rates of subglacial erosion preserved old bedrock features, leading to the highly weathered landscape visible today.

Work at two different sites in western Greenland has shown that ice characteristics can vary appreciably over distances as short as 500 kilometers. Ice retreat in Upernavik was almost twice as rapid as in Ilulissat, likely because it was driven by ice berg calving of the predominately marine-based margin. Subglacial landscape sculpting

148

occurred efficiently in Ilulissat due to the presence of thick, warm-based, highly erosive ice. Conversely, little subglacial landscape sculpting occurred in Upernavik, especially at high elevations, because the ice was thin, cold-based, and non-erosive. These contrasts demonstrate that, even though the two sites were glaciated by the same body of ice, the behavior of that ice seems to have been dictated by local or regional factors.

In both Ilulissat and Upernavik, deglaciation took place on human time scales. Retreat rates of 100 to several hundred meters per year would have evident effects on landscape, sea level, and climate noticeable over human lifetimes. The rapidity with which ice loss can take place is an important consideration in light of anthropogenic climate change; it implies that deglaciation in Greenland, and resulting sea level rise, can have real implications for modern-day civilizations.

2. Future Work

Although this work has provided insight about ice behavior at two sites in western Greenland, more information is needed to improve the depth of understanding. At present, the basal thermal regime of the Greenland Ice Sheet is poorly constrained. Performing a similar study at various locations along the ice sheet margin could provide information about what areas of the ice sheet are warm-based, therefore efficiently eroding the landscape, and what areas are cold-based, therefore performing little erosion on the landscape. Tighter constraints on the spatial distribution of erosion rates would provide information about how erosive the Greenland Ice Sheet is as a whole. Modeling could quantify the total flux of material removed from Greenland's land surface and

transported to the sea, thereby constraining the geomorphic impact of one of the largest erosive agents on Earth.

Future work could also focus on climatic implications. I hypothesize that the differences in ice retreat rates between Ilulissat and Upernavik were caused by ice berg calving at the primarily marine-based Upernavik ice margin; however, investigation at more sites is required to test this assertion. Future work could use a similar study design to quantify post-glacial ice retreat rates at more sites, some with terrestrial-based ice margins and others with marine-based ice margins. It is probable that this comparison would yield a detectable difference in retreat rates between the two types of ice margins. A deeper understanding of topographic controls on ice retreat characteristics would show which areas of the ice sheet margin are at risk for rapid disintegration.

If there are indeed real differences in retreat rates, further work could focus on quantifying the current state of the Greenland Ice Sheet through this lens. This work could consider what portion of the ice sheet margin is currently marine-based, the volume of ice these areas encompass, and the sea level equivalent of this ice. Ice loss through calving is a positive feedback; melting ice causes sea level rise, which causes terrestrial-based ice to float and be susceptible to calving. Therefore, it would also be helpful to quantify how much of the Greenland Ice Sheet would be marine-based in various scenarios of sea level rise, and to model how this positive feedback would play out. Modeling these scenarios would greatly improve the forecasts in the Intergovernmental Panel on Climate Change reports, providing critical information about changes in both ice sheet extent and global sea level in the future.

COMPREHENSIVE BIBLIOGRAPHY

Alley, R., 2000, The Younger Dryas cold interval as viewed from central Greenland: Quaternary Science Reviews, v. 19, p. 213-226.

Alley, R., and Ágústsdóttir, A., 2005, The 8k event: cause and consequences of a major Holocene abrupt climate change: Quaternary Science Reviews, v. 24, p. 1123-1149.

Alley, R., Anandakrishnan, S., Dupont, T., Parizek, B., and Pollard, D., 2007, Effect of sedimentation on ice-sheet grounding-line stability: Science, v. 315, p. 1838-1841.

Alley, R., Andrews, J., Brigham-Grette, J., Clarke, G., Cuffey, K., Fitzpatrick, J., Funder, S., Marshall, S., Miller, G., and Mitrovica, J., 2010, History of the Greenland Ice Sheet: paleoclimatic insights: Quaternary Science Reviews, v. 29, p. 1728-1756.

Alley, R., Clark, P., Huybrechts, P., and Joughin, I., 2005, Ice-sheet and sea-level changes: Science, v. 310, p. 456-460.

Alley, R., Mayewski, P., Sowers, T., Stuiver, M., Taylor, K., and Clark, P., 1997, Holocene climatic instability: a prominent, widespread event 8200 yr ago: Geology, v. 25, p. 483-486.

Andrews, J., 1973, The Wisconsin Laurentide ice sheet: dispersal centers, problems of rates of retreat, and climatic implications: Arctic and Alpine Research, v. 5, p. 185-199.

Axford, Y., Briner, J., Miller, G., and Francis, D., 2009, Paleoecological evidence for abrupt cold reversals during peak Holocene warmth on Baffin Island, Arctic Canada: Quaternary Research, v. 71, p. 142-149.

Balco, G., 2011, Contributions and unrealized potential contributions of cosmogenic-nuclide exposure dating to glacier chronology, 1990-2010: Quaternary Science Reviews, v. 30, p. 3-27.

Balco, G., Briner, J., Finkel, R., Rayburn, J., Ridge, J., and Schaefer, J., 2009, Regional beryllium-10 production rate calibration for late-glacial northeastern North America: Quaternary Geochronology, v. 4, p. 93-107.

Balco, G., Stone, J., Lifton, N., and Dunai, T., 2008, A complete and easily accessible means of calculating surface exposure ages or erosion rates from ^{10}Be and ^{26}Al measurements: Quaternary Geochronology, v. 3, p. 174-195.

Bennike, O., 2000, Palaeoecological studies of Holocene lake sediments from west Greenland: Palaeogeography, Palaeoclimatology, Palaeoecology, v. 155, p. 285-304.

----, 2008, An early Holocene Greenland whale from Melville Bugt, Greenland: Quaternary Research, v. 69, p. 72-76.

Bennike, O., and Björck, S., 2002, Chronology of the last recession of the Greenland Ice Sheet: Journal of Quaternary Science, v. 17, p. 211-219.

Bentley, C., 1987, Antarctic ice streams: a review: Journal of Geophysical Research, v. 92, p. 8843-8858.

Berger, A., 1988, Milankovitch theory and climate: Reviews of Geophysics, v. 26, p. 624-657.

Bierman, P., 1994, Using in situ produced cosmogenic isotopes to estimate rates of landscape evolution: A review from the geomorphic perspective: Journal of Geophysical Research, v. 99, p. 13885-13896.

Bierman, P., and Steig, E., 1996, Estimating rates of denudation using cosmogenic isotope abundances in sediment: Earth Surface Processes and Landforms, v. 21, p. 125-139.

Bierman, P., Gillespie, A., and Caffee, M., 1995, Cosmogenic ages for earthquake recurrence intervals and debris flow fan deposition, Owens Valley, California: Science, v. 270, p. 447-450.

Bierman, P., Marsella, K., Patterson, C., Davis, P., and Caffee, M., 1999, Mid-Pleistocene cosmogenic minimum-age limits for pre-Wisconsinan glacial surfaces in southwestern Minnesota and southern Baffin Island: a multiple nuclide approach: Geomorphology, v. 27, p. 25-39.

Bierman, P.R., and Nichols, K.K., 2004, Rock to sediment- slope to sea with ^{10}Be- rates of landscape change: Annual Review of Earth and Planetary Sciences, v. 32, p. 215-255.

Bintanja, R., and Van De Wal, R.S.W., 2008, North American ice-sheet dynamics and the onset of the 100,000-year glacial cycles: Nature, v. 454, p. 869-872.

Bougamont, M., and Tulaczyk, S., 2003, Glacial erosion beneath ice streams and ice stream tributaries: constraints on temporal and spatial distribution of erosion from numerical simulations of a West Antarctic ice stream: Boreas, v. 32, p. 178-190.

Briner, J., and Swanson, T., 1998, Using inherited cosmogenic ^{36}Cl to constrain glacial erosion rates of the Cordilleran ice sheet: Geology, v. 26, p. 3-6.

Briner, J., Bini, A., and Anderson, R., 2009, Rapid early Holocene retreat of a Laurentide outlet glacier through an Arctic fjord: Nature Geoscience, v. 2, p. 496-499.

Briner, J., Miller, G., Davis, P., Bierman, P., and Caffee, M., 2003, Last Glacial Maximum ice sheet dynamics in Arctic Canada inferred from young erratics perched on ancient tors: Quaternary Science Reviews, v. 22, p. 437-444.

Briner, J., Stewart, H., Young, N., Phillips, W., and Losee, S., 2010, Using proglacial-threshold lakes to constrain fluctuations of the Jakobshavn Isbrae ice margin, western Greenland, during the Holocene: Quaternary Science Reviews, v. 29, p. 3861-3874.

Brown, E., Edmond, J., Raisbeck, G., Yiou, F., Kurz, M., and Brook, E., 1991, Examination of surface exposure ages of Antarctic moraines using in situ produced ^{10}Be and ^{26}Al: Geochimica et Cosmochimica Acta, v. 55, p. 2269-2283.

Brown, E., Stallard, R., Larsen, M., Raisbeck, G., and Yiou, F., 1995, Denudation rates determined from the accumulation of in situ-produced ^{10}Be in the Luquillo Experimental Forest, Puerto Rico: Earth and Planetary Science Letters, v. 129, p. 193-202.

Corbett, L., Bierman, P., Graly, J., Neumann, T., Rood, D., and Finkel, R., 2009, In situ cosmogenic ^{10}Be estimates of deglaciation timing and glacial erosion efficiency, western Greenland: Geological Society of America Abstracts with Programs, v. 41, p. 621.

Corbett, L., Young, N., Bierman, P., Briner, J., Neumann, T., Graly, J., and Rood, D., 2011, [10]Be concentrations in bedrock and boulder samples resulting from early Holocene ice retreat near Jakobshavn Isfjord, western Greenland: Quaternary Science Reviews, v. DOI 10.1016/j.quascirev.2011.04.001.

Csatho, B., Schenk, T., Van der Veen, C., and Krabill, W., 2008, Intermittent thinning of Jakobshavn Isbræ, West Greenland, since the Little Ice Age: Journal of Glaciology, v. 54, p. 131-144.

Cuffey, K., and Marshall, S., 2000, Substantial contribution to sea-level rise during the last interglacial from the Greenland ice sheet: Nature, v. 404, p. 591-594.

Dahl-Jensen, D., Mosegaard, K., Gundestrup, N., Clow, G., Johnsen, S., Hansen, A., and Balling, N., 1998, Past temperatures directly from the Greenland Ice Sheet: Science, v. 282, p. 268-271.

Dansgaard, W., White, J., and Johnsen, S., 1989, The abrupt termination of the Younger Dryas climate event: Nature, v. 339, p. 532-534.

De Vernal, A., and Hillaire-Marcel, C., 2008, Natural variability of Greenland climate, vegetation, and ice volume during the past million years: Science, v. 320, p. 1622-1625.

Delmas, M., Gunnell, Y., Braucher, R., Calvet, M., and Bourles, D., 2008, Exposure age chronology of the last glaciation in the eastern Pyrenees: Quaternary Research, v. 69, p. 231-241.

Ditchburn, R., and Whitehead, N., 1994, The separation of [10]Be from silicates, 3rd Workshop of the South Pacific Environmental Radioactivity Association, p. 4-7.

Dyke, A., 1979, Quaternary geomorphology, glacial chronology, and climatic and sea-level history of southwestern Cumberland Peninsula, Baffin Island, Northwest Territories, Canada: Arctic and Alpine Research, v. 11, p. 179-202.

England, J., 1987, Glaciation and the evolution of the Canadian high arctic landscape: Geology, v. 15, p. 419-423.

Escher, J., and Pulvertaft, T., 1995, Geological Map of Greenland 1:2,500,000, Geologic Survey of Greenland, Copenhagen.

Fabel, D., and Harbor, J., 1999, The use of in-situ produced cosmogenic radionuclides in glaciology and glacial geomorphology: Annals of Glaciology, v. 28, p. 103-110.

Fairhall, A., 1960, The Radiochemistry of Beryllium, Nuclear Science Series: Washington, DC, National Academy of Sciences and National Research Council.

Fredskild, B., 1985, The Holocene vegetational development of Tugtuligssuaq and Qeqertat, northwest Greenland, Museum Tusculanum Press, 20 p.

Funder, S., Abrahamsen, N., Bennike, O., and Feyling-Hanssen, R.W., 1985, Forested arctic: evidence from north Greenland: Geology, v. 13, p. 542-546.

Gardner, T., Jorgensen, D., Shuman, C., and Lemieux, C., 1987, Geomorphic and tectonic process rates: Effects of measured time interval: Geology, v. 15, p. 259-261.

Gillespie, A.R., and Bierman, P.R., 1995, Precision of terrestrial exposure ages and erosion rats estimated from analysis of cosmogenic isotopes produced *in situ*: Journal of Geophysical Research, v. 100, p. 24,637-24,649.

Glasser, N.F., and Ghiglione, M.C., 2009, Strutctual, tectonic, and glaciological controls on the evolution of fjord landscapes: Geomorphology, v. 105, p. 291-302.

Gosse, J., and Phillips, F., 2001, Terrestrial in situ cosmogenic nuclides: theory and application: Quaternary Science Reviews, v. 20, p. 1475-1560.

Gosse, J., Grant, D., Klein, J., and Lawn, B., 1995, Cosmogenic [10]Be and [26]Al constraints on weathering zone genesis, ice cap basal conditions, and Long Range Mountain (Newfoundland) glacial history: CANQUA-CGRG conference abstracts, v. CA19.

Gosse, J., Grant, D., Klein, J., Klassen, R., Evenson, E., Lawn, B., and Middleton, R., 1993, Significance of altitudinal weathering zones in Atlantic Canada, inferred from in situ produced cosmogenic radionuclides: Geological Society of America Abstracts with Programs, v. 25, p. A394.

Granger, D., and Muzikar, P., 2001, Dating sediment burial with in situ-produced cosmogenic nuclides: theory, techniques, and limitations: Earth and Planetary Science Letters, v. 188, p. 269-281.

Granger, D., Kirchner, J., and Finkel, R., 1996, Spatially averaged long-term erosion rates measured from in situ-produced cosmogenic nuclides in alluvial sediment: The Journal of Geology, v. 104, p. 249-257.

Gregory, J., Huybrechts, P., and Raper, S., 2004, Threatened loss of the Greenland ice-sheet: Nature, v. 428, p. 616.

Håkansson, L., Alexanderson, H., Hjort, C., Moller, P., Briner, J., Aldahan, A., and Possnert, G., 2008, Late Pleistocene glacial history of Jameson Land, central East Greenland, derived from cosmogenic [10]Be and [26]Al exposure dating: Boreas, v. 38, p. 244-260.

Hanna, E., Huybrechts, P., Steffen, K., Cappelen, J., Huff, R., Shuman, C., Irvine-Fynn, T., Wise, S., and Griffiths, M., 2008, Increased runoff from melt from the Greenland Ice Sheet: a response to global warming: Journal of Climate, v. 21, p. 331-341.

Harbor, J., Stroeven, A., Fabel, D., Clarhäll, A., Kleman, J., Li, Y., Elmore, D., and Fink, D., 2006, Cosmogenic nuclide evidence for minimal erosion across two subglacial sliding boundaries of the late glacial Fennoscandian ice sheet: Geomorphology, v. 75, p. 90-99.

Heyman, J., Stroeven, A., Harbor, J., and Caffee, M., 2010, Too young or too old: Evaluating cosmogenic exposure dating based on an analysis of compiled boulder exposure ages: Earth and Planetary Science Letters, v. 302, p. 71-80.

Holland, D., Thomas, R., De Young, B., Ribergaard, M., and Lyberth, B., 2008, Acceleration of Jakobshavn Isbrae triggered by warm subsurface ocean waters: Nature Geoscience, v. 1, p. 659-664.

Hunt, A., Larsen, J., Bierman, P., and Petrucci, G., 2008, Investigation of factors that affect the sensitivity of accelerator mass spectrometry for cosmogenic [10]Be and [26]Al isotope analysis: Analytical Chemistry, v. 80, p. 1656-1663.

Hunt, A., Petrucci, G., Bierman, P., and Finkel, R., 2006, Metal matrices to optimize ion beam currents for accelerator mass spectrometry: Nuclear Instruments and Methods in Physics Research Section B: Beam Interactions with Materials and Atoms, v. 243, p. 216-222.

154

Huybrechts, P., 1996, Basal temperature conditions of the Greenland ice sheet during the glacial cycles: Annals of Glaciology, v. 23, p. 226-236.

Huybrechts, P., Letreguilly, A., and Reeh, N., 1991, The Greenland ice sheet and greenhouse warming: Global and Planetary Change, v. 3, p. 399-412.

Imbrie, J., Boyle, E.A., Clemens, S.C., Duffy, A., Howard, W.R., Kukla, G., Kutzbach, J., Martinson, D.G., McIntyre, A., Mix, A.C., Molfino, B., Morley, J.J., Peterson, L.C., Pisias, N.G., Prell, W.L., Raymo, M.E., Shackleton, N.J., and Toggweiler, J.R., 1992, On the structure and origin of major glaciation cycles 1, linear response to Milankovitch forcing: Paleoceanography, v. 7, p. 701-738.

IPCC, 2007, Climate Change 2007: The Physical Science Basis. Contribution of Working Group I to the Fourth Assessment Report of the Intergovernmental Panel on Climate Change, Cambridge University Press.

Joughin, I., Abdalati, W., and Fahnestock, M., 2004, Large fluctuations in speed on Greenland's Jakobshavn Isbrae glacier: Nature, v. 432, p. 608-610.

Kelly, M., 1980, Preliminary investigations of the Quaternary of Melville Bugt and Dundas, northwest Greenland: Rapport Gronlands Geologiske Undersogelse, v. 100, p. 33-38.

Kelly, M., Lowell, T., Hall, B., Schaefer, J., Finkel, R., Goehring, B., Alley, R., and Denton, G., 2008, A [10]Be chronology of lateglacial and Holocene mountain glaciation in the Scoresby Sund region, east Greenland: implications for seasonality during lateglacial time: Quaternary Science Reviews, v. 27, p. 2273-2282.

Klein, J., and Middleton, R., 1984, Accelerator mass spectrometry at the University of Pennsylvania: Nuclear Instruments and Methods in Physics Research Section B: Beam Interactions with Materials and Atoms, v. 5, p. 129-133.

Koerner, R., 1989, Ice core evidence for extensive melting of the Greenland ice sheet in the last interglacial: Science, v. 244, p. 964-968.

Kohl, C., and Nishiizumi, K., 1992, Chemical isolation of quartz for measurement of in-situ-produced cosmogenic nuclides: Geochimica et Cosmochimica Acta, v. 56, p. 3583-3587.

Lal, D., 1988, In situ-produced cosmogenic isotopes in terrestrial rocks: Annual Review of Earth and Planetary Sciences, v. 16, p. 355-388.

----, 1991, Cosmic ray labeling of erosion surfaces: in situ nuclide production rates and erosion models: Earth and Planetary Science Letters, v. 104, p. 424-439.

Lanford, W.A., Parker, P.D., Bauer, K., Turekian, K.K., Cochran, J.K., and Krishnaswami, S., 1980, Measurements of [10]Be distributions using a Tandem Van De Graaff accelerator: Nuclear Instruments and Methods, v. 168, p. 505-510.

Larsen, H., Saunders, A., Clift, P., Beget, J., Wei, W., and Spezzaferri, S., 1994, Seven million years of glaciation in Greenland: Science, v. 264, p. 952-955.

Letréguilly, A., Reeh, N., and Huybrechts, P., 1991, The Greenland ice sheet through the last glacial-interglacial cycle: Global and Planetary Change, v. 4, p. 385-394.

Licciardi, J.M., Schaefer, J.M., Taggart, J.R., and Lund, D.C., 2009, Holocene glacier fluctuations in the Peruvian Andes indicate northern climate linkages: Science, v. 325, p. 1677-1679.

Lilly, K., Fink, D., Fabel, D., and Lambeck, K., 2010, Pleistocene dynamics of the interior of the East Antarctic ice sheet: Geology, v. 38, p. 703-706.

Lisiecki, L., and Raymo, M., 2005, A Plio-Pleistocene stack of 57 globally distributed benthic ^{18}O records: Paleoceanography, v. 20, p. 522–533.

Lloyd, J., Park, L., Kuijpers, A., and Moros, M., 2005, Early Holocene palaeoceanography and deglacial chronology of Disko Bugt, West Greenland: Quaternary Science Reviews, v. 24, p. 1741-1755.

Long, A., 2009, Back to the future: Greenland's contribution to sea-level change: GSA Today, v. 19, p. 4-10.

Long, A., and Roberts, D., 2002, A revised chronology for the 'Fjord Stade' moraine in Disko Bugt, West Greenland: Journal of Quaternary Science, v. 17, p. 561-579.

----, 2003, Late Weichselian deglacial history of Disko Bugt, West Greenland, and the dynamics of the Jakobshavns Isbrae ice stream: Boreas, v. 32, p. 208-226.

Long, A., Roberts, D., and Dawson, S., 2006, Early Holocene history of the West Greenland Ice Sheet and the GH-8.2 event: Quaternary Science Reviews, v. 25, p. 904-922.

Marquette, G., Gray, J., Gosse, J., Courchesne, F., Stockli, L., Macpherson, G., and Finkel, R., 2004, Felsenmeer persistence under non-erosive ice in the Torngat and Kaumajet mountains, Quebec and Labrador, as determined by soil weathering and cosmogenic nuclide exposure dating: Canadian Journal of Earth Sciences, v. 41, p. 19-38.

Marsella, K., Bierman, P., Davis, P., and Caffee, M., 2000, Cosmogenic ^{10}Be and ^{26}Al ages for the last glacial maximum, eastern Baffin Island, Arctic Canada: Geological Society of America Bulletin, v. 112, p. 1296-1312.

Merchel, S., Arnold, M., Aumaitre, G., Benedetti, L., Bourles, D., Braucher, R., Alfimov, V., Freeman, S., Steier, P., and Wallner, A., 2008, Towards more precise ^{10}Be and ^{36}Cl data from measurements at the 10^{-14} level: Influence of sample preparation: Nuclear Instruments and Methods in Physics Research Section B: Beam Interactions with Materials and Atoms, v. 266, p. 4921-4926.

Milankovitch, M., 1969, Canon of isolation and the Ice-Age problem: Jerusalem, Israel Program for Scientific Translations, 484 p.

Nichols, K.K., Bierman, P.R., Foniri, W.R., Gillespie, A.R., Caffe, M., and Finkel, R., 2006, Dates and rates of arid region geomorphic processes: GSA Today, v.16, p. 4-11.

Nishiizumi, K., 2004, Preparation of ^{26}Al AMS standards: Nuclear Instruments and Methods in Physics Research Section B: Beam Interactions with Materials and Atoms, v. 223, p. 388-392.

Nishiizumi, K., Finkel, R., Ponganis, K., Graf, T., Kohl, C., and Marti, K., 1996, *In situ* produced cosmogenic nuclides in GISP2 rock core from Greenland summit: EOS Transactions of the American Geophysical Union, v. 77, p. Abstract 06945142.

Nishiizumi, K., Imamura, M., Caffee, M., Southon, J., Finkel, R., and McAninch, J., 2007, Absolute calibration of ^{10}Be AMS standards: Nuclear Instruments and Methods in Physics Research Section B: Beam Interactions with Materials and Atoms, v. 258, p. 403-413.

Nishiizumi, K., Kohl, C., Arnold, J., Klein, J., Fink, D., and Middleton, R., 1991, Cosmic ray produced ^{10}Be and ^{26}Al in Antarctic rocks: exposure and erosion history: Earth and Planetary Science Letters, v. 104, p. 440-454.

Nishiizumi, K., Lal, D., Klein, J., Middleton, R., and Arnold, J., 1986, Production of ^{10}Be and ^{26}Al by cosmic rays in terrestrial quartz in situ and implications for erosion rates: Nature, v. 319, p. 134-136.

Nishiizumi, K., Winterer, E., Kohl, C., Klein, J., Middleton, R., Lal, D., and Arnold, J., 1989, Cosmic ray production rates of ^{10}Be and ^{26}Al in quartz from glacially polished rocks: Journal of Geophysical Research, v. 94, p. 17907.

Otto-Bliesner, B., Marshall, S., Overpeck, J., Miller, G., and Hu, A., 2006, Simulating Arctic climate warmth and icefield retreat in the last interglaciation: Science, v. 311, p. 1751-1753.

Overpeck, J., Otto-Bliesner, B., Miller, G., Muhs, D., Alley, R., and Kiehl, J., 2006, Paleoclimatic evidence for future ice-sheet instability and rapid sea-level rise: Science, v. 311, p. 1747-1750.

Pallas, R., Rodes, A., Braucher, R., Carcaillet, J., Ortuno, M., Bordonau, J., Bourles, D., Vilaplana, J., Masana, E., and Santanach, P., 2006, Late Pleistocene and Holocene glaciation in the Pyrenees: a critical review and new evidence from ^{10}Be exposure ages, south-central Pyrenees: Quaternary Science Reviews, v. 25, p. 2937-2963.

Peterson, R., 2003, Settlements, kinship and hunting grounds in traditional Greenland, 327 pp. p.

Phillips, F., Zreda, M., Smith, S., Elmore, D., Kubik, P., and Sharma, P., 1990, Cosmogenic chlorine-36 chronology for glacial deposits at Bloody Canyon, eastern Sierra Nevada: Science, v. 248, p. 1529-1532.

Portenga, E.W., and Bierman, P.R., *In Press*, Understanding Earth's eroding surface with ^{10}Be: GSA Today.

Porter, S., 1989, Late Holocene fluctuations of the fiord glacier system in Icy Bay, Alaska, USA: Arctic and Alpine Research, v. 21, p. 364-379.

Rinterknecht, V., Gorokhovich, Y., Schaefer, J., and Caffee, M., 2009, Preliminary ^{10}Be chronology for the last deglaciation of the western margin of the Greenland Ice Sheet: Journal of Quaternary Science, v. 24, p. 270-278.

Roberts, D., and Long, A., 2005, Streamlined bedrock terrain and fast ice flow, Jakobshavns Isbrae, West Greenland: implications for ice stream and ice sheet dynamics: Boreas, v. 34, p. 25-42.

Roberts, D., Long, A., Schnabel, C., Davies, B., Xu, S., Simpson, M., and Huybrechts, P., 2009, Ice sheet extent and early deglacial history of the southwestern sector of the Greenland Ice Sheet: Quaternary Science Reviews, v. 28, p. 2760-2773.

Rood, D., Hall, S., Guilderson, T., Finkel, R., and Brown, T., 2010, Challenges and opportunities in high-precision Be-10 measurements at CAMS: Nuclear Instruments and Methods in Physics Research Section B: Beam Interactions with Materials and Atoms, v. 268, p. 730-732.

Schildgen, T., Phillips, W., and Purves, R., 2005, Simulation of snow shielding corrections for cosmogenic nuclide surface exposure studies: Geomorphology, v. 64, p. 67-85.

Shackleton, N., Backman, J., Zimmerman, H., Kent, D., Hall, M., Roberts, D., Schnitker, D., Baldauf, J., Desprairies, A., and Homrighausen, R., 1984, Oxygen isotope calibration of the onset of ice-rafting and history of glaciation in the North Atlantic region: Nature, v. 307, p. 620-623.

Sharma, P., and Middleton, R., 1989, Radiogenic production of ^{10}Be and ^{26}Al in uranium and thorium ores: Implications for studying terrestrial samples containing low levels of ^{10}Be and ^{26}Al: Geochimica et Cosmochimica Acta, v. 53, p. 709-716.

Smith, A., Murray, T., Nicholls, K., Makinson, K., Adalgeirsdottir, G., Behar, A., and Vaughan, D., 2007, Rapid erosion, drumlin formation, and changing hydrology beneath an Antarctic ice stream: Geology, v. 35, p. 127-130.

Smith, J., Finkel, R., Farber, D., Rodbell, D., and Seltzer, G., 2005, Moraine preservation and boulder erosion in the tropical Andes: interpreting old surface exposure ages in glaciated valleys: Journal of Quaternary Science, v. 20, p. 735-758.

Southon, J., Vogel, J., Nowikow, I., Nelson, D., Korteling, R., Ku, T., Kusakabe, M., and Huh, C., 1983, The measurement of ^{10}Be concentrations with a tandem accelerator: Nuclear Instruments and Methods in Physics Research, v. 205, p. 251-257.

Steig, E.J., and Wolfe, A.P., 2008, Sprucing up Greenland: Science, v. 320, p. 1595-1596.

Stone, J., 2000, Air pressure and cosmogenic isotope production: Journal of Geophysical Research, v. 105, p. 23753-23759.

Stone, J., Balco, G., Sugden, D., Caffee, M., Sass III, L., Cowdery, S., and Siddoway, C., 2003, Holocene deglaciation of Marie Byrd Land, West Antarctica: Science, v. 299, p. 99-102.

Stone, J., Ballantyne, C., and Keith Fifield, L., 1998, Exposure dating and validation of periglacial weathering limits, northwest Scotland: Geology, v. 26, p. 587-590.

Stroeven, A., Fabel, D., Hättestrand, C., and Harbor, J., 2002, A relict landscape in the centre of Fennoscandian glaciation: cosmogenic radionuclide evidence of tors preserved through multiple glacial cycles: Geomorphology, v. 44, p. 145-154.

Stuiver, M., and Grootes, P., 2000, GISP2 oxygen isotope ratios: Quaternary Research, v. 53, p. 277-284.

Sugden, D., 1977, Reconstruction of the morphology, dynamics, and thermal characteristics of the Laurentide Ice Sheet at its maximum: Arctic and Alpine Research, v. 9, p. 21-47.

----, 1978, Glacial erosion by the Laurentide ice sheet: Journal of Glaciology, v. 20, p. 367-391.

Sugden, D., and Watts, S., 1977, Tors, felsenmeer, and glaciation in northern Cumberland Peninsula, Baffin Island: Canadian Journal of Earth Sciences, v. 14, p. 2817-2823.

Sugden, D., Balco, G., Cowdery, S., Stone, J., and Sass III, L., 2005, Selective glacial erosion and weathering zones in the coastal mountains of Marie Byrd Land, Antarctica: Geomorphology, v. 67, p. 317-334.

Suter, M., 1990, Accelerator mass spectrometry: state of the art in 1990: Nuclear Instruments and Methods in Physics Research Section B: Beam Interactions with Materials and Atoms, v. 52, p. 211-223.

Swift, D.A., Persano, C., Stuart, F.M., Gallagher, K., and Whitman, A., 2008, A reassessment of the role of ice sheet glaciation in the long-term evolution of the East Greenland fjord region: Geomorphology, v. 97, p. 109-125.

Taylor, K., Lamorey, G., Doyle, G., Alley, R., Grootes, P., Mayewski, P., White, J., and Barlow, L., 1993, The 'flickering switch'of late Pleistocene climate change: Nature, v. 361, p. 432-436.

Taylor, K., Mayewski, P., Alley, R., Brook, E., Gow, A., Grootes, P., Meese, D., Saltzman, E., Severinghaus, J., and Twickler, M., 1997, The Holocene-Younger Dryas transition recorded at Summit, Greenland: Science, v. 278, p. 825-827.

Vinther, B., Buchardt, S., Clausen, H., Dahl-Jensen, D., Johnsen, S., Fisher, D., Koerner, R., Raynaud, D., Lipenkov, V., and Andersen, K., 2009, Holocene thinning of the Greenland ice sheet: Nature, v. 461, p. 385-388.

Von Blanckenburg, F., 2005, The control mechanisms of erosion and weathering at basin scale from cosmogenic nuclides in river sediment: Earth and Planetary Science Letters, v. 237, p. 462-479.

Von Blanckenburg, F., Belshaw, N., and O'Nions, R., 1996, Separation of ^{9}Be and cosmogenic ^{10}Be from environmental materials and SIMS isotope dilution analysis: Chemical geology, v. 129, p. 93-99.

Weidick, A., 1968, Observations on some Holocene glacier fluctuations in West Greenland: *Medd. om Gronland*, v. 165(6), p. 194 pp.

Weidick, A., and Bennike, O., 2007, Quaternary glaciation history and glaciology of Jakobshavn Isbrae and the Disko Bugt region, west Greenland: a review: Geologic Survey of Denmark and Greenland Bulletin, v. 14, p. 1-13.

Weidick, A., Oerter, H., Reeh, N., Thomsen, H., and Thorning, L., 1990, The recession of the Inland Ice margin during the Holocene climatic optimum in the Jakobshavn Isfjord area of West Greenland: Global and Planetary Change, v. 2, p. 389-399.

Wiles, G., and Calkin, P., 1993, Neoglacial fluctuations and sedimentation of an iceberg-calving glacier resolved with tree rings (Kenai Fjords National Park, Alaska): Quaternary International, v. 18, p. 35-42.

Willerslev, E., Cappellini, E., Boomsma, W., Nielsen, R., Hebsgaard, M.B., Brand, T.B., Hofreiter, M., Bunce, M., Poinar, H.N., and Dahl-Jensen, D., 2007, Ancient biomolecules from deep ice cores reveal a forested southern Greenland: Science, v. 317, p. 111-114.

Wouters, B., Chambers, D., and Schrama, E., 2008, GRACE observes small-scale mass loss in Greenland: Geophysical Research Letters, v. 35, p. L20501.

Young, N., Briner, J., Stewart, H., Axford, Y., Csatho, B., Rood, D., and Finkel, R., 2011, Response of Jakobshavn Isbrae, Greenland, to Holocene climate change: Geology, v. 39, p. 131-134.